Copyright Warning & Restrictions

The copyright law of the United States (Title 17, United States Code) governs the making of photocopies or other reproductions of copyrighted material.

Under certain conditions specified in the law, libraries and archives are authorized to furnish a photocopy or other reproduction. One of these specified conditions is that the photocopy or reproduction is not to be "used for any purpose other than private study, scholarship, or research." If a, user makes a request for, or later uses, a photocopy or reproduction for purposes in excess of "fair use" that user may be liable for copyright infringement,

This institution reserves the right to refuse to accept a copying order if, in its judgment, fulfillment of the order would involve violation of copyright law.

Please Note: The author retains the copyright while the New Jersey Institute of Technology reserves the right to distribute this thesis or dissertation

Printing note: If you do not wish to print this page, then select "Pages from: first page # to: last page #" on the print dialog screen

ABSTRACT

MODELING OF NON-UNIFORM HYDRODYNAMICS AND CATALYTIC REACTION IN A SOLIDS-LADEN RISER

by
Rajeshkumar Patel

The riser reactors are widely used in a variety of industrial applications such as polymerization, coal combustion and petroleum refinery because of the strong mixing of gas and solids that yields high heat and mass transfer rates, and reaction rates. In a Fluid Catalytic Cracking (FCC) process, the performance of riser reactor is strongly dependent on the interaction between the fluid and catalysts, since the reaction takes place on the active surface of the catalysts. This is why, the local coupling between hydrodynamics and reaction kinetics is critical to the development of riser reaction models. The local gas-solids flow structure in riser reactors is highly heterogeneous both in axial and radial direction with back-mixing of catalyst. The radial non-uniform gas-solid flow structure is presented as core-annulus regime, with up-flow of dilute suspension of fresh catalyst and hydrocarbon vapor in the core regime, which is surrounded by dense down-flow of deactivated catalyst in the wall regime. As a result, the reaction characteristics in core and wall regions are strikingly different. The performance of the riser reactor is also strongly dependent on the vaporization and reaction characteristics in the feed injection regime of the riser reactors. From the modeling point of view, to predict the reaction characteristics in riser reactors, there is a need to develop hydrodynamics model, which can predicts both axial and radial nonuniform distribution of hydrocarbon vapor and catalyst and back-mixing of catalyst. There is also need for reasonable description of mechanistic coupling between nonuniform flow hydrodynamics and the cracking kinetics.

This dissertation is aimed to develop the mechanistic model for nonuniform hydrodynamics and catalytic reactions in a FCC riser reactor. A mechanistic model for multiphase flow interactions, vaporization of droplets and reactions in the feed injection regime is developed for to decide proper input boundary conditions for FCC riser reaction models. The dissertation is divided into the three major parts: 1) development of governing mechanisms and modeling of the axial and radial nonuniform distribution of the gas-solids transport properties in riser reactors 2) development of mechanistic model that gives a quantitative understanding of the interplay of three phase flow hydrodynamics, heat/mass transfer, and cracking reactions in the feed injection regime of a riser reactor 3) modeling of nonuniform hydrodynamics coupled reaction kinetics in the core and wall regime of the riser reactors.

For the modeling of the axial nonuniform distribution of gas-solids transport properties, a new controlling mechanism in terms of impact of pressure gradient along the riser on the particles transport is introduced. A correlation for inter-particle collision force is proposed which can be used for any operation conditions of riser, riser geometry and particle types. For simultaneous modeling of axial and radial nonuniform distribution of the gas-solids phase transport properties, a continuous modeling approach is used. In this dissertation, governing mechanisms for radial nonuniform distribution of gas-solids phase is proposed based on which a mechanistic model for radial nonuniform distribution of the gas and solid phase transport properties is proposed. With the proposed model for radial nonuniform phase distribution, the continuous model can successfully predicts both axial and radial nonuniform distribution of phase transport properties.

As the performance of the riser reactor is strongly influence by the vaporization and reactions in the feed injection regime, in this dissertation, a detailed mechanistic model for the multiphase flow hydrodynamics, vaporization and reaction characteristics in feed injection regime is established. To simulate the conditions of industrial riser reactor, the four nozzle spray jets were used, while overlapping of the spray jets is also considered.

Finally, in this dissertation, a modeling concept for the reactions in the core and wall regime of the riser reactor is explored. The proposed modeling concept takes into the account very important missed out physics such as, non-thermal equilibrium between the hydrocarbon vapor and the feed, back mixing and recirculation of the deactivated catalyst, activity of catalyst in core and wall regime, and coupling between the flow hydrodynamics and reaction kinetics.

MODELING OF NON-UNIFORM HYDRODYNAMICS AND CATALYTIC REACTION IN A SOLIDS-LADEN RISER

by
Rajeshkumar Patel

A Dissertation
Submitted to the Faculty of
New Jersey Institute of Technology
in Partial Fulfillment of the Requirements for the Degree of
Doctor of Philosophy in Mechanical Engineering

Department of Mechanical and Industrial Engineering

May 2011

APPROVAL PAGE

MODELING OF NON-UNIFORM HYDRODYNAMIC AND CATALYTIC REACTION IN A SOLIDS-LADEN RISER

Rajeshkumar Patel

Dr. Chao Zhu, Dissertation Advisor — Date
Professor of Mechanical & Industrial Engineering, NJIT

Dr. Pushpendra Singh, Committee Member — Date
Professor of Mechanical & Industrial Engineering, NJIT

Dr. Teh C. Ho, Committee Member — Date
Sr. Research Associate, ExxonMobil Co.

Dr. Anthony D. Rosato, Committee Member — Date
Professor of Mechanical & Industrial Engineering, NJIT

Dr. Ian S. Fischer, Committee Member — Date
Professor of Mechanical & Industrial Engineering, NJIT

BIOGRAPHICAL SKETCH

Author: Rajeshkumar Patel

Degree: Doctor of Philosophy

Date: May 2011

Undergraduate and Graduate Education:

- Doctor of Philosophy in Mechanical Engineering,
  New Jersey Institute of Technology, Newark, NJ, 2011
- Master of Engineering in Thermal Science,
  M. S. University, Vadodara, India, 2002
- Bachelor of Engineering in Mechanical Engineering,
  S. P. University, Vallabh Vidyanagar, India, 1999

Major: Mechanical Engineering

Presentations and Publications:

Rajesh Patel, Dawei Wang, Chao Zhu, Teh C. Ho, "Coupling of Hydrodynamics, Vaporization and Reaction with Liquid Spray Injection into a High-Temperature Gas-Solid Reactor", Proceedings of the ASME/JSME 2011 8th Thermal Engineering Joint Conference, March 13-17, 2011, Honolulu, Hawaii, USA.

Chao Zhu, You Jun, Rajesh Patel, Dawei Wang, Teh C. Ho "Interactions of Flow and Reaction in Fluid Catalytic Cracking Risers" AIChE Journal, 2011.

Jun You, Rajesh Patel, Dawei Wang, Chao Zhu, "Role of Inter-particle Collision on Solids Acceleration in Risers", Particuology, 8: 13-18, 2010.

Rajesh Patel, Dawei Wang, Chao Zhu, "Coupling of Hydrodynamics and Catalytic Reaction in Core Flow of Riser Reactors", AIChE Annual Meeting, Nashville, TN on November 10, 2009.

Jun You, Rajesh Patel, Dawei Wang, Chao Zhu, "Hydrodynamic Modeling of Gas-solids Riser Flows", AIChE Annual meeting: Philadelphia, PA on November 17, 2008.

This dissertation is dedicated to my beloved daughter, Kanishka; my wife, Seema and my parents for their love and support.

ACKNOWLEDGMENT

I would like to express my deepest appreciation to Dr. Chao Zhu, for his remarkable guidance, constant supervision, sincere friendship and moral support throughout my research. I would also like to express my sincere thanks to Dr. Teh C. Ho for his valuable guidance and for participating in my dissertation committee. I express my sincere thanks to Dr. Pushpendra Singh, Dr. Anthony D. Rosato and Dr. Ian S. Fischer for actively participating in my dissertation committee.

I would like to express my grateful to Department of Mechanical Engineering of New Jersey Institute of Technology, for giving me Teaching Assistantships during my study. I appreciate the friendship and cooperation of my colleagues Dr. Jun You, Dr. Dawei Wang, Mr. Raivat Patel and Mr. Pengfei He during my research in the Particulate Multiphase Flow Laboratory.

I would like to express my endless gratitude to my beloved parents, who have always supported my academic pursuits and helped me in every possible way. Last, but not least, I would like to express deep heated gratitude to my lovely wife, Seema and my adorable daughter, Kanishka for their love, support and encouragement throughout these years.

TABLE OF CONTENTS

TABLE OF CONTENTS
(Continued)

Chapter **Page**

TABLE OF CONTENTS
(Continued)

Chapter **Page**

TABLE OF CONTENTS
(Continued)

LIST OF TABLES

LIST OF FIGURES

LIST OF FIGURES
(Continued)

LIST OF FIGURES
(Continued)

LIST OF FIGURES
(Continued)

LIST OF SYMBOLS

Symbol	Meaning
A	area
C	molar concentration
C	specific heat
C_D	drag coefficient
CTO	catalyst to oil ratio
d	diameter
D	diameter
D	diffusion transport coefficient
E	activation energy
E	energy
F	force
f	friction coefficient
F_D	drag force
G_s	solid flux
h	convection heat transfer coefficient
k	reaction rate constant
L	latent heat of vaporization
l	perimeter
$\dot{m}$	mass flow rate
M	molecular weight
n	number density

N_u	Nusselt number
P	pressure
P_r	Prandtl number
r	radial position
R	radius
R	universal gas constant
Re	Reynolds number
St	Strokes number
T	temperature
u	velocity
u_{pt}	particle terminal velocity
v	velocity
Z	height

Greek letters

ρ	density
ε	emissivity
θ	injection angle
ξ	jet trajectory
γ	partition function
σ	Stefan Boltzmann constant
μ	viscosity of fluid
α	volume fraction

τ	wall shear stress
σ	wall stress

Subscript

0	center of riser
c	collision
c	convection heat transfer
D	diffusion
d	droplet
e	entrainment
f	fluid
g	gas
gs	gas-solid mixture
j	spray jet
n	power index
p	particle
R	reaction
Rad	radiation heat transfer
s	solid
T	turbulent
v	vapor
w	wall

CHAPTER 1

INTRODUCTION

1.1 Background

1.1.1 Riser Reactor Structure, Functions and Applications

Interaction between the gases and the solid particles is often necessary in many industries such as refinery, pharmaceutical, utility, mineral processes, polymerization process and many other applications. Risers are employed in most of the industrial applications, where the interaction between the gases and particles takes place. Depending upon the nature of the process, the particles may serve as catalyst for reacting gases i.e., catalytic cracking, particles may be chemically converted different compounds i.e., coal combustion process. The potential technologies available for carrying out the gas-solids interacting reactions are fixed beds or moving beds reactor where, the particles move slowly downward and interact with each other and also with reacting gas phase; Fluidized bed reactors in which the particles are suspended by gas or liquid which is introduced at the bottom of the bed through a distributor; Circulating Fluidized Bed (CFB) reactor system in which the solid particles are recirculated through vertical transport unit known as riser by the gases. Circulating fluidized bed riser reactors are employed in chemical, petroleum, pharmaceutical many other industrial applications to perform reactions in presence of particles.

The schematic diagram of industrial Circulating Fluidized Bed (CFB) gas-solid riser reactor is shown in Figure 1.1, which is consisting of a riser, separator, down-comer and feed systems for solids and for the fluid, which is shown in Figure 1.1. The riser is a tall vertical column in which hot particles are conveyed upward in presence of the lubricating gases. The reaction occurs in risers due to the interaction between the reacting gases and particles. The gas and solid particles are separated at the top of the reactor by cyclones and the particles are returned to the riser via down-comer. The feed is supplied from the bottom of the riser for reaction.

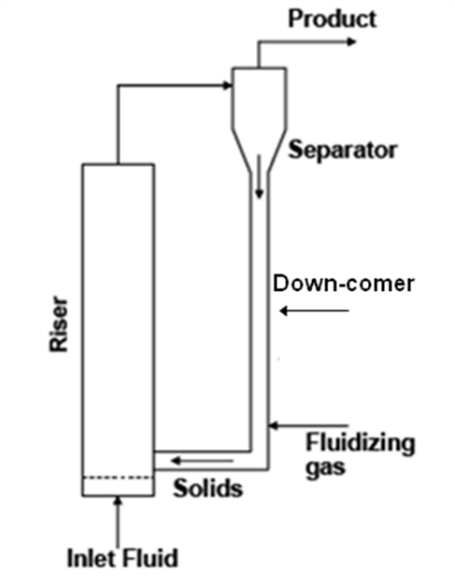

Figure 1.1 Schematic diagram of Circulating Fluidized Bed Riser.

1.1.2 Coupling between the Hydrodynamics and Reaction Kinetics in Riser Reactor

The performance of the riser reactors is strongly dependent on the interaction between the particles and the reactant which may be the gas or liquid. The efficiency of the reactions process in riser reactors is strongly dependent on the effective contact of particles with

fluid as majority of reactions takes place on the surface of the particles. The conversion of reactant in reaction process is strongly dependant on catalyst temperature (depending upon the nature of reaction process i.e., endothermic or exothermic process), local catalyst concentration and reaction time duration. All of these influencing factors are dictated by the local hydrodynamics that is highly heterogeneous due to wall effects and particle acceleration. Unfortunately, most riser reactor models ignore these non-uniform flow characteristics in riser. To predict correctly local reaction rates into the riser reactor, it is essential to develop mechanistic approach for coupling between the local flow hydrodynamics and local reaction kinetics.

1.1.3 Hydrodynamics of Multiphase Flows in Riser Reactors

The actual flow structure of gas-solids in a riser reactor is very complex with transient, multidimensional variations (axial, radial and azimuthally directions), multi-scaled phase interaction, and other complications from solid cohesions to electrostatic charges (He and Rudolph, 1995). The gas-solids flow structure in the CFB risers is unsteady and highly heterogeneous both in axial and in radial directions (Rautiainen *et al.*, 1999). The heterogeneity in gas-solids riser flow may be categorized into phase heterogeneity and hydrodynamic heterogeneity. The phase heterogeneity refers to the non-uniform distribution of a mixture of solids in forms of individual particles, clusters and agglomerates. The hydrodynamic heterogeneity refers to the non-uniform distribution of solids concentration and phase velocities in axial and radial directions. The axial non-uniformity is mainly due to the phase interactions and inter-particle collisions, which is represented by “S” shaped distribution of particle volume fraction and velocity as shown in Figures 1.2 (a) and 1.2 (b). An axial non-uniform gas-solids flow structure in riser

reactor is represented as a bottom dense phase regime, acceleration phase regime and top dilute phase regime which are shown in Figure 1.2 (c).

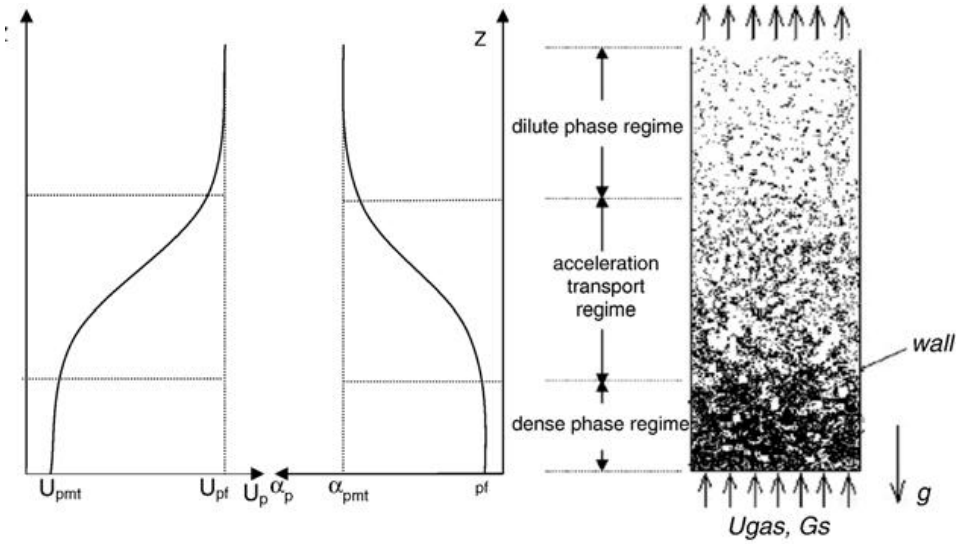

(a) Velocity (b) Solid Volume fraction (c) Flow Regimes

Figure 1.2 Flow regime and axial solid phase distribution. (Zhu & You 2007)

The radial non-uniform gas-solids flow structure in the riser reactor is consisting of rapid up flow of dilute suspension of solids in a core regime while slow downward flow of dense suspension of solids in wall regime (Herb *et al*., 1992; Brereton and Grace, 1993; Horio and Kuroki, 1994; Rhodes *et al*., 1998; Issangya *et al*., 2000), as shown in Figure 1.3 (a).

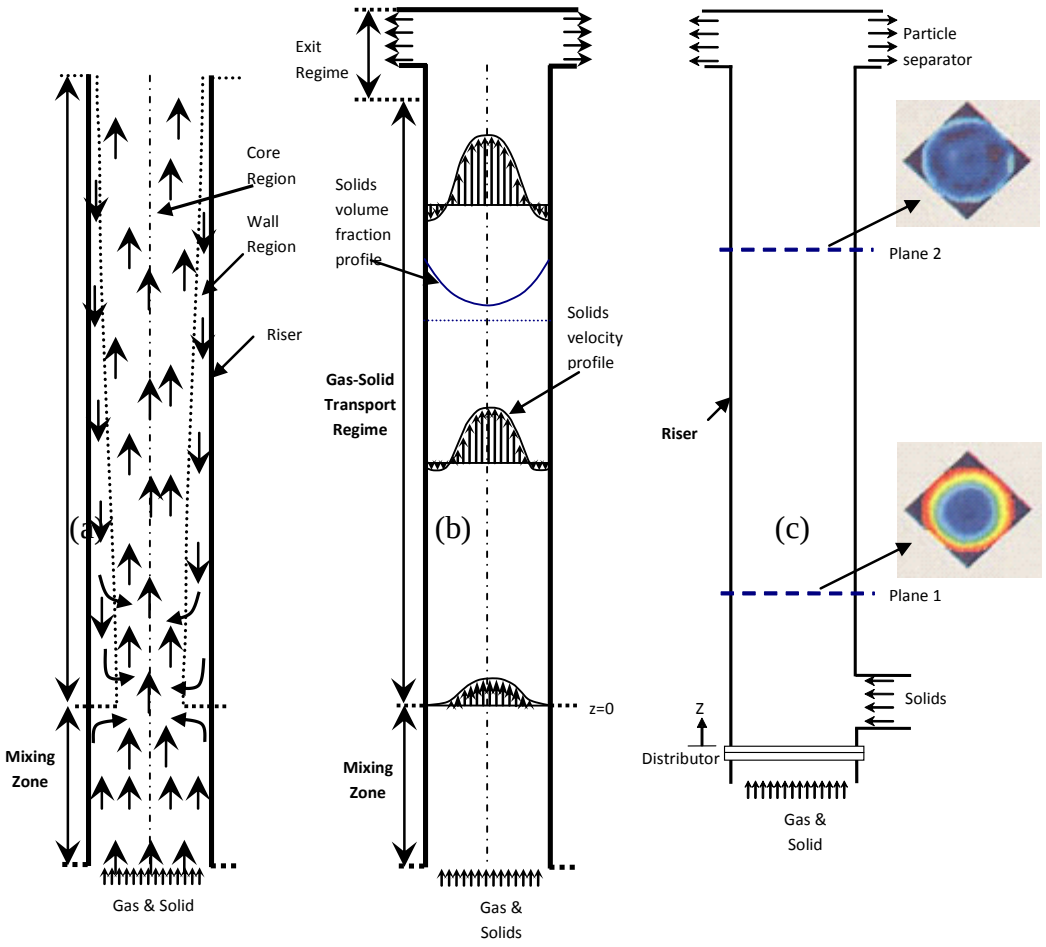

Figure 1.3 Heterogeneous radial phase distributions in riser: (a) core-annulus two-zone gas-solids transport; (b) continuous solids velocity distributions (from Wang, *et al*., 2008); (c) radial profiles of solids concentration (ECT measurements from Du *et al*., 2004).

Radial nonuniform distribution of gas and solid phase is mainly caused by the riser wall effects, turbulent and collisional diffusive mass transfer of gas and solids in radial direction. In a radially nonuniform gas-solids flow, there is an extensive back-mixing of solids from the wall regime. The ECT measurements (Du *et al*., 2004) of solid concentration also reveal core-annulus flow structure in riser reactor, which is shown in the Figure 1.3 (c). The non-uniform gas-solids flow structure with back-mixing of the particles in riser reactors may have significant impact on momentum transfer, heat and

mass transfer, which may have significant impact on the reaction characteristics in riser reactors. Riser reactors are employed in a variety of industrial applications because of the strong mixing between gas and solids that yields high heat and mass transfer rates, and relative ease of regenerating spent solid catalyst, among other reasons. To improve the existing facility and for development of new processes, better understanding of riser hydrodynamics and local coupling between hydrodynamics and reaction kinetics is critical to the development of riser reaction models.

1.1.4 Challenges and Unsolved Issues of Riser Flow Hydrodynamics

Despite of applications of riser reactors in many important industrial applications, from the modeling point of view, the understanding of riser flow hydrodynamics is still very poor. There are many important characteristics of riser flow hydrodynamic, which has been observed experimentally but never explained and modeled (quantified) due to very complex gas-solids flow structure and lake of suitable and accurate measurement techniques for dense flow regime of riser. The experimental studies on flow structure of particles in the riser reactor reveals an “S” shaped axial distribution of the solids concentration and velocity in the riser reactor. An axial non-uniform gas-solids flow structure in riser reactor is represented as a bottom dense phase regime, acceleration phase regime and top dilute phase regime. The flow regimes in the riser reactor mainly depend on the fluid-particles and particle-particle interactions. The inter-action between the fluid and particle is generally represented by the drag force while the particle-particle interaction is represented by the inter-particle collision force. The drag force on the single particle in unbounded flow has been derived by Stokes in early 60’s. In the solid laden riser flows, the particles are surrounded by neighboring particles and flow is no longer

unbound. The use of single particle drag for accelerating gas-solids flow is still questionable. There are many empirical correlations for the drag force available in literature, but all the correlations are derived from non-accelerating gas-solids flow. The inter-particle interactions play a vital role in deciding gas-solids flow structure. The formulation of inter-particle collision force is far from complete due to complex inter-particle collision mechanism. Modeling efforts to interpret the effect of inter-particle collisions on the solid flow distributions are mostly based on the kinetic theory of granular flow and two-fluid model with apparent viscosity in solid phase. In fluidization, most of the inter-particle collisions are off-center or oblique, in which the energy dissipation is not only dependant on the loss of normal component collision but also dependant on the loss due to sliding and micro-slip friction in tangential and rolling contacts. The application of kinetic theory of granular flows for riser reactor may lead to appreciable biased predictions in particle flow hydrodynamics, especially in energy or pressure distributions due to the assumptions of friction free and center-to-center particle collision in vacuum. Which modeling approach or the semi-empirical formulation of the collision force should be used for the application of the riser reactor, which can reasonably predict the axial pressure gradient and solids volume fraction distribution in riser reactor?

For most riser reactors which are operating in the fast fluidization regime, the gas-solids flow structure is nonuniform in radial direction with back-mixing of the particles from the wall regime. The riser wall not only leads to the non-uniform radial profiles of phase transport but also causes a back flow of spent particles. Such lateral mixing and recirculation of the particles increases the residence time of the particles in the riser

reactors, which is desirable for some industrial application like combustion while it is undesirable for fluid catalytic cracking process due to deactivation of the catalyst which may affect the in product yield. The only operating parameters know for typical riser reactors are the inlet conditions (i.e., flux, temperature, velocity, pressure etc.) and outlet conditions. Hence, the fundamental understanding of the mechanism for lateral mixing and recirculation of the particles is very important to maximize the product. From the modeling point of view it is very important to determine what will be the back-mixing of the particles and its residence time for given operating conditions of the riser reactor?

The radial heterogeneous gas-solids flow structure in gas-solids riser is known as core-annulus flow structure. The radial heterogeneity in transport is resulted from a combined effect of flow turbulence, phase diffusion and wall boundary. Most of the hydrodynamics models for gas-solids riser flow fall into two categories; uniform radial distribution of phases (one-dimensional uniform flow model) or core-annulus two-zone radial phase distribution with back-mixing of particles. The former modeling approach fails to account for the back flow and wall boundary effect; whereas the later modeling approach mostly relies on artificial demarcation of the two zones and limited empirical correlations for back flow. In addition, there is no reliable hydrodynamics model for the dense-phase and acceleration regime where most catalytic reactions occur. For realistic riser reactor models, the determination of core-annulus boundary (distribution of core and wall area) and back-mixing of particles from mechanistic models is crutial.

1.1.5 Challenges and Unsolved Issues of Coupling between Flow Hydrodynamics and Reaction Kinetics in FCC reactors

The efficiency of the reactions process in petroleum refining process is strongly dependent on the effective contact of catalyst with feed oil as majority of cracking takes place on the active sites inside the pores of catalyst. Vacuum gas oils (VGO) are typical feed-stocks whose conversion depends on catalyst temperature, local catalyst-to-oil ratio (CTO), spent-fresh catalyst composition, and reaction time duration. All of these influencing factors are dictated by the local hydrodynamics that is highly heterogeneous due to wall effects and catalysts acceleration.

From a mechanistic point of view, the hydrodynamics of catalyst particles should play a nontrivial role in determining FCC conversion and yield structure. The coupling between flow hydrodynamics and reaction kinetics is must from the process modeling point of view. There are challenges and unsolved issues related to coupling between flow hydrodynamics and reaction kinetics, which are listed below.

Local Catalyst-to-Oil Ratio (rather than overall CTO): The rate of cracking reactions depends strongly on the local CTO. Due to vaporization and cracking, the hydrocarbon vapor expands, thus drastically increasing the velocities of vapor and catalysts and the consequent decrease in the catalyst concentration. Hence, the CTO decreases significantly from the bottom (dense phase) to the top (dilute phase) of riser. Even the CTO varies considerably with radial locations due to wall effect. Even the direction catalyst flow is different in the wall and center regime of the reactor. Unfortunately, most riser reactor models ignore these non-uniform flow characteristics in riser. As a result, a constant, overall CTO is used throughout the riser and flow is treated without proper wall effects.

Reaction Temperature: Due to the endothermic reaction and different thermal capacities of vapor and catalysts, the temperature of reacting vapors can be significantly lower than that of catalysts. Since catalytic reactions predominantly occur inside the catalyst pores, the heat of reaction is supplied by regenerated catalyst. So, the temperature that drives the reaction should be the catalyst temperature rather than equilibrium temperature. So far most reaction models simplified the matters by assuming thermal equilibrium between the catalyst and hydrocarbon feed, which was used for reaction temperature. So what would be the temperature for reaction, a catalyst or hydrocarbon feed or hybrid?

Spent-Fresh Catalyst Composition: The heterogeneous structure (axial as well as radial non-uniformity) of solids flow in the riser has been well recognized. In most of the annulus (wall) region, deactivated catalysts move downwards which cause the back flow or back-mixing of deactivated catalyst from wall to core regime. The reaction rates in the presence of deactivated catalysts are completely different from the fresh catalyst. These deactivated catalysts not only affect the hydrodynamics of fresh/deactivating catalysts and energy balance but also contribute to the cracking with a lower activity. Most modeling approaches in the literature so far did not consider back-mixing of deactivated catalyst and its impact on the final product yield.

1.1.6 Inlet Conditions for Riser Reactor Models from Spray Zone Regime

In FCC process, the liquid hydrocarbon feed (VGO) is injected into the dense cross-flow of hot gas-solids flow through the multiple feed injection nozzles, which is located below the riser main body. There have been no systematic for hydrodynamics of three phase

flows and hydrodynamics coupled reactions in a spray zone regime of FCC reactors. This is hardly surprising due to the complexity of the problem, which involves transfers of momentum, heat and mass transfer in a three-phase interacting system that is coupled with catalyst-influenced cracking reaction. Due to the lake of information on the reaction in the feed injection regime, most published literature model for FCC riser reactor are based on the assumption of instantaneous vaporization or no catalytic reaction in the feed injection regime. The understating of three phase interaction, heat transfer, vaporization and reaction in the this regime is very important to determine the actual performance of the riser reactor by providing true input boundary conditions for existing riser reactor model.

1.2 Dissertation Objectives and Structure

For optimal design and development of new/existing processes in riser reactor, it is essential to gain a predictive understanding of heterogeneous gas-solids flow structure, the local coupling of hydrodynamics and reaction kinetics, and the effect of the particle back-mixing and recirculation on the performance of the riser reactor.

In this dissertation, Fluid Catalytic Cracking (FCC) process has been taken as an example of riser reactors to address the key issues related to riser reactor, such as heterogeneous gas-solids flow structure, the local coupling of hydrodynamics and reaction kinetics, and the effect of the particle back-mixing and recirculation on the performance of the riser reactor, which have received scant attention at best and have never been systematically investigated. The FCC process is designed to crack a high-

boiling hydrocarbon stream, such as vacuum gas oil (VGO) into more valuable lighter hydrocarbons; the schematic diagram of FCC riser reactor is given in Figure 1.4.

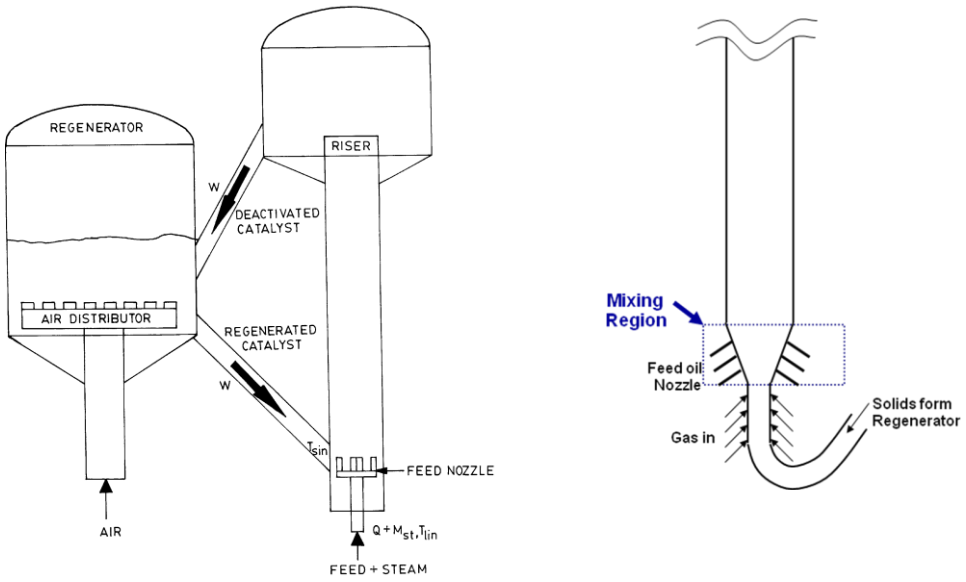

Figure 1.4 (a) Simplified schematic of commercial FCC unit (b) Feed injection regime of riser reactor with J-bend inlet.

The interaction mechanism between the gases-droplet-solid phases in the FCC riser reactor is schematically presented in Figure 1.5. In the FCC riser, the hydrocarbon feed in form of droplet is supplied at the bottom of the riser through the feed injection nozzle, where it comes in contact with hot regenerated catalyst coming from the regenerator, which is shown in Figure 1.4. The objective of this dissertation is to address some important issues related to hydrodynamics and reactions in solid laden riser reactors, which have not been studied systematically so far. The major focused issues are; the impact of non-uniform gas-solids flow structure on the reaction characteristics in the riser reactor; the impact of pre-reactions in the feed injection regime on the performance of riser reactors. To be more specific, the objectives of the dissertation can be further

break down into four parts, which are 1) Hydrodynamic modeling of axial distribution of uniform flow transport properties of gas-solids flow in risers, with constitutive modeling of collision force; 2) Hydrodynamic modeling of axial and radial nonuniform flow structure in riser reactor with back-mixing of particles; 3) Coupling of nonuniform flow hydrodynamics with reaction kinetics and; 4) Modeling of flow hydrodynamics coupled reaction characteristics in entrance regime of the reactor.

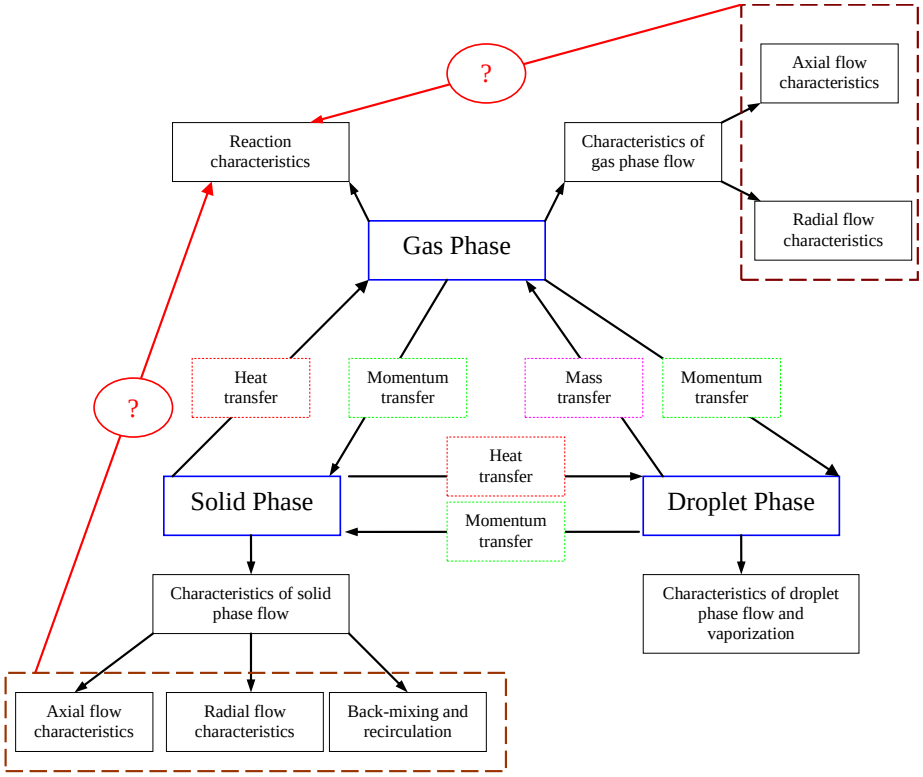

Figure 1.5 Interaction between three phase flow (droplet-gas-solids) phases in riser reactor.

In Chapter 3, one-dimensional uniform flow model for gas-solids transport in riser presented. The impact of pressure gradient along the riser on the particle transport is built in one-dimensional model by introduction of pressure gradient partition in solid phase momentum equation. The semi-empirical correlation for the drag force on the particle in

presence of surrounding particles is formulated from sedimentation experiment data of Richardson and Zaki, 1954. The constitutive correlation for inter-particle collision force is also proposed in this chapter. The one-dimensional uniform model with proposed new physics and constitutive relations is validated by comparing model predictions of axial phase distribution with experiment data. The uniform flow model prediction were reasonably matches with the experiment data of axial distribution of solid volume fraction and pressure gradient with proposed formulations of collision force.

In Chapter 4, a predictive continuous modeling approach for axial and radial non-uniform gas-solids flow structure is proposed. The purpose of such modeling is to identify the fresh and spent catalyst and boundary for the core-annulus flow regime of riser reactor by modeling of radial transport of the gas-solids phase in the riser reactor. The proposed modeling approach is based on the one dimensional and continuous modeling of radial hydrodynamic characteristics of flow, which was initially proposed by (Wang 2010 PhD Thesis). The radial nonuniform gas-solids flow structure is approximated by 3^{rd} order polynomial distribution. The mechanism of the radial transport of both gas and solid phase has been discussed and modeled. The proposed continuous modeling approach for multiphase flow in risers can simultaneous predicts both radial and axial direction distribution of gas-solids phase transport properties. The motions of two solid “species," namely, the downward flow of particles in the wall regime and upward flow of particles in the core regime with back-mixing of particles can be identified from the model predictions. The boundary for core-wall regimes was also calculated from proposed model predictions.

In Chapter 5, a mechanistic model has been proposed to predict the reaction characteristics both in core and wall regime of the riser reactor. The local flow hydrodynamics and reaction kinetics has been coupled to take into account the effects of local flow hydrodynamics on the reaction rates (e.g., hydrocarbon vapor and deactivated/deactivating catalysts concentrations and corresponding temperatures). The amount of back-mixing of deactivated/deactivation catalyst and the core-wall regime has been modeled from the hydrodynamic model proposed in Chapter 4. The proposed model is low cost tool for determining the effect of radial non-uniform flow and solid back-mixing on the final product of the FCC reactor.

In Chapter 6, the hydrodynamics and reaction characteristics in the entrance regime of the FCC reactor has been modeled. A mechanistic model has been proposed that gives a quantitative understanding of the interplay of three phase flow (gas-liquid-solid) hydrodynamics, heat/mass transfer, vaporization and cracking reactions along the spray jet. The cross-section averaged approach then has been used to find the average hydrodynamic and reaction characteristics at the end of the entrance regime in case of multiple spray jet injections. The proposed model can reasonably answer the import question related to feed injection regime such as; 1) the length of the feed injection regime 2) Conversion three phase flow (gas-droplet-solid) in feed injection regime into the two-phase flow (gas-solid) in the main body of the riser reactor 3) The hydrodynamic characteristics and reaction characteristics of phases at the end of the feed injection regime.

CHAPTER 2

LITERATURE SURVEY

2.1 Introduction of Area of Literature Survey

Fluid Catalytic cracking (FCC) is the most important and profitable process in petroleum refining industry. To improve the existing facilities and new process development, there is need to understand the complex gas-solids flow hydrodynamics, unknown multiple reactions coupled with heat and mass transfer and vaporization of feed. Many research efforts have been made on feed atomization and vaporization, gas-sold flow hydrodynamics, cracking kinetics, inter-phase heat and mass transfer, and catalyst deactivation. The inter-action between gas-solid-droplet phases in terms of momentum transfer, heat and mass transfer in FCC riser reactors is shown in Figure 2.1. Following is the summary of the key literatures related to flow hydrodynamics and reaction kinetics in riser reactor. The literature review presented in this section is focused on 1) experiment observation and modeling methods for non-uniform gas-solids flow structure in the riser reactor 2) modeling of the flow hydrodynamics and reaction kinetics characteristics along the riser reactor and 3) the hydrodynamic of three phase flow and reaction in the feed injection regime (entrance regime) of the riser reactor.

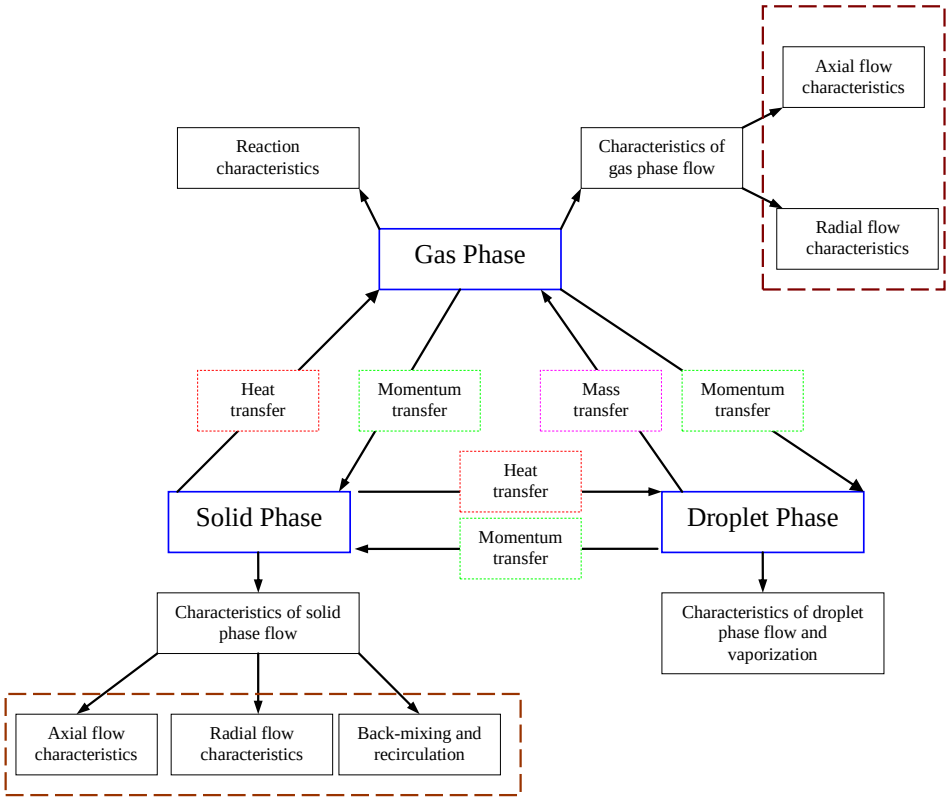

Figure 2.1 Schematic representation of area of literature review for FCC riser reactor.

2.2 Non-Uniform Hydrodynamics of Gas-solids Riser flows (Cold Flow)

The gas-solids flow structure in the CFB riser is heterogeneous both in axial and in radial directions and unsteady (Rautiainen *et al.*, 1999). The heterogeneity may be categorized into phase heterogeneity and hydrodynamic heterogeneity. The phase heterogeneity refers to the non-uniform distribution of a mixture of solids in forms of individual particles, clusters and agglomerates. The hydrodynamic heterogeneity refers to the non-uniform distribution of solids concentration and phase velocities, both in axial and radial directions. The axial heterogeneity of gas-solids flow in riser in general can be represented as a dense region at the bottom of the riser, a dilute regime at the top of the

riser and a acceleration region which is also known as transition region between them (Li and Kwauk, 1980; Bai *et al*., 1992; Rhodes *et al*., 1998; Pärssinen and Zhu, 2001; Yan and Zhu, 2004). The experiment measurements for radial phase distribution shows that, the radial non-uniformity of gas-solids flow structure can be represented as a dilute core region where, there is a up-flow of dilute suspension of particles, which is surrounded by dense annulus (wall) region with particles down-flow along the wall (Weinstein *et al*., 1984; Bader *et al*., 1988; Hartge *et al*., 1988; Zhang *et al*., 1991; Herb *et al*., 1992; Brereton and Grace, 1993; Nieuwland *et al*., 1996). According to Harris and Davidson (1994), the modeling of gas-solids hydrodynamics in risers can be broadly categories as: (i) the models that predict the axial variation of the solid suspension density, but not the radial variation; (ii) the models that predict the radial variation and the high average slip velocities by assuming two or more regions, such as core-annulus or clustering annulus flow models; and (iii) the models which are based on the numerical modeling of the conservation equations for mass, momentum, and energy for gas and solid phases.

The complete modeling of gas-solids flow in CFB is rather difficult. The simplest modeling approach is to assume uniform flow in radial direction i.e., modeling of axial non-uniformity of gas-solids riser flows with assumption of cross-sectioned averaged flow properties. There are many published models for one-dimensional, cross-section averaged axial distribution of gas-solids transport properties for cold flow risers (Louge *et al*., 1991; Bussing and Reh, 2001). Most literature models have similar modeling approach in describing the main governing equations for mass and momentum conservation for gas-solids phase; the significant differences are found in the simplifying

assumptions, limitations in applications for riser flow regimes and sub-models for phase interactions.

Significant research efforts have been made for modeling of radial distribution of gas and solid phase in riser, but most published models used experimental measurements to propose a correlation for radial phase profiles. The applicability of proposed correlations is limited by the operating range and geometry of CFB risers. For example, a core-annulus model proposed by Capes and Nakamuka, (1977), to account for their experiment observations. Shimizu *et al*., 1987 who proposed a two-region model for very dilute fluidized beds, which can not be applied to the bottom dense regime of the riser. A modeling of two-regime (core-annulus) was first presented by Bolton and Davidson, (1988); Bolton and Davidson, (1994), assuming up-flow of the dilute suspension of particles in the center of riser, while down flow dense suspension of the particles adjacent to the riser wall. For modeling of radial transport of gas and solids Bolton and Davidson, (1988), they only considered the radial mass transfer of the solid due to the turbulent diffusion and ignored the diffusive mass transfer of the particles and radial transport of gas phase. The core and wall regimes were predefined as fraction of riser area used by core and annulus regime. The above literature review shows that, most of the proposed models for two-zone (core-annulus) models are over simplified by pre-defining the core-annulus flow regimes, the radial transport of gas-solids phase are not truly based on the governing mechanisms but built in the models by defining the transport coefficients. Above all, published models are validated by comparing model predictions of the radial non-uniform distribution of the phases, transfer coefficient, and annulus thickness but

never validate for axial distribution of the phases i.e., axial distribution of the solid volume fraction, pressure gradient in the axial direction and particle velocity.

The radial nonuniform distribution of gas-solids results in severe back-mixing and internal recirculation of solids in risers. In a FCC riser reactor, internal circulation of deactivating catalyst particles affects the reactor performance by reducing the quality of catalyst. For back-mixing of catalyst, Wirth (1991) developed a model based the momentum transfer arising from collisions between discrete particles and clusters dispersed throughout the riser cross-section. The model for radial particle transport was based on radial momentum transfer due to inter-particle collision, but they neglect the radial particle transport due to the turbulence fluctuation induced radial transport of the particles. Later on (Pugsley and Berruti 1995) modified the model of Wirth (1991) by considering the solids flow in core and annulus regions and calculated the core-to-annulus solids interchange coefficient. Senior and Brereton (1992) showed that a value of 0.2 m/s for core-to-annulus solid interchange coefficient gave the best fit of their experimental data of axial suspension density profile. The lateral mixing or the back-mixing of the catalyst was determined from mass and momentum balance from pre-defined core-annulus regimes for risers, and the lateral mixing coefficient was adjusted to fit the experiment data. The radial transport of the particle is mainly governed by the turbulence fluctuation of particle and inter-particle collision induced diffusion of the particles. Hence, radial transport and recirculation of the gas and particles in riser flow should be governed by mechanism rather than constant transport coefficient.

2.3 Flow Hydrodynamics Coupled Reaction Kinetics of Riser Reactor

Fluid Catalytic Cracking (FCC) units are used widely in refineries across the world to produce higher value gasoline from heavy oil. The effect of the complex multiphase hydrodynamics in an FCC riser has been pointed out by Derouin *et al.*, (1997) who conducted in depth measurements of catalyst distribution and product concentration in the unit. Recently, Zhu *et al.*, (2011) has proposed modeling approach for coupling between local flow-hydrodynamics with reaction kinetics for FCC riser reactor. Literatures have been documented for modeling of hydrodynamics and reaction kinetics in FCC unit. The first attempt to model the hydrodynamics and reactions in an FCC unit was described by Theologos and Markatos (1993). They used basic conservation equations for the gas and solids flow and a simple 3-lumps model to simulate the cracking reactions. Many other models are also found in literature for reaction in FCC unit (e.g., Arandes and Lasa, 1992; Arbel *et al*., 1995; Han and Chung, 2001; Ali and Rohani, 1997; Bollas, 2007) describes the riser reactions in reactors by one-dimensional governing equations for mass, energy and chemical species balances. Unfortunately most reaction model for riser reactors, ignored the coupling between the hydrodynamics and reaction kinetics, also simplified matters by using cross-sectional averaged flow and ignored the wall effect and solids back-mixing. In addition, most of them under predicted the effect of inter-particle collisions on the dense phase transport of solids. Most modeling efforts discussed above assumes thermal equilibrium between the hydrocarbon feed and the catalyst, which is not the case for real FCC process.

With the advancement in the CFD techniques and computing capacity, CFD modeling had been used for the riser reactor for a full-scale numerical simulation of gas–

solids riser flows with reaction. For FCC riser modeling, most works used Eulerian–Eulerian approach where the dispersed solid particles are treated as interpenetrating continuum (e.g., Theologos and Markatos, 1993; Benyahia *et al*., 2003; Zimmermann and Taghipour, 2005; Lan *et al.,* 2009). Few works have used Eulerian–Lagrangian approach (e.g., Nayak *et al*., 2005; Wu *et al.*, 2010). In Eulerian–Lagrangian approach, the motion of solid catalyst particles is modeled in the Lagrangian framework and the motion of continuous phase is modeled in the Eulerian framework. The hydrodynamic characteristics can be significantly influence by the inter-particle collision, for which the kinetic theory of granular flows has been introduced to account for inter-particle collisions (e.g., Mathesian *et al.,* 2000; Neri and Gidaspow, 2000; Van Wachem *et al*., 2001). The restitution coefficient represents the elasticity of particle collisions and ranges from fully inelastic (e = 0) to fully elastic (e =1). The proper selection of restitution coefficient is important for correct prediction of hydrodynamic characteristics. However, these models may be inadequate for simulating complex gas–solid flows at high solids flux Ranade (2002) and for handling inter-particle collisions and other interactions in the dense-phase and transition/acceleration regimes of solids transport (e.g., You *et al*., 2008; You *et al*., 2010; Wang *et al*., 2010), in addition to a significantly increased requirement on computational resources.

Describing the kinetic mechanism for the cracking of petroleum fractions is difficult because of the presence of thousands of unknown components in a petroleum fraction. However, the important chemical reactions occurring during catalytic cracking are given by Gates *et al.,* (1979). The simplest kinetic model Weekman, (1968) has 3 lumps: unconverted gas oil, gasoline, and light gas plus coke. An improved yet simple 4-

lump kinetic model (e.g., Yen *et al.*, 1987; Lee *et al*., 1989) considers coke as an independent lump rather combined with light gas, which was used by several other investigators (e.g., Farag *et al.*, 1993; Zheng, 1994; Gianetto *et al*., 1994; Ali and Rohani, 1997; Blasetti *et al.*, 1997; Gupta and Rao, 2001; Han and Chung, 2001a; Abul Hamayel *et al*., 2002; Jia *et al*., 2003; Nayak *et al.*, 2005; Hernandez-Barajas *et al.*, 2009). This simple lumping approach for kinetic modeling was further extended by various researchers by increasing the number of lumps in their models. More detailed lumped models have also been developed (e.g., 5-lump by Corella *et al.*, 1991; and Larocca *et al.*, 1990; 10-lump by Jacob *et al.*, 1976) in order to improve the predictability of the effects of feedstock composition.

2.4 Reaction in Entrance Regime of Riser Reactor

In the FCC unit, the liquid hydrocarbon feed (VGO) is injected into the dense feed injection zone at bottom of the riser reactor in the form of spray through the multiple injection nozzles. The understanding of flow gas-liquid-solid flow structure, heat transfer, vaporization and reaction in this regime is very important because the reaction starts as soon as the liquid feed vaporizes. A significant portion of the cracking and catalyst deactivation occurs in the feed injection zone where the temperature is the highest. With today's high-activity catalysts, the contact time in the FCC riser has been shortened significantly over the years. Thus, the feed injection zone plays an increasingly important role in determining the FCC riser performance. Considerable effort has been devoted for better understanding of hydrodynamics and reaction in feed injection into FCC reactor by conducting experiments, theoretical modeling, and numerical simulation of process.

Extensive studies on the effects of particle loading on the gas entrainment of free jets are reported (e.g., Field, 1963; Ricou and Spalding, 1961; Subramanian and Ganesh, 1982; Subramanian and Ganesh, 1984; Subramanian and Venkatram, 1985). Later on, extensive experimental studies on multiphase jet injection into the gas-solids flows have been reported by Edelman *et al.*, (1971); Chen *et al.*, (1994); Wu *et al*., (1998). Ariyapadi *et al.*, (2004) measured the penetration length of the horizontal gas–liquid jets into the gas–solid fluidized bed for different nozzle geometries. By analyzing the test results, they proposed an analytical expression to evaluate jet penetration length. Experimental studies on vaporizing liquid jets in gas-solids flows were conducted in the late 90's by Skouby, (1998); Zhu *et al*., (2000) followed up by modeling studies by Zhu *et al*., (2001); Zhu *et al*.,(2002). Later on, Zhu *et al*., (2000) investigated the liquid nitrogen spray jets in dilute gas-solids flows to illustrate the effect of solid concentration on microstructures of the evaporative liquid jets, especially the jet evaporation length. The study indicated that the jet evaporation length significantly decreased with an increase in the solid concentration. A parametric model was developed by Zhu *et al.*, (2002) for the study of mixing characteristics of an evaporative liquid jet in gas-solids suspension flows. Fan *et al*., (2001) studied the fundamental characteristics of evaporative liquid jets in gas-liquid-solid systems for both dilute and dense solid phase conditions. Studies on parametric models of jet flows have also been actively pursued for both single-phase jets in early years and multi-phase spray jet recently. Extensive studies and reviews on the hydrodynamic characteristics of single-phase jets were summarized as early as 1960's (e.g., Abramovich 1963; Platten, and Keffer, 1968; Campbell and Schetz, 1973; Rajaratnam 1976). The characteristics of single-phase jet are then extended to multiphase

jet by similarity laws of the jet (e.g., Forney and Kwon, 1976; D'Souza *et al*., 1990; Li and Karagozian, 1992; Han and Chung, 1992-a; Han, and Chung, 1992-b). Experimental studies on evaporating liquid jets in gas–solid flows are reported since late 1990s (e.g., Skouby, 1998; Zhu, 2000; Chang *et al*., 2001) and followed up by modeling studies by Zhu *et al*., (2001); Zhu *et al*., (2002); Qureshi and Zhu, (2006). Studies on parametric models of jet flows have also been actively pursued for both single-phase jets in early years and multi-phase spray jet recently. Parametric modeling of non-reacting jet flows into gas-solids flows have also been reported for both single-phase (e.g., Platten and Keffer, 1968; Campbell and Schetz, 1973) and multi-phase spray jets (e.g., Li and Karagozian, 1992; Han and Chung, 1992). The latter studies invoked similarity laws for jet flow.

In recent years, a tremendous effort has been made to develop simulation models, incorporating FCC reaction kinetics and complex hydrodynamics in a single model. Numerical simulations of evaporative spray jets in concurrent gas-solids pipe flows and gas-solids cross-flows with Eulerian–Lagrangian approach were conducted by Wang *et al*., (2004); Qureshi and Zhu (2006). Theologos and Markatos (1993) had developed a CFD model to assess changes in operating parameters on FCC riser reactions, including the impact of feed-injector geometry on hydrodynamics, particularly near the bottom of the reactor. Theologos *et al*., (1999) incorporated an atomization modeling scheme into their CFD model to evaluate atomization effects on feedstock vaporization rates, cracking reactions initiation, reactor selectivity and overall reactor performance. Gupta and Rao (2003) developed a three-phase model for predicting conversions and yield patterns in a FCC riser taking into account the effect of feed atomization. A three-dimensional, three-

phase reacting flow computational fluid dynamics code, ICRKFLO, was developed in Argonne National Laboratory, and it was used to study the interactions of multiphase hydrodynamics, droplet evaporation, and cracking reactions in FCC riser reactors (Chang *et al*., 2001; Chang and Zhou, 2003). There are many other attempts to simulate entire FCC unit (e.g., Arbel *et al*., 1995; Gupta and Sharma, 1995; Ali *et al.*, 1997; Malay *et al*., 1999; Arandes *et al*., 2000; Han and Chung, 2001a,b) but these simulations were based on the assumption of instantaneous vaporization of feed at riser entry.

The brief literature review indicates that previous theoretical, experimental and CFD simulation studies on injection of a vaporizing liquid jet into gas-solids flow are most relevant to the present work. There have been no published studies on the reaction-hydrodynamics coupling in a vaporizing liquid jet penetrating into a gas-solids flow. This is hardly surprising given the complexity of the problem, which involves transfers of momentum, heat and mass transfer in a three-phase interacting system that is coupled with catalyst-influenced cracking reaction. Due to the lack of information on the extent of cracking reactions in the feed injection zone, the reaction model presented in previous section of literature survey, neglect this zone and assume instantaneous vaporization and thermal equilibrium between catalyst and hydro-carbon feed (Zhu *et al*., 2010). However, the validity of this assumption has not been established. The reactions in the feed injection zone are believed to be significant and should not be ignored without justification.

CHAPTER 3

MODELING OF AXIAL DISTRIBUTION OF UNIFORM FLOW PROPERTIES OF GAS-SOLID FLOW IN RISER

3.1 Problem Statement and Challenges

Gas-solids transport has found widespread applications in a variety of industrial processes such as fluid catalytic cracking, pulverized solid fuel combustion, coal gasification, and pneumatic conveying. The hydrodynamics of gas-solids flow in risers have become major concern of interest to provide a general understanding for the design and operation principles, and in turn, the productivity. In this chapter, a one-dimensional, uniform flow model for gas-solids transport in risers has been presented. An important physics governing the particle transport is introduced in solid momentum equation. The pressure gradient along the riser height provides an additional force to the particle transport, which has been introduced into the particle momentum equations by partition of pressure gradient for solids phase. The empirical correlation for the drag force on the particle in the presence of surrounding particles has been derived from the experiment data of Richardson & Zaki, 1954 for sedimentation. In addition, a constitutive correlation for the inter-particle correlation force for particle transport is also proposed.

Vertical gas-solids flows in risers are known to be inherently heterogeneous and unsteady (Rautiainen *et al.*, 1999). The heterogeneity in gas-solids flow may be categorized into the phase heterogeneity and hydrodynamic heterogeneity. The phase heterogeneity refers to the nonuniform distribution of solids in the form of individual particles, clusters and agglomerates.

The hydrodynamic heterogeneity refers to the nonuniform distribution of solids concentration and phase velocities, both in axial and radial directions (Gidaspow, 1994). This chapter is focused only on the axial nonuniform gas-solids flow, while ignored any phase heterogeneity in gas-solids transport system. The axial non-uniformity of gas-solids flow is mainly due to the phase acceleration and inter-particle collision force. The pressure drop in a riser, from hydrodynamic energy conservation point of view, can be interpreted as the sum of the changes in potential energy and kinetic energy of solids and gas phase, dissipation of kinetic energy due to interfacial friction, and energy dissipation due to inter-particle collision (He and Rudolph, 1996). In particular, the inter-particle collision plays an important role on the particle dynamics as well as the evolution of gas-solids flow. The traditional approach of equating the static pressure drop to the bulk weight in riser section overlook the effects of solids acceleration and inter particle collisions, which leads to overestimation of local solids holdup (Zhu and You, 2007). The overestimation of solids holdup is very significant in the acceleration and dense phase transport regions.

The detailed modeling of axial and radial nonuniform gas-solids flow in risers is rather difficult. Therefore, it is necessary to develop simplified modeling approaches, which can describe the gas–solids flow structure with reasonable accuracy. The simplest modeling approach is to ignore radial non-uniformity of gas-solids flow structure and to simulate only the axial nonuniform distribution of phase transport properties. Most published literatures models have similar modeling approach for describing the main governing equations for axial nonuniform distribution phase distribution; the significant differences are found in the sub-models for phase interactions. In vertical gas-solids

transport risers there exists a pressure gradient along the height. The pressure gradient along the riser height provides an additional force on the particle phase, which has significant influence on the solid phase distribution, should be taken into account in the solid phase momentum equation in terms of fraction of pressure gradient for solid phase transport. The pressure gradient in the dense phase regime is very high, which may also affect the inter-particle collision force in this regime. To take in to account the effect of pressure gradient on the particles transport, the pressure gradient is partitioned for the gas and particle phase and solid momentum equation is modified by pressure gradient force. Most of the models in the literature do not completely take into account the performance of the bottom zone of the riser, where the inter particle collisions and solid acceleration plays an important role in axial distribution of solid phase. The kinetic theory of granular flow has been used so far to take into account the inter-particle collision in the bottom of the riser. But the kinetic theory of granular is not sufficient to account for inter particle collisions due to the assumptions of center to center collisions of particle in vacuum (Zhu and You 2007). Recently a semi-empirical correlation for the inter-particle collision force has been proposed for the riser transport system to take into account the energy dissipation by inter-particle collision in the dense and acceleration phase regime (Jun *et al*., 2010; Wang *et al*., 2010). In their studies (Jun *et al*., 2010; Wang *et al*., 2010), ignored the impact of pressure gradient in the riser on the solid phase transport. The inter-particle collision force in presence of pressure gradient is considerable different and has same order of magnitude as drag force. In this dissertation, a constitutive correlation is proposed for inter-particle collision force. The interfacial drag force per unit volume in a gas-solids mixture plays a significant role in the momentum balance for the gas and

solids phase. An accurate description for this force is important in order to evaluate the flow hydrodynamics. An empirical expression for drag force in presence of neighboring particles is derived from sedimentation and fluidization data for liquid-solid systems.

In this chapter, a simplified one zone, one-dimensional cross-sectioned averaged uniform flow model with the following physics and constitutive correlation has been presented. 1) the effect of pressure gradient on the phase transport is taken into account by partition pressure gradient for gas and solid phase momentum equation 2) A constitutive equation for inter-particle collision force is proposed for solid phase momentum balance, which has the same order of magnitude of drag force in dense and acceleration phase regime, while it approaches zero in the dilute regime of the riser. 3) an empirical correlation for the drag force on a particle in swamp of neighbor particles provided for to predict the hydrodynamic characteristics in the dense and acceleration zone of the riser.

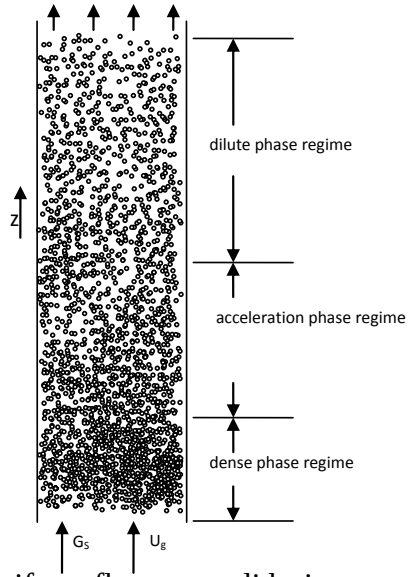

Figure 3.1 Flow regime of uniform flow gas-solid riser.

The detailed description of drag force and collision force is discussed in details in later section. The proposed model reasonably predicts axial distribution of gas-solids transport properties in dense phase, acceleration phase and top dilute phase regime. The proposed model is validated against published experimental data of axial pressure drop and solid volume fraction profile. With the inclusion of pressure gradient force and semi-empirical correlation for collision force in the momentum equation, the proposed model predictions reasonably matches the experimental data of pressure drop and solid volume fraction along the riser, specifically in dense and acceleration phase regime.

3.2 Modeling Approach

Consider a steady, isothermal gas-solids flow in riser as shown in Figure 3.1. The following assumptions are made to simplify the problem. The effect of solid deceleration of solids at the top of the riser and the intensive turbulent mixing regime at the inlet of the riser are ignored. All the properties of the gas and solid phase are assumed to be cross-sectioned averaged i.e., uniform flow properties over the cross-section of the riser. The wall frictions between gas and solids phases are also ignored. The gas phase follows the ideal gas law.

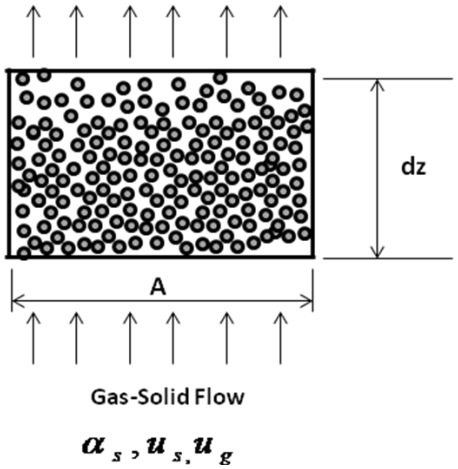

Figure 3.2 Control volume for unifrom flow model.

With the above simplifying assumptions, the mass and momentum conservations equation for gas and solid phase over a control volume as shown in Figure 3.2 can be written in terms of cross-section averaged phase properties. The mass conservation equation for gas and solid phase can be written as;

Gas Phase:

$$\frac{d\left(\alpha_g \rho_g u_g\right)}{dz} = 0 \tag{3.1}$$

Solid Phase:

$$\frac{d\left(\alpha_s \rho_s u_s\right)}{dz} = 0 \tag{3.2}$$

The momentum equation for the gas and solid phase can be written by balancing the forces over the control volume as shown in Figure 3.2. This can be written as;

Gas Phase:

$$-\frac{dP}{dz} = \alpha_g \rho_g g + \alpha_g \rho_g u_g \frac{du_g}{dz} + F_{gs} \tag{3.3}$$

Solid Phase:

$$\alpha_s \rho_s u_s \frac{du_s}{dz} = F_{gs} - \alpha_s \rho_s g - F_c \tag{3.4}$$

Where, F_{gs} represent force due to gas-solids phase inter-phase inter-action, F_c represents the inter-particle collision force.

The volumetric fraction relations of gas and solids phase can be written as;

$$\alpha_g + \alpha_s = 1 \tag{3.5}$$

The equation of state of gas phase, according to ideal gas law can be written as;

$$\rho_g = \frac{P}{RT} \tag{3.6}$$

The governing Equations (3.1) to (3.6) for the gas-solids riser flow can be solved coupled, provided appropriate sub-models or semi-empirical equation for gas-solids

phase inter-phase inter-action force F_{gs} and inter-particle collision force F_c. The governing Equations (3.1) to (3.6) can be solved to find cross-section averaged pressure (P), solid volume fraction (α_s), solid velocity (u_s), gas velocity (u_g), gas density (ρ_g) along the riser height.

3.3 Modeling of Constitutive Relations

3.3.1 Gas-solid phase Interaction Force F_{gs}

The interaction force between gas and solid phase can be divided into drag force due to slip between gas and solid phase (F_D), and the force due to pressure gradient along the riser (F_P). The pressure along the riser decreases, and the energy is utilized for gas and solid lift up, gas and solid acceleration, inter-particle collision and wall friction. In presence of pressure gradient along the riser, an additional force also acts on the particles. Using the axi-symmetric condition, the force on the spherical particle due to the pressure gradient can be written as;

$$f_p = -2\pi\left(\frac{d_s}{2}\right)^3 \int_0^{\pi} \frac{dP}{dz} \sin\theta \cos^2\theta d\theta = -\frac{dP}{dz}\frac{\pi {d_s}^3}{6} \tag{3.7}$$

The negative sign indicates that pressure gradient decreases along the riser, which means the force on the spherical particle is acting in the opposite direction of pressure gradient. The total force on the solid phase due to the pressure gradient can be written as;

$$F_p = n_p f_p \tag{3.8}$$

Where, f_p and n_p represents pressure gradient force on single particle and number of particles per unit volume.

$$F_p = \frac{\alpha_s}{\frac{\pi}{6} d_s^{\,3}} f_p \tag{3.9}$$

Combining Equations (3.7) and (3.9), the total force on the solid phase due to the pressure gradient can be written as;

$$F_p = -\alpha_s \frac{dp}{dz} \tag{3.10}$$

With the use of the pressure gradient force F_p, the gas and solid momentum Equations (3.3) and (3.4) can be written as;

$$-\alpha_g \frac{dP}{dz} = \alpha_g \rho_g g + \alpha_g \rho_g u_g \frac{du_g}{dz} + F_D \tag{3.11}$$

$$\alpha_s \rho_s u_s \frac{du_s}{dz} = F_D - \alpha_s \rho_s g - F_c - \alpha_s \frac{dP}{dz} \tag{3.12}$$

3.3.2 Drag Force on Settling of Suspension of Particles

The drag force is defined as force due to the interaction and contact of a solid body with a fluid (liquid or gas). In the fluidization the drag force is defined as the inter-phase momentum transfer between gas and solids. When suspension of particles is settling, each particle is suspended freely in the fluid and the drag force exerted by the fluid on each particle is equal to its weight in the fluid, but not equal to the weight in the suspension. In case of settling of uniform suspension, the resistance force to the motion of individual particle also depends on the presence of the other particles since they affect flow pattern. The restriction of the flow spaces between the particles with increase of concentration results in steeper velocity gradient in the fluid and consequently greater shearing stresses compare to setting single particle. The drag coefficient for settling of a single spherical particle (C_{D0}) infinite medium and settling a particle forming part of suspension (C_D) can be written in terms of relative velocity of particle and fluid (Richardson & Zaki, 1954).

$$\frac{C_D}{C_{D0}} = \left(\frac{u_{r0}}{u_r} \right)^2 \tag{3.13}$$

Experiments on settling of suspension of particles in finite volume tubes have been performed to find the settling velocity of the suspension. The lake of clear terminology for sedimentation results in misleading or misinterpretation among the particle terminal velocity, settling velocity and relative velocity with fluid. When a single particle settles in an infinite fluid medium, the particle settling velocity, terminal velocity and relative velocity are same and fluid velocity is zero. However, when suspension of particles settles in a finite fluid medium with the closed end of tube, the particle motion is

resisted by the upward movement of the fluid and so the settling velocity (observed velocity) of particles is different from the terminal velocity. Consider a case of settling of particle suspension in a finite volume cylindrical tube with the closed end as shown in Figure 3.3. In any cross-section with in the settling suspension, from a material balance, the relationship between, particle relative velocity (u_r), particle terminal velocity and particle settling velocity can be written as;

$$u_s = u_{pt} - u_f \tag{3.14}$$

$$u_r = u_s + u_f \tag{3.15}$$

The relative velocity of particle in suspension can be written in terms of voidage and settling velocity (observed falling velocity) of suspension;

$$u_r = \frac{u_s}{\alpha} \tag{3.16}$$

In 1954, Richardson and Zaki, performed experiments on the settling of suspension of particles in vertical cylindrical tube similar to shown in Figure 3.3. They measure the falling rate of particles in tube by reading the marking on tube, which is the settling velocity of the suspension. Many researches believe that the observed falling velocity of suspension is the terminal velocity of the suspension, which is not the case. From the results of experiments, Richardson and Zaki, 1954 proposed a correlation for

observed falling velocity (u_s) which is the settling velocity of suspension in terms of the settling velocity of single particle (u_{pt0}) in an infinite fluid medium.

$$\frac{u_s}{u_{pt0}} = \alpha^n \tag{3.17}$$

The settling velocity of the single particle is equal to its terminal velocity and relative velocity with fluid. While for settling of the suspension particles, the relative velocity and settling velocity of suspension in terms of gas phase volume fraction can be represented by Equation (3.17).

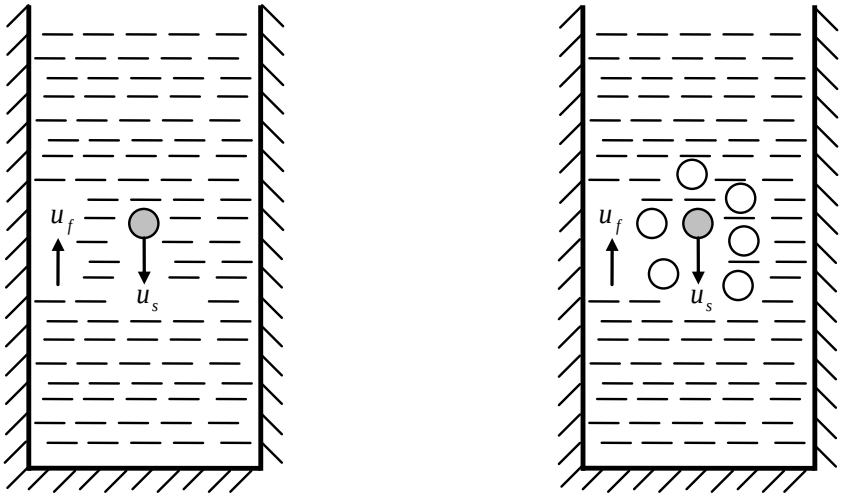

(a) Settling of single particle (b) Settling of suspension

Figure 3.3 Settling experiment setup for (a) single particle in infinite fluid medium (b) suspension in finite fluid medium.

The drag coefficient for particle settling in swamp of neighboring particle in terms of drag coefficient of single particle settling in infinite fluid medium give by Equation (3.13);

$$\frac{C_D}{C_{D0}} = \alpha^{-2(n-1)} \tag{3.18}$$

The drag force on the particle, which is the part of the suspension of the particles, can be represented in terms of drag coefficient of single particle using Equation (3.18).

$$F_{D0} = \frac{\rho_f u^2_r}{2} A_p C_D \tag{3.19}$$

$$F_{D0} = \frac{\rho_f u^2_r}{2} A_p C_{D0} \alpha^{-2(n-1)} \tag{3.20}$$

The total drag force on the particles in the gas-solids phase flow can be written as;

$$F_D = n_p F_{D0} \tag{3.21}$$

Where

$$F_{D0} = \frac{3}{4} C_{D0} \rho_f \left(u_g - u_s\right).\left|u_g - u_s\right|.\frac{\alpha_s}{\left(1-\alpha_s\right)^{-2(n-1)}}.\frac{1}{d_s} \tag{3.22}$$

Where the exponent 'n' is the slope of the curve of log u_s against α. The results of experiment, the empirical correlation for exponent 'n' had been proposed by Richardson & Zaki, 1954, in terms d_p/D and particle Reynolds number.

For $0.2 < Re_p < 1$

$$n = \left(4.35 + 17.5\frac{d_p}{D}\right)\mathrm{Re}_p^{-0.03} \tag{3.23}$$

For $1 < Re_p < 200$

$$n = \left(4.45 + 18\frac{d_p}{D}\right)\mathrm{Re}_p^{-0.1} \tag{3.24}$$

For $200 < Re_p < 500$

$$n = 4.45\,\mathrm{Re}_p^{-0.1} \tag{3.25}$$

The relationship between drag coefficient for settling of single particle $\left(C_{D0}\right)$ and particle Reynolds number was give by (Dallavalle, 1948), which can be represented as;

$$\begin{aligned} C_{D0} &= \frac{24}{\mathrm{Re}_p} && \mathrm{Re}_p < 2 \\ C_{D0} &= 0.4 + \frac{24}{\mathrm{Re}_p} && 2 < \mathrm{Re}_p < 500 \\ C_{D0} &= 0.44 && 500 < \mathrm{Re}_p < 2 \text{ x } 10^5 \end{aligned} \tag{3.26}$$

3.3.3 Inter-particle Collision Force

The coexistence of dense phase at bottom of the riser, dilute phase at top of the riser with intermediated acceleration phase, and "S" shape distribution of solid volume concentration was experimentally demonstrated first by (Kwauk *et al*., 1986). The high slip velocity or low solid velocity in the dense phase in mainly due to energy dissipation by inters particle collision. The energy dissipation by inter particle collision decreases as the solid volume fraction decreases along the riser. In the dense phase regime the drag force is much higher than the gravitational force, and the drag force is mainly balanced by the collision force, and so there is no solids acceleration. The collision force $\left(F_c\right)$ can be represented as a function of drag force and riser height. The collision force is a function of properties of solid flux, solid velocity, gas velocity and particle properties. The formulation of the collision force from the basic principles is very complicated due to normal, tangential and oblique collision among the particles, so in this dissertation, a phenomenological semi-empirical correlation for collision force as a function of drag force is proposed.

$$F_c = F_D\left(1-K_1\right) \tag{3.27}$$

Where, K_1 is the coefficient represents the "S" shaped distribution along the riser height, which can be written as;

$$K_1 = A+\tan^{-1}\left(\frac{H-z_i}{B}\right)/C \tag{3.28}$$

Where A, B, and C are the coefficient which can be adjusted to fit the experiment data. The constants A, B, and C are the function of the operating conditions, physical and hydrodynamic properties of phases. The formulation of the function K_1 is similar to that proposed by (Kwauk *et al*., 1986) for "S" shape distribution of the solid volume fraction. The value of B is unity for high solid flux risers.

3.4 Results and Discussion

In this section, the uniform flow model for gas-solids transport in riser is validated by comparing the model predictions with available published experimental data. The impact of axial pressure gradient on the solid phase transport is considered by introducing partition of pressure gradient for gas and solid phase in their momentum balance. The proposed correlation for inter-particle collision force is calibrated by comparing the model predictions of axial gradient of pressure and solid volume fraction against published experiment data. The significance of inter-particle collision force is further analyzed by comparing model predictions of solid volume fraction distribution with and without collision force against experiment data. The input parameters for the model predictions are kept identical with the experiment conditions. In order to examine the model robustness and rationality of working conditions, the relevant parameters of experiments were purposely chosen in wide range for particle type, gas velocity, solid mass flux and riser geometry. The operating conditions of the experiments used for the comparison of the proposed model predictions are shown in Table 3.1.

Table 3.1 Experiment Conditions for Model Input and Validation

Case/ [Ref.]	**Particle Type**	**d_p** (μm)	**G_s** ($kg/m^2.s$)	**U_g** (m/s)	**ρ_s** (kg/m^3)	**Z** (m)	**D** (m)
1[Arena *et al*., 1985]	Glass Beads	88	600	7	2600	6.4	0.041
2[Arena *et al*., 1985]	Glass Beads	88	382	7	2600	6.4	0.041
3[Arena *et al*., 1985]	Glass Beads	88	199	7	2600	6.4	0.041
4[Knowlton, 1995]	FCC	76	489	5.2	1712	14.0	0.041
5[Knowlton, 1995]	FCC	76	489	7.6	1712	14.0	0.041
6[Knowlton, 1995]	FCC	76	489	11	1712	14.0	0.041
7[Knowlton, 1995]	Sand	120	50	4.2	2600	14.0	0.041
8[Pugsley & Berruti, 1996]	Sand	208	400	8.5	2580	5.0	0.05
9[Pugsley & Berruti, 1996]	Sand	208	240	8.5	2580	5.0	0.05
10[Pugsley & Berruti, 1996]	Sand	208	700	8.5	2580	5.0	0.05
11[Schlichthaerle & Werther, 1999]	Quartz Sand	105	23	4	2600	15.6	0.04

As a part of model validation, the model predictions of solid volume fraction for case 1-3 are compared with experiment data. The input conditions for the model predictions are similar to experiment conditions given in Table 3.1. To make comparison of different cases more representatives, the dimensionless riser height (z/D) is used.

As shown in Figure 3.4, the model predictions for solid volume fraction fit the experimental data satisfactory along the riser height. The result shows that, in the lower part of the riser (dense regime), the solid volume fraction is high, with the increase in riser height the solid are then accelerated due to the interaction with gas phase and it reaches to steady state volume fraction at the upper dilute phase regime of the riser. As shown in Figure 3.4, in dilute phase transport regime, solid volume fraction remains constant for all three cases. The model predictions demonstrate the similar trend for the

solid volume fraction distribution as experimental measurement and quantitatively match with their values along the riser with reasonable accuracy specifically in dilute phase regime. The under prediction of solid volume fraction in the dense phase regime is due to assumption of cross-section average properties, which ignores any radial nonuniformity in flow structure and back mixing of particles in this regime. The actual flow structure in the riser is two-zone (core-annulus) along the riser height with back-mixing of solids from wall to core regime, which current model does not include.

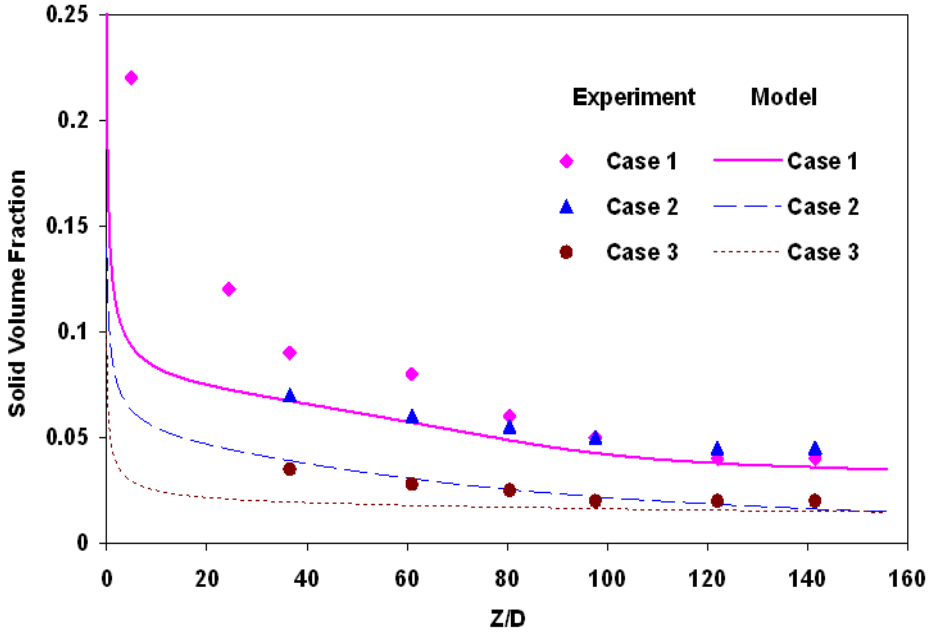

Figure 3.4 Model predictions of axial profile of solid volume fraction against experiment data (Arena *et al*., 1985).

The model is validated for the axial gradient of pressure by comparing model prediction of axial gradient of pressure with experiment data of Pugsley and Berruti, 1996 (case 8, 9, and 10). The model input parameters are similar to experiment conditions given in Table 3.1.

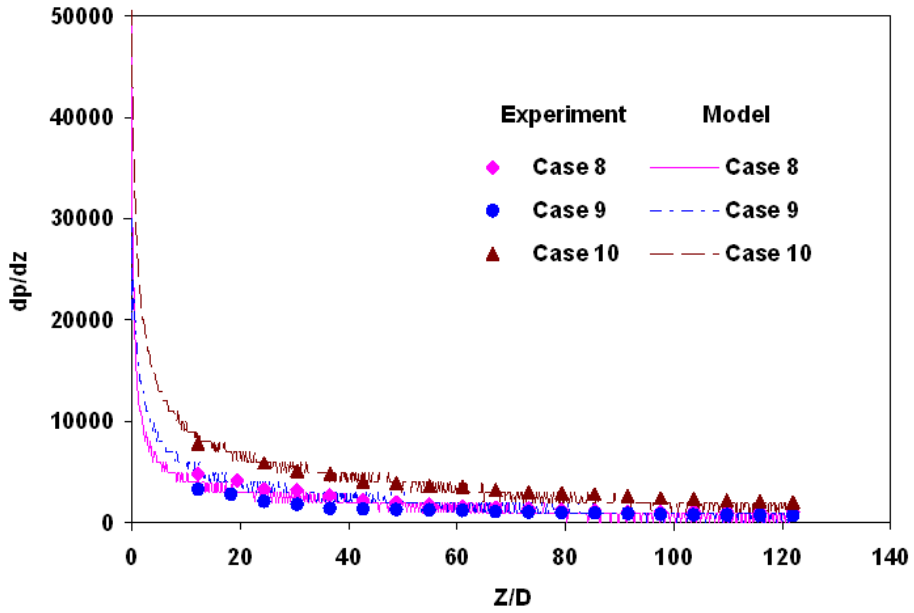

Figure 3.5 Model prediction of axial pressure gradient profile against experiment data (Pugsley and Berruti, 1996).

Figure 3.5 shows reasonable agreement between model prediction and experimental data for axial gradient of pressure. As demonstrated in Figure 3.5, in the lower dense phase regime of the riser, the axial pressure gradients are much steeper than in the upper dilute phase regime. The reason for such steep pressure gradient in the dense phase regime is due to the energy dissipation caused by severe inter-particle collision. The energy dissipation due to inter particle collision is much higher in dense phase regime than in the upper part of the riser, where the energy dissipation is mainly by friction loss and gravity. The particles are accelerated gradually with the increase of riser height and the dense gas-solids flow enters in to the acceleration transition regime and then dilute transport regime. Along the riser height, the solid volume fraction decreases and so the energy dissipation due to inter particle collision also decreases. In the dilute phase regime, inter-particle collision is very small and the energy dissipation is dominated only by friction loss between gas/solid and wall. This is the reason for the

steep pressure gradient in the dense phase regime and quite steady axial pressure gradient in the upper dilute transport regime of the riser.

In order to demonstrate the importance of the energy dissipation by inter-particle collision in gas-solids transport in risers, the model predictions of solid volume fraction distribution with and without inter-particle collision force are compared with the experiment data which is shown in Figures 3.6 and 3.7.

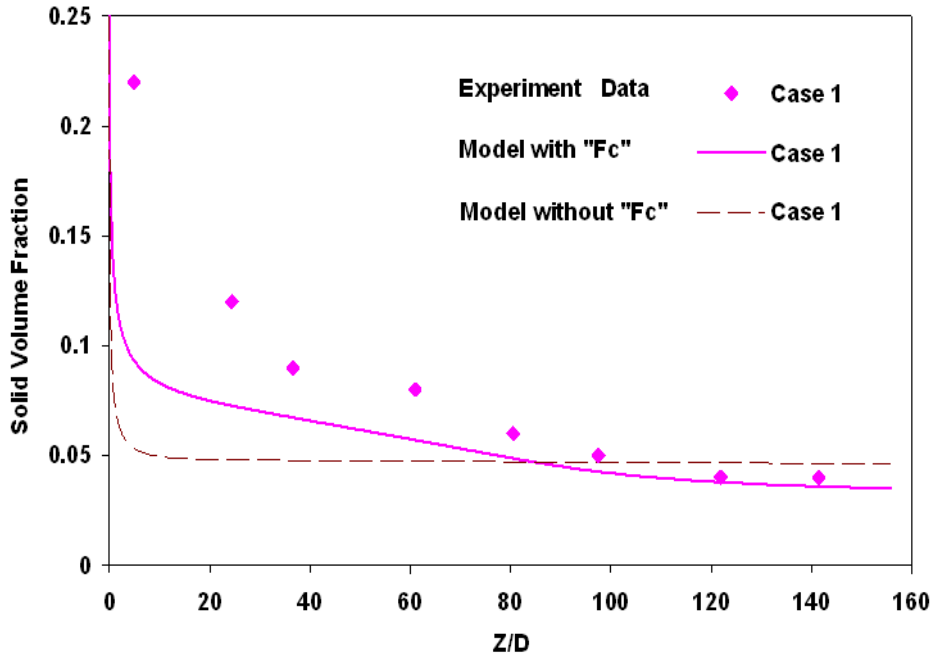

Figure 3.6 Model prediction of axial distribution of solid volume fraction with and without inter-particle collision force against experiment data (Arena *et al.*, 1985).

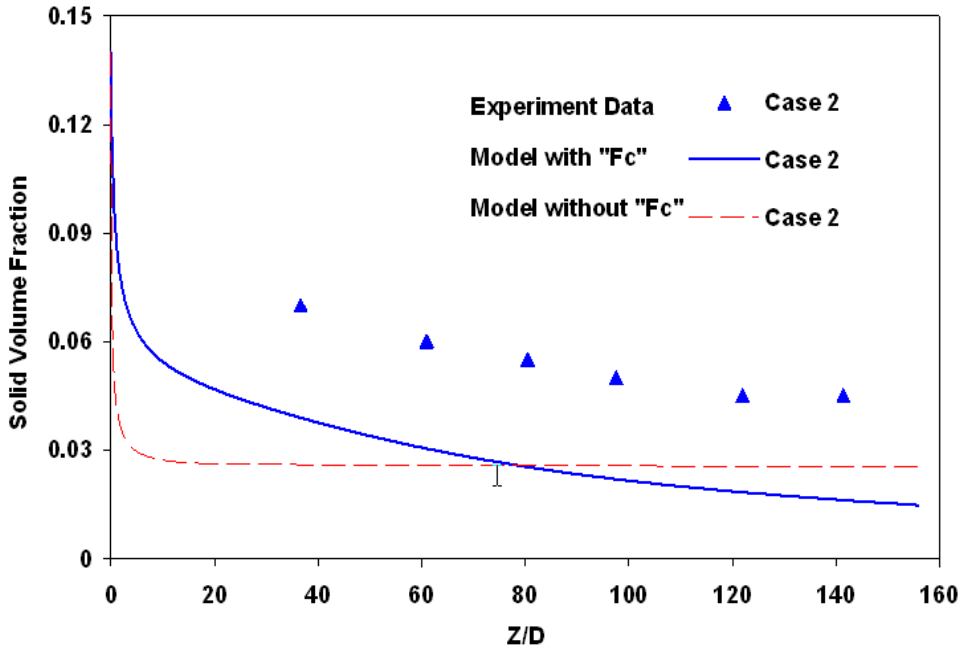

Figure 3.7 Model prediction of axial distribution of solid volume fraction with and without inter-particle collision force against experiment data (Arena *et al*., 1985).

As shown in Figures 3.6 and 3.7, without inter-particle collision force, the particles are accelerated to the dilute transport regime in couple of centimeters length of risers, while the experiment data and model predictions with collision force, shows gradual acceleration particles to the dilute phase transport regime. The result shows that, the particles acceleration into the dense phase transport regime is damped out due to intensive inter-particle collision and hence, the solid volume fraction is high in this regime. When the particle volume fraction reduces, the particles are accelerated in presence of collision force and reach to steady state value in the dilute transport regime. This results shows that, the energy dissipation due to inter-particle collision is significant and cannot be ignored, especially in dense phase transport regime.

3.5 Summary of Chapter

1. A simple mechanistic model is developed, which describes the gas-solids flow hydrodynamics in the riser. The proposed model predicts well axial distribution of phase transport properties.
2. Introduced the impact of pressure gradient along the riser on the particle transport by partition of the pressure gradient for the gas and solid momentum equation.
3. An intrinsic correlation for inter-particle collision force is proposed for particle momentum balance to take into account the energy dissipation by inter-particle collision specifically in the dense and acceleration phase regime.
4. Formulated the drag force on a particle in the presence of neighboring particles in gas-solids riser flow by modifying the drag force on the single particle by correction factor formulated from sedimentation experiments of Richardson-Zaki correction factor.
5. With enforcing pressure gradient impact on solid phase transport and inter-particle collision in solid momentum balance, the model predictions reasonably fits the experiment data of axial distribution of solid volume fraction and pressure gradient. Specifically in absence of inter-particle collision force the model predictions are significantly different from the experiment data.
6. The proposed uniform flow model for axial distribution can be later on used to take into account the radial nonuniformity of phase distribution in terms of wall effect and radial particle transport and particle back-mixing from wall regime.

CHAPTER 4

HYDRODYNAMICS OF AXIAL AND RADIAL NON-UNIFORM GAS-SOLID FLOW STRUCTURE OF COLD FLOW RISER

4.1 Problem Statement and Challenges

Gas-solids risers are widely adopted for transportation and reactors in many industrial applications such as fluidized catalytic cracking (FCC) of petroleum, coal combustion and pneumatic conveying of drug powders. Despite of their widespread applications, the hydrodynamics of riser transport is still not very well understood, partly due to complex gas-solids flow structure which complicates a thorough theoretical understanding and description, and difficulties in measurement of local transport properties in the dense gas-solids flows. It is essential for the optimal design and improvement in existing industrial facilities to understand the flow structure and hydrodynamics of gas-solids in risers. In this chapter, a continuous modeling approach is proposed for simultaneous prediction of axial and radial nonuniform distribution of gas-solids transport properties. There are many challenges for modeling of nonuniform gas-solids risers flow, which are discussed in next section.

Experimental studies clearly demonstrate that the gas-solids flow structure is heterogeneous both in axial and radial direction and the down flow of solids in wall region (e.g., Gajdos and Bierl 1978; Bi *et al.*, 1996; Namkung and Kim, 1998). The axial non-uniformity of gas-solids flow is mainly due to the phase acceleration and inter-particle collision while the radial heterogeneity is mainly due to wall boundary effect, turbulent convection and collisional diffusive mass transfer of solids.

The axial heterogeneity of gas-solids flow in riser in general can be represented as a dense region at the bottom of the riser, a dilute regime at the top of the riser and a acceleration region between them which is also known as transition region (e.g., Li and Kwauk, 1980; Bai *et al*., 1992; Rhodes *et al.*, 1998; Parssinen and Zhu, 2001; Yan and Zhu, 2004). Radial nonuniform distribution of gas-solids flow in risers is presented as a dilute core region where particles are flowing upward and dense annulus (wall) region with solids mostly down flow along the wall (e.g., Weinstein *et al*., 1984; Bader *et al*., 1988; Hartge *et al.*, 1988; Zhang *et al*., 1991; Herb *et al*., 1992; Brereton and Grace, 1993; Nieuwland *et al*., 1996). Axial and radial non-uniform gas-solids flow structure in riser is shown in Figure 4.1.

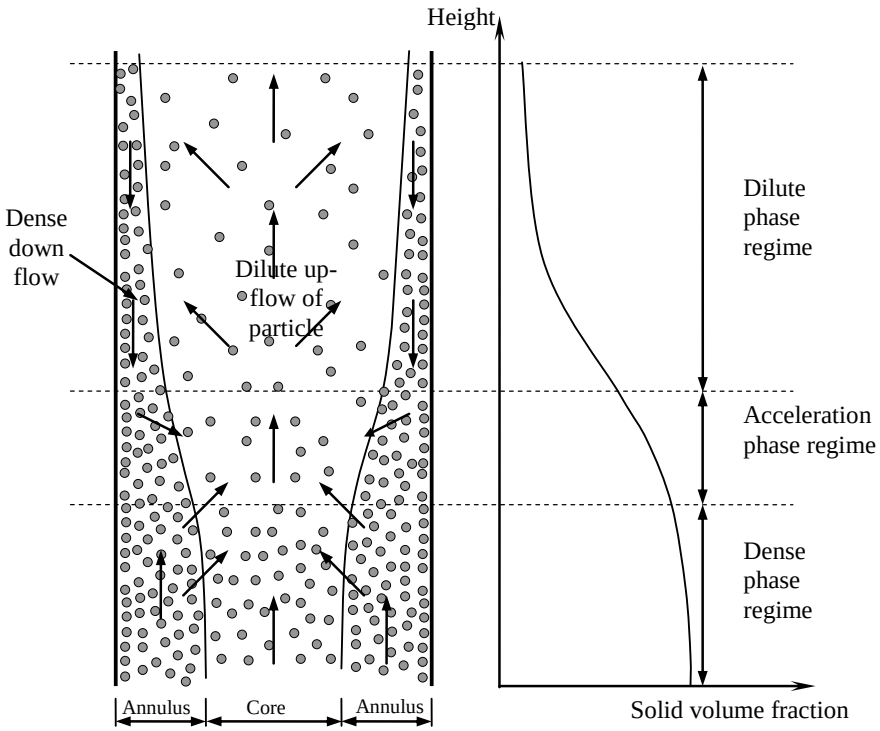

Figure 4.1 (a) Schematic representation of core-annulus riser regimes with radial transport mechanism (b) Flow regimes along of riser.

Most modeling efforts for the axial distribution of gas-solids flow are based on the assumptions of one-dimensional flow with cross-section averaged properties of phases. In uniform flow modeling approach, due to the assumption of radial uniform phase distribution, the area for upward flow of particle suspension and mass fluxes of gas and solids phases remains constant along the riser, and there is no back-mixing of particles. The one zone, one-dimensional model for gas-solids flow with the assumption of cross-section average phase property is reasonable for engineering approximation with error in model predictions. The gas-solids risers are mostly employed in petroleum, chemical and other industries, where intensive heat and mass transfer and reaction takes place due to interaction between gas and solid phases. The nonuniform distribution of gas-solids phase with back-mixing particles may have significant impact on heat and mass transfer rates and reaction characteristics. The hydrodynamic characteristics of gas-solids flow in core and annulus (wall) regimes are strikingly different; consequently, it is not physical to combine the transport properties of two regions as a uniform flow. To aid the design of riser reactors and other two-phase up-flow suspension systems, it become obvious to develop a modeling approach for axial and radial nonuniform distribution of gas-solids transport properties in risers.

This chapter is aimed to develop a one-dimensional continuous modeling for simultaneous prediction of radial and axial nonuniform distribution of gas-solids phase in risers. The governing equations for gas-solids transport are presented in form of differential-integral form for proposed modeling approach. The radial nonuniform phase distribution is approximated as 3^{rd} order polynomial distribution. A mechanistic model for radial transport of gas and solid phase is also proposed to determine the radial

nonuniform phase distribution. The mechanism for radial nonuniform phase distribution is discussed in details in Section 4.2.

Many research efforts have reported in literature for the predictions of radial distribution of gas and solid phase profiles, but most of the previous published work used experimental data to propose a correlation for radial phase profiles. The proposed correlations can be applicable for certain operating range and geometry of CFB risers. It should be emphasized that, the measurements of transport properties near the wall, specifically, in the dense phase regime are extremely difficult. The radial distributions of the phases based on such empirical correlations are not universe, limited by rise operating conditions and mostly used for dilute phase transport regime. The literature survey for modeling of radial nonuniform distribution of gas-solids flow in riser is presented in Chapter 2. From the literature survey, it can be concluded that, the proposed models for radial nonuniform phase distribution (two-zone (core-annulus) models) are over simplified by pre-defining the core-annulus flow regimes. The radial transport of the particles, in published core-annulus flow models, are not truly based on the governing mechanisms but built in the models by defining the transport coefficients. Above all, most published models are validated by comparing model predictions of the radial non-uniform distribution of the phases, transfer coefficient, and annulus thickness with experiment data but never validate for axial distribution of the phases i.e., axial distribution of the solid volume fraction, pressure gradient in the axial direction and particle velocity.

Against the above backdrop, in this chapter we proposed a one-dimensional continuous modeling approach for predictions of both radial and axial distribution of gas-

solid flow properties. The proposed modeling is very useful for determination of core-wall area and back-mixing of particles. Our preliminary studies shows that the published experiment data on radial distribution of the gas-solids phase profile can be reasonably approximated by 3^{rd} order polynomial with very small error. The maximum error (in some cases) with 3^{rd} order polynomial approximation for radial distribution of the phases is less than 20% in comparison with the experiment data, which is mostly in the dense phase regime. The 3^{rd} order polynomial distribution for radial distribution of gas and solid phase is used for this study. The axial distribution of gas-solids flow properties was then simultaneously determined by averaging the terms of mass and momentum conservation equation of each phase over the cross-section of riser.

4.2 Mechanisms for Wall Induced Radial Transport of Phases

The radial non-uniform distribution of gas and solid phase in riser is mainly due to the riser wall. The gas velocity at the wall is zero due to the no slip condition. As the gas velocity near the wall is very low compare to the gas velocity at the center of the riser, the particles which comes in contact with riser wall or very close to riser wall will lose their momentum and depending upon the momentum transfer to the particles by gas (drag force), the particles may be moving upward or downward in the wall regime. If the momentum transfers to the particles higher than the weight of the particles, the particles will slowly move upwards otherwise it will flow in downward direction. The particles concentration at the center of the riser is low (dilute) and the flow is highly turbulent. Due to the turbulence induced fluctuation of the particles, the particles have equal probability in moving in all direction, the schematic diagram of this mechanism is shown

in Figure 4.2(a). Due to high turbulence induced fluctuation of particles in the core regime, there is a radial transport of the particle from center (core) of the riser to wall. When these particles collide with riser wall or with down-flowing particles in wall regime, they may bounce back or may loss their momentum and captured by the downward moving particles in the wall regime. This way the particles are accumulated into the wall regime and form a dense flow of particles in the wall regime.

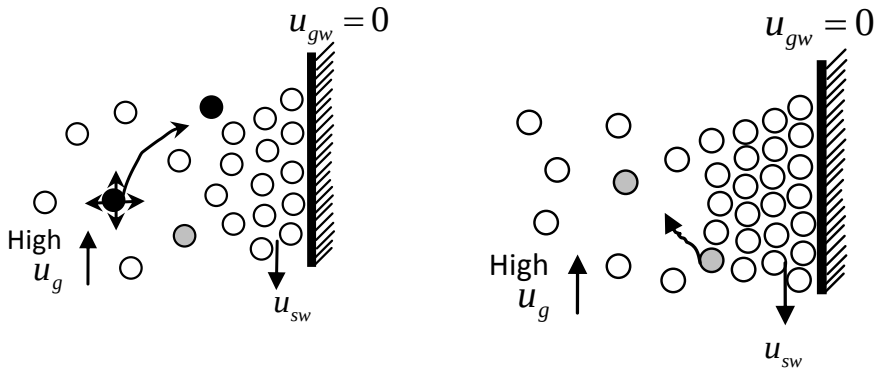

(a) (b)

Figure 4.2 Schematics of (a) Turbulent fluctuation induce particle transport from core to wall regime (b) Particle pickup from wall to core regime.

Due to the development of the dense layer of the particles in the wall regime, the gas velocity in the core regime is increased due to reduction in the flow area of the riser. The particles in the outermost layer of the wall regimes are in contact with high velocity gas, which are easily pickup by high velocity gas from the outermost layer of the wall regime to core regime, schematic of such mechanism is shown in Figure 4.2 (b). This is the mechanism by which the wall regime is developed in incipient circulating fluidized

bed riser flow. These non-uniform distributions of the phases will produce particle velocity and concentration gradient in the radial direction of the riser.

Once the gas-solids riser flow is fully developed, the radial transport of the particles and the wall layer thickness is governed by the turbulence fluctuation induced transfer of particles from core to wall regime and wall collision induced transfer of particles from wall to core regime. Above all, the direction of particle flow in the wall regime is mainly dependent upon the superficial velocity of gas, solid mass flux and riser geometry (specially the diameter of riser). Under the high solid mass flux and high superficial gas velocity flow condition in the riser, the particles are moving upward in the wall regime, which has been observed in high density circulating fluidized beds experiments.

In the dense phase regime of the riser, the particles are in the highly packed flow model, the particles turbulence in theses regime is damped out due to inter-particle collision. In the dense phase regime of the riser, the radial transport of the particles from the core to wall regime is limited due to the damping of particle turbulence by inter-particle collision. At the same time the particles in the outermost layer of the packed wall regime interact with high velocity gas in the core regime, some of the particles are picking up by high velocity gas and there is a radial transport of particles from wall to core-regime. As the drag force is very high and the particles are in the packed conditions in dense phase regime, even though there is gas stagnation on the wall, still the particles are slowly moving upward in this regime. The mechanism of radial transport of particle in the dense phase regime is shown in Figure 4.1.

In the fully developed dilute transport regime at the top of the riser, the solid volume fraction in the wall is higher than in the core regime but the particles are loosely packed. The particle turbulence and the gas velocity is very high in the core regime of the riser, which causes particle turbulence induced radial transfer of the particles from core to wall regime. When high velocity particles from the core regime collide with the particles/wall into the wall regime, depending upon the radial component of the particle momentum, the particle may bounce back on collision with particle/wall or captured by the particles in the wall regime. The radial transport of the particles from the wall to core regime is mainly governed by the particle-particle collision or particle-wall collision induce bouncing back of the particle into the core regime, the shear lifting of the particles in the wall regime due to steep gas phase velocity gradient in the wall regime and the radial particle concentration gradient. In the dilute phase transport regime, the net radial transport of the particles is from core to wall regime as shown in Figure 4.1.

4.3 One-dimensional Modeling Approach for Gas-solids Transport with Axial and Radial Non-Uniform Gas-solids Flow Structure in Risers

Consider a steady, isothermal axial and radial nonuniform gas-solids riser as shown in Figure 4.3. The radial distributions of the gas and solid phase in the riser flow are shown in Figure 4.3. The following simplifying assumptions are made for this study. The effect of solids deceleration at the top of the riser and the intensive turbulent mixing regime at the inlet of the riser is ignored in proposed modeling. The variation of gas pressure in the radial direction is much less than the axial variation in the pressure; so the pressure and the density of the gas in the radial direction are assumed constant. For the simplification,

the frictions between the wall and the gas and solids phases are also ignored. The gas phase follows the ideal gas law.

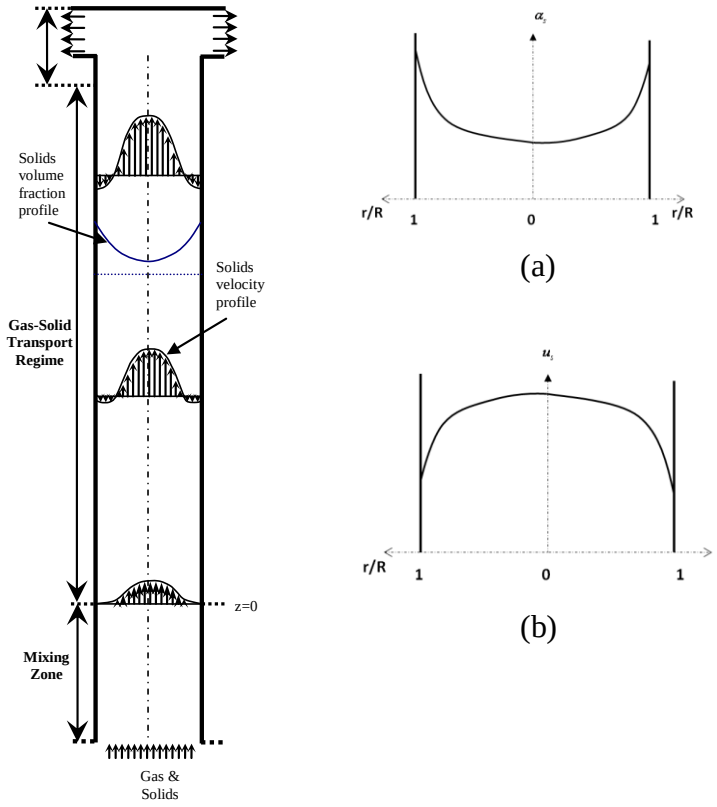

Figure 4.3 Radial nonuniform phase distribution in risers (a) solid volume fraction (b) solid velocity.

With the simplifying assumptions, taking into account the radial nonuniformity of gas-solids phase distributions, the governing equations for the cross-section average axial distribution of gas and solids phase can be written in terms of differential-integral equation. Based on the first principle of conservation, the governing equations for the mass and momentum conservations for the gas and solid phase can be written as;

$$\frac{d}{dz}(\int_A \alpha_g \rho_g u_g dA) = 0 \tag{4.1}$$

$$\frac{d}{dz}(\int_A \alpha_s \rho_s u_s dA) = 0 \tag{4.2}$$

$$-\bar{\alpha}_g \frac{dP}{dz} = \frac{1}{A}\int_A \alpha_g \rho_g g dA + \frac{1}{A}\frac{d(\int_A \alpha_g \rho_g u_g^2 dA)}{dz} + \frac{1}{A}\int_A F_D dA \tag{4.3}$$

$$\frac{1}{A}\frac{d(\int_A \alpha_s \rho_s u_s^2 dA)}{dz} = \frac{1}{A}\int_A F_D dA - \frac{1}{A}\int_A \alpha_s \rho_s g dA - \frac{1}{A}\int_A F_c dA - \bar{\alpha}_s \frac{dp}{dz} \tag{4.4}$$

The relation between the solid and gas volume fraction can be written as;

$$\alpha_g + \alpha_s = 1 \tag{4.5}$$

The equation of the state, following the ideal gas law can be written as;

$$\rho_g = \frac{P}{RT} \tag{4.6}$$

Where, α_g , α_s, ρ_g, u_g and u_s represents the local radially nonuniform voidage, solid fraction, gas velocity and solids velocity respectively.

The integral term in the Equations (4.1) to (4.4) represents the cross-sectioned averaged properties of the phases. For radial uniform flow or cross-section averaged one-

dimension model, the local radial nonuniform transport properties (say volume fractions and velocities) in above equations can be replaced by cross-sectional averaged values and the integrals in above equation could be expressed as explicit functions of these averaged values. The axial distribution of the gas and solid phase transport properties can be predicted by solving coupled governing Equations (4.1) to (4.5) provided the radial nonuniform distribution of gas-solids transport properties and formulation for cross-section averaged drag force and collision force.

For the modeling of non-uniform flow structure both in radial and axial directions, the integrals terms in above Equations (4.1) to (4.4) can be integrated only when the radial distributions of each phase is explicitly expressed. The governing Equations (4.1) to (4.4) can be solved only four unknown cross-section averaged or uniform flow properties of phases, otherwise intrinsic mechanisms or semi-empirical correlations should be provided.

4.4 Modeling of Constitutive Relations

4.4.1 Mechanistic Modeling of Radial Non-Uniform Flow Structure in Riser

Preliminary study shows that, the published experiment data for radial distribution of transport properties of gas-solids in the riser can be reasonably fit by 3rd order polynomial approximation. In this study, around 70 cases of experiment data for radial distribution of transport properties of solid phase from different research groups (e.g., Nieuwland, 1996; Wei *et al*., 1998; Issangya *el al*., 2000; Parssinen and Zhu, 2001; Xiao-Bo *et al*., 2008), operated under different flow conditions and riser geometry, were reviewed and most of them were reasonably fit by 3rd order polynomial approximation. The least square method with axi-symmetric condition is used for riser to fit the experiment data point for radial

phase distribution. Figures (4.4) to (4.9) shows demonstrative example from each group for 3rd order polynomial fit. The operating conditions of experiment and measurement locations are summarized in Tables (4.1) to (4.6). In this study, 3rd order polynomial approximation for radial phase distribution is adopted without losing the characteristics of the flow in the riser. From the experiment data, it was also found that the pressure gradient in the axial direction is much higher than in the radial direction, the uniform pressure in the radial direction is used i.e., pressure is constant over any cross-section of the riser, which implies, the gas density is also constant over cross-section.

Table 4.1 Experiment Conditions and Measurement Location for Radial Distribution of Particle Velocity

Parssinen and Zhu 2001	**Case 1**	**Case 2**	**Case 3**	**Case 4**
Particle Type	FCC	FCC	FCC	FCC
Particle diameter (μm)	67	67	67	67
Particle Density (kg/m^3)	1500	1500	1500	1500
Riser Diameter (m)	0.076	0.076	0.076	0.076
Riser height (m)	10	10	10	10
Solid mass flux (kg/m^2/s)	300	300	300	300
Superficial gas velocity (m/s)	5.5	5.5	5.5	5.5
Measurement location above distributor height (m)	1.53	2.73	3.96	8.74

Source: Parssinen, J.H., Zhu, J.X. (2001). Particle velocity and flow development in a long and high-flux circulating fluidized bed riser. *Chemical Engineering Science*, 56, 5295-5303.

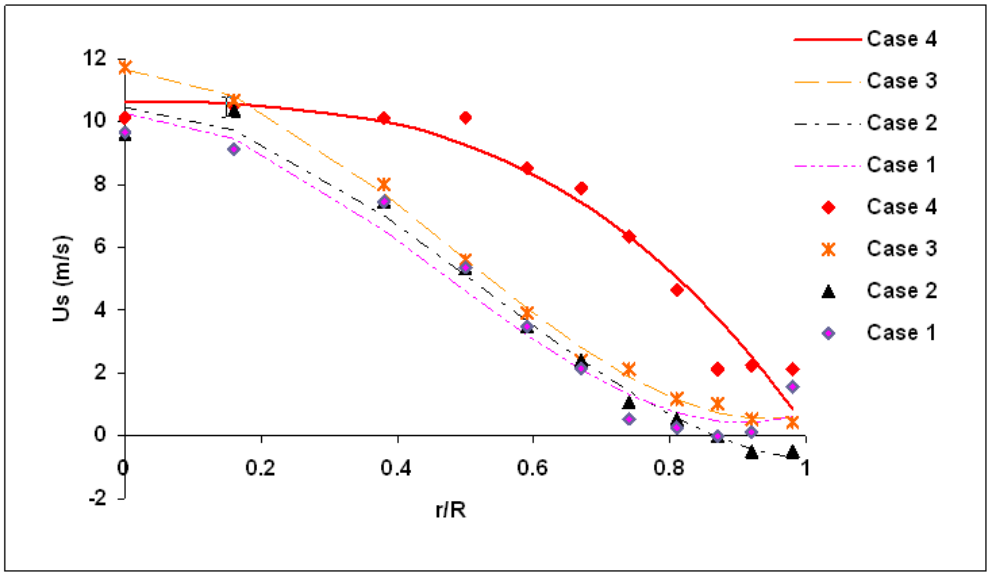

Figure 4.4 3rd order polynomial representation against experiment data for radial solid velocity distribution (Parsinen and Zhu, 2001).

Table 4.2 Experiment Conditions and Measurement Location for Radial Distribution of Particle Velocity

Neieuwland *et al.*, 1996	**Case 1**	**Case 2**
Particle Type	Sand	Sand
Particle diameter (μm)	129	129
Particle Density (kg/m^3)	2540	2540
Riser Diameter (m)	0.054	0.054
Riser height (m)	10.0	10.0
Solid mass flux (kg/m^2/s)	300	300
Superficial gas velocity (m/s)	10	7.5
Measurement location above distributor height (m)	1.8	1.8

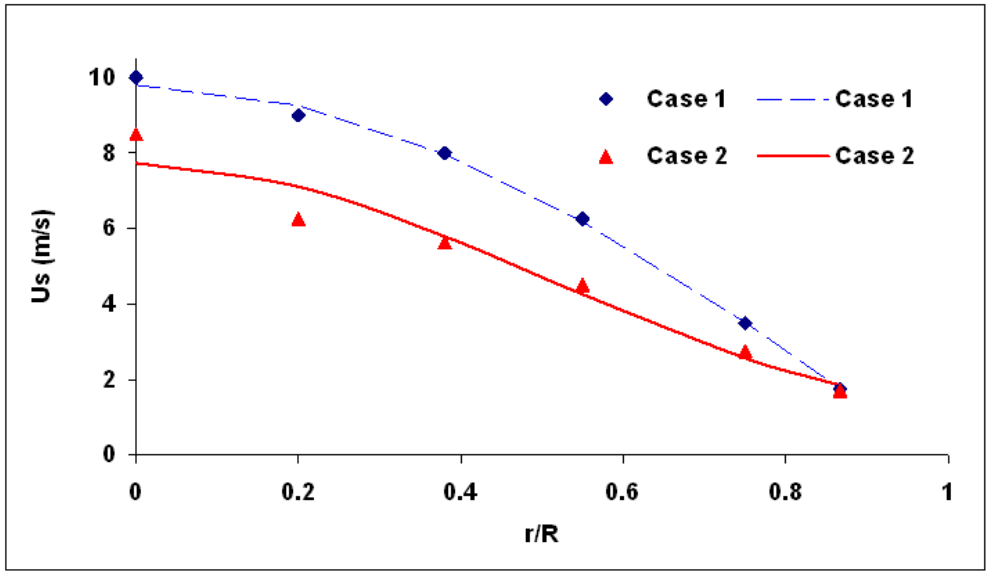

Figure 4.5 3rd order polynomial representation against experiment data for radial solid velocity distribution (Neieuwland *et al.*, 1996).

Table 4.3 Experiment Conditions and Measurement Location for Radial Distribution of Particle Velocity, Parssinen and Zhu, 2001

Parssinen and Zhu, 2001	**Case 1**	**Case 2**	**Case 3**	**Case 4**
Particle Type	FCC	FCC	FCC	FCC
Particle diameter (μm)	67	54	54	54
Particle Density (kg/m^3)	1500	1398	1398	1398
Riser Diameter (m)	0.076	0.186	0.186	0.186
Riser height (m)	10.0	8.0	8.0	8.0
Solid mass flux (kg/m^2/s)	100	100	300	550
Superficial gas velocity (m/s)	8.0	8.0	8.0	8.0
Measurement location above distributor height (m)	2.73	3.96	6.34	TOP

Source: Parssinen, J.H., Zhu, J.X. (2001). Particle velocity and flow development in a long and high-flux circulating fluidized bed riser. *Chemical Engineering Science*, 56, 5295-5303.

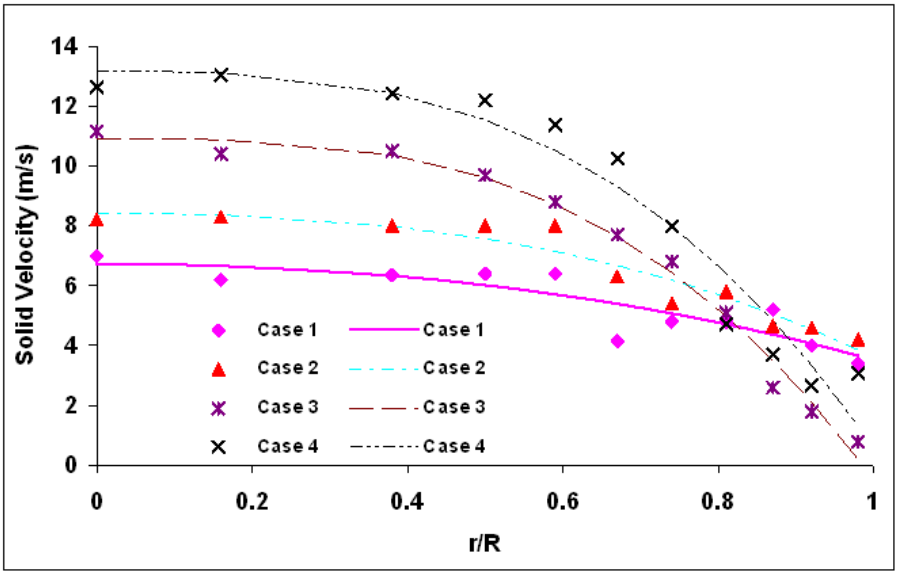

Figure 4.6 3rd order polynomial representation against experiment data for radial solid velocity distribution (Parsinen and Zhu, 2001).

Table 4.4 Experiment Conditions and Measurement Location for Radial Distribution of Particle Solid Volume Fraction

Issangya *et al*., 2001	**Case 1**	**Case 2**
Particle Type	FCC	FCC
Particle diameter (μm)	70	70
Particle Density (kg/m^3)	1600	1600
Riser Diameter (m)	0.0762	0.0762
Riser height (m)	6.1	6.1
Solid mass flux (kg/m^2/s)	391	249
Superficial gas velocity (m/s)	7.5	7.0
Measurement location above distributor height (m)	3.4	5.23

Source: Issangya, A.S., Grace, J.R., Bai, D., and Zhu, J. (2000). Further measurements of flow dynamics in a high-density circulating fluidized bed riser. *Powder Technology*, 111, 104-113.

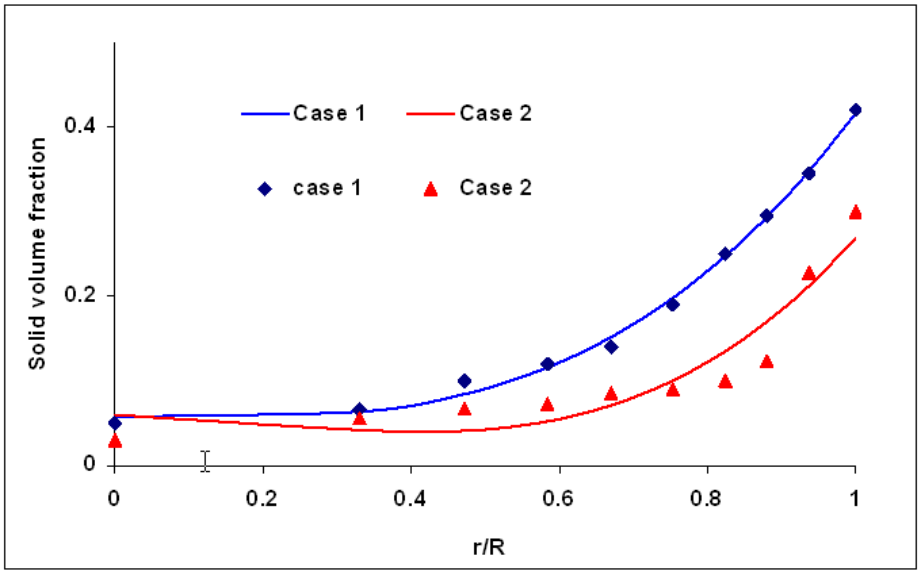

Figure 4.7 3rd order polynomial representation against experiment data for radial solid volume fraction distribution (Issangya *et al.*, 2001).

Table 4.5 Experiment Conditions and Measurement Location for Radial Distribution of Particle Solid Volume Fraction

Qi *et al.*, 2008	**Case 1**	**Case 2**	**Case 3**	**Case 4**
Particle Type	FCC	FCC	FCC	FCC
Particle diameter (μm)	67	67	67	67
Particle Density (kg/m^3)	1500	1500	1500	1500
Riser Diameter (m)	0.762	0.762	0.762	0.762
Riser height (m)	15.1	15.1	15.1	15.1
Solid mass flux (kg/m^2/s)	100	100	100	100
Superficial gas velocity (m/s)	3.5	3.5	3.5	3.5
Measurement location above distributor height (m)	0.95	2.59	8.16	14.08

Source: Xiao-Bo Qi, Wei-Xing Huang and Jesse Zhu (2008). Comparison of flow structure in circulating fluidized bed risers with FCC and sand particles. *Chem. Eng. Technol*., 31(4), 542-553.

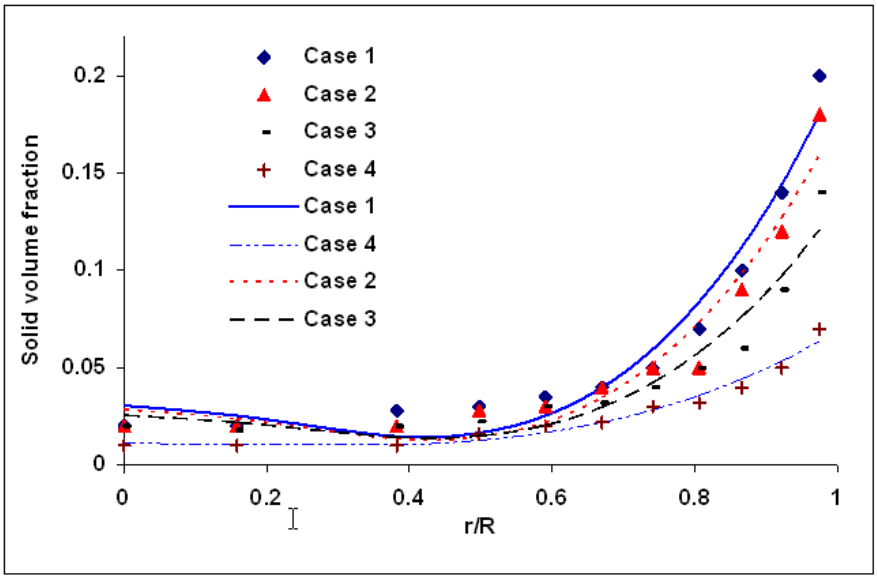

Figure 4.8 3rd order polynomial representation against experiment data for radial solid volume fraction distribution (Qi *et al.*, 2008).

Table 4.6 Experiment Conditions and Measurement Location for Radial Distribution of Particle Solid Volume Fraction

Wei *et al.*, 1998	**Case 1**	**Case 2**	**Case 3**
Particle Type	FCC	FCC	FCC
Particle diameter (μm)	54	54	54
Particle Density (kg/m^3)	1398	1398	1398
Riser Diameter (m)	0.186	0.186	0.186
Riser height (m)	8.0	8.0	8.0
Solid mass flux (kg/m^2/s)	98.8	98.8	98.8
Superficial gas velocity (m/s)	3.25	3.25	3.25
Measurement location above distributor height (m)	6.26	3.92	2.31

Source: Wei, F., Lin, H., Cheng, Y., Wang, Z., and Jin, Y. (1998). Profile of particle velocity and solid volume fraction in a high-density riser. *Powder Technology*, 100, 183-189.

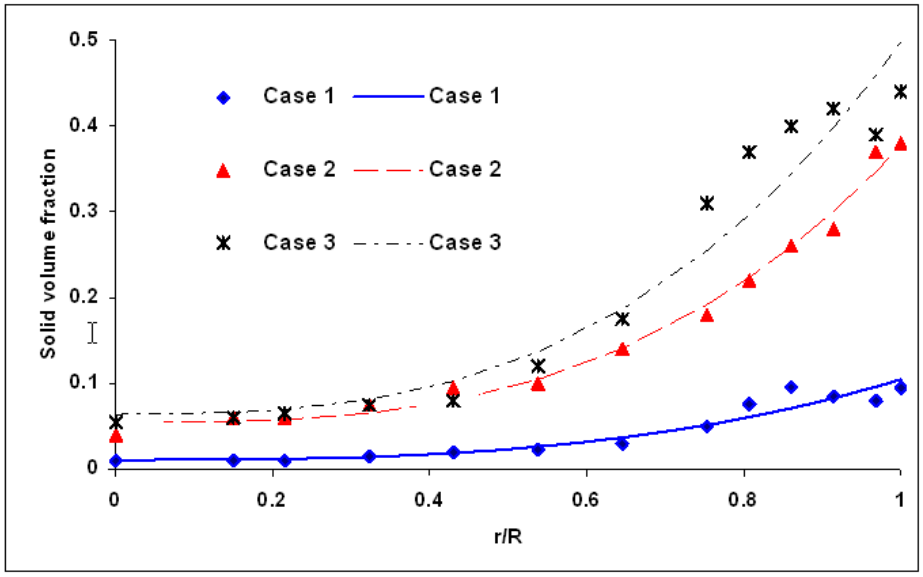

Figure 4.9 3rd order polynomial representation against experiment data for radial solid volume fraction distribution (Wei *et al.*, 1998).

With above assumptions and without losing generality of riser flow, the radial distribution of solid volume fraction $\alpha_s(r)$, solid velocity $u_s(r)$ and gas velocity $u_g(r)$ at any axial location (z) can be expressed by following 3rd polynomial distribution as given by Equation (4.7);

$$\phi(r,z) = \sum_{i=0}^{3} c_{\phi i}(z) \cdot r^i \tag{4.7}$$

The Equation (4.7) can be expanded and written as;

$$\phi(r,z) = c_{\phi 3}(z) r^3 + c_{\phi 2}(z) r^2 + c_{\phi 1}(z) r + c_{\phi 0} \tag{4.8}$$

Here $\phi(r,z)$ can be $u(r,z)$ and $\alpha(r,z)$ for gas and solid phase, which represents radial distribution of phase property at any section of the riser (z). The radial distribution of transport parameters $u(r,z)$ and $\alpha(r,z)$) of gas and solid phase can be determined from Equation (4.8), provided characteristics values of four coefficients $c_{\phi i}$ for each transport property at any cross-section of the riser. According to axi-symmetric nature of riser, the gradient of each transport parameter at the center line of the riser should be zero i.e., $\left.\frac{\partial \phi_i}{\partial r}\right|_{r=0} = 0$, which results in $c_{\phi 1} = 0$. With this condition, the Equation (4.8) will be reduced to;

$$\phi(r,z) = c_{\phi 3}(z) r^3 + c_{\phi 2}(z) r^2 + c_{\phi 0} \tag{4.9}$$

In order to solve above equation for radial distribution of each transport parameter, we need three characteristic values of coefficient $c_{\phi i}$ at any radial location of the riser. In this study, the other three characteristic values for $c_{\phi i}$ were determined from local transport properties of each phase at wall boundary (ϕ_w) , center line (ϕ_0) and cross-sectioned averaged $\left(\bar{\phi}\right)$ at any cross-section of the riser.

The cross-section average value of any transport parameter can be written as;

$$\bar{\phi} = \frac{1}{A}\int_0^R \phi(r)\, dA \tag{4.10}$$

The centerline (r = 0) property of each phase at any cross-section can be written as;

$$\phi_0 = c_{\phi 0} \tag{4.11}$$

The property of transport parameter at wall (r = R) at any cross-section of can be written as;

$$\phi_w = c_{\phi 3} R^3 + c_{\phi 2} R^2 + c_{\phi 0} \tag{4.12}$$

For know values of transport property of each phase (e.g., volume fraction and velocity of gas and solid phase) at wall, centerline and average value over the cross-section of the riser, the characteristic values of coefficient $c_{\phi i}$ at any cross-section of the riser can be determined by solving Equations (4.9) to (4.12) as;

$$c_{\phi 0} = \phi_0 \tag{4.13}$$

$$c_{\phi 2} = \frac{10\bar{\phi} - 4\phi_w - 6\phi_0}{R^2} \tag{4.14}$$

$$c_{\phi 3} = \frac{5\left(\phi_w + \phi_0 - 2\bar{\phi}\right)}{R^3} \tag{4.15}$$

Knowing the three values of coefficient $c_{\phi i}$ at any cross-section of the riser, the radial distribution of the each transport properties for gas and solid phase can be determined from Equation (4.9). For modeling of both radial and axial non-uniform distribution of gas and solid phase, there are 11 unknowns namely, average solid volume fraction $\bar{\alpha}_s$, solid volume fraction at center of riser α_{s0}, solid volume fraction at wall α_{sw}, average particle velocity $\bar{u}_s$, particle velocity at center of riser u_{s0}, particle velocity at wall u_{sw}, average gas velocity $\bar{u}_g$, gas velocity at center of riser u_{g0}, gas velocity at wall u_{gw}, average pressure P, and average gas density ρ_g. The five governing Equations (4.1) to (4.4) and (4.6), which can be solved for five cross-section averaged transport properties i.e., cross-section average solid volume fraction $\bar{\alpha}_s$, gas velocity $\bar{u}_g$, particle velocity $\bar{u}_s$, pressure P, and average gas density ρ_g. To close the problem, additional six intrinsic mechanism or empirical correlations are required.

4.4.2 Radial Transport of Gas and Solids and Riser Wall Effects

4.4.2.1 Radial Mass Transfer. The riser wall blocks the radial motion of both gas and solid phase. The radial transport of the solid is mainly due to the turbulent fluctuation induced particle transport and collision diffusive mass transfer of solids particles. The intensity of turbulent induced mass transfer is dependent on the local particle turbulent intensity and the velocity gradient of particles in the radial direction and is from high turbulent fluctuation of the particles to the low turbulent fluctuation of particles. The intensity of collision diffusive mass transfer is dependent on the local solids

concentration and the concentration gradient of particles in the radial direction, the direction is from high concentration to low concentration. Taking the radial transport of phase from core to the wall is positive; the net radial transport of particles at the wall of the riser (which is zero), which can be written as;

$$\left(\overline{\alpha'_s \rho_s \vec{v}'_{sT}}\right)_w - \left(\overline{\alpha'_s \rho_s \vec{v}'_{sD}}\right)_w = 0 \tag{4.16}$$

The radial transport of the particles due to the turbulence induced particle fluctuation can be best approximated in terms of the solid phase velocity at the center of the riser, because the particle fluctuation is dependent on the particle velocity.

$$\overline{< v'_{sT} >} = k_{sT} u_{s0} \tag{4.17}$$

Where k_{sT} is the dimensionless number, which is a function Reynolds number based on the velocity of gas at the center of the riser and the Stokes number. In the core regime of the riser the particle volume fraction is the lowest compare to any other radial location at a given cross-section of the riser. The particle turbulence and fluctuation is highest in the core regime of the riser, so k_{sT} is defined from the Reynolds number based on the gas velocity at the center of the riser.

$$k_{sT} = \frac{St}{\mathrm{Re}} \tag{4.18}$$

Where St represents Stokes number;

Using Boussinesq's approximation (Boussinesq, 1877), by introducing a transport coefficient, thus the second term in above Equation (4.16) can be expressed as;

$$\overline{<\alpha_s' v_{sD}'>} = -D_{Ds}\nabla\alpha_s \tag{4.19}$$

Where D_D represents the particle mass diffusion mass transport coefficient due to collisional diffusion of the particles in the radial direction, while the negative sign indicates that the direction of transport is down the gradient. The collisional diffusion particle transport coefficient D_D can be determined by the kinetic theory of the gases. According to the kinetic theory of the gases, the particle transport by the self diffusion can be written as

$$D_D = \frac{1}{3}\langle v_c \rangle \lambda \tag{4.20}$$

Where, $\langle v_c \rangle$ and λ represents the average collision velocity and mean free path of the particle respectively.

The radial mass transfer of the gas phase is due to the turbulent fluctuation of gas phase in the core of the riser and also due to the diffusive radial gas transport due to the concentration gradient in the radial direction. Such radial transports of gases results in dilution of solid volume concentration in the wall regime.

$$\left(\overline{\alpha'_g \rho_g \vec{v}'_{gT}}\right)_w + \left(\overline{\alpha'_g \rho_g \vec{v}'_{gD}}\right)_w = -\bar{u}_g \rho_g \delta \frac{d\alpha_{sw}}{dz} \tag{4.21}$$

Here, δ represents average thickness of wall boundary layer, where the compression of the gas results in dilution of solid concentration.

The radial transport of the gases due to the turbulence induced gas fluctuation can be best approximated in terms of the gas phase velocity at the center of the riser,

$$\overline{< v'_{gT} >} = k_{gT} u_{g0} \tag{4.22}$$

Where k_{gT} represents coefficient of the turbulence fluctuation for gas phase, which is defined as the ratio of fluctuation velocity component of the gas phase to the mean velocity the gas phase, which can be expressed as;

$$k_{gT} = \frac{\left\langle v'^{\,2}_g \right\rangle^{\frac{1}{2}}}{\bar{u}_g} \tag{4.23}$$

According to the Boussinesq's approximation, the second term in Equation (4.17) can be expressed as;

$$\overline{< \alpha_g' v_{gD}' >} = -D_{Dg} \nabla \alpha_g \tag{4.24}$$

Where D_{Dg} represents the diffusion mass transport coefficient of the gas phase. The radial transport of the gases due to the turbulence induced gas fluctuation can be best approximated in terms of the gas phase velocity at the center of the riser,

4.4.2.2 Radial Momentum Transfer

Gas Phase: The turbulent and diffusive gas transfer of gas is due to the turbulent fluctuation of gas phase in the core and radial gradient of the voidage respectively. The net radial transport of the gas momentum exerts pressure on the riser wall. If the measurement of the pressure (momentum) exerted by the gas phase on the riser wall is known, the radial momentum of the gas phase at the wall can be written as;

$$\left(\overline{\alpha'_g \rho_g \bar{v}'_{gT}}\right)_w v_{gT} - \left(\overline{\alpha'_g \rho_g \bar{v}'_{gD}}\right)_w v_{gD} = \sigma_{wg}(z) \tag{4.25}$$

Here, v_{gT} and v_{gD} represent the radial gas transport velocity due to the gas turbulence and diffusion. In this study, v_{gT} and v_{gD} were approximated in terms of average gas velocity as;

$$v_{gT} = x_{gT}\bar{u}_g \qquad v_{gD} = x_{gD}\bar{u}_g \tag{4.25-1}$$

σ_{gw} in Equation (4.25) represents the radial pressure on the wall exerted by the radial momentum of the gas phase, which can be measured along the height of the riser using the suitable measurement technique. The Pitot tube may be used to measure the gas

pressure at the wall. The schematic diagram for the experiment setup is shown in the Figure 4.9.

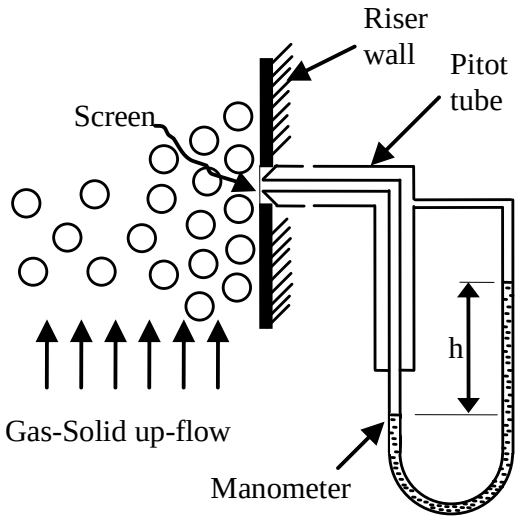

Figure 4.10 Experiment set up for measurement of radial gas pressure on riser wall.

Figure 4.10 shows the experiment set up to measure the radial gas pressure on the riser wall. A pitot tube with the manometer can be used at the riser wall to measure the radial pressure of gas on the wall. Screen is used at the tip of the pitot tube to prevent the blockage of the pitot tube by particles and prevent also preventing the particles from striking with the pitot tube. Only gas is allowed to pass through the pitot tube.

In absence of measurements for σ_{gw}, the radial gas pressure on the wall was expressed in terms of cross-section average transport properties of gas as;

$$\sigma_{wg}(z) = k\bar{\alpha}_g \rho_g \bar{u}_g^{\,2} \tag{4.26}$$

Here “k” is coefficient to correlate the axial acceleration of gas with the radial gas pressure on the wall.

Solid Phase: The radial transfer of particles in the riser exerts force on the riser wall by particles collision on the wall, which induces stress on the wall. If suitable measurement technique is used to measure the stress on the riser wall by particle collision on the wall, then the axial distribution of the radial stress on the wall can be measure for given flow conditions. The radial momentum of the solid phase can be written as;

$$\left(\overline{\alpha'_s \rho_s \vec{v}'_{sT}}\right)_w v_{sT} - \left(\overline{\alpha'_s \rho_s \vec{v}'_{sD}}\right)_w v_{sD} = \sigma_{ws} \tag{4.27}$$

Here, v_{sT} and v_{sD} represent the radial gas transport velocity due to the particle turbulence induced fluctuation and diffusion due to concentration gradient. In this study, v_{sT} and v_{sD} were approximated in terms of average gas velocity as;

$$v_{gT} = x_{sT}\bar{u}_s \qquad v_{gD} = x_{sD}\left|u_{sw}\right| \tag{4.25-1}$$

Where σ_{ws} represents the particle collision induces wall stress.

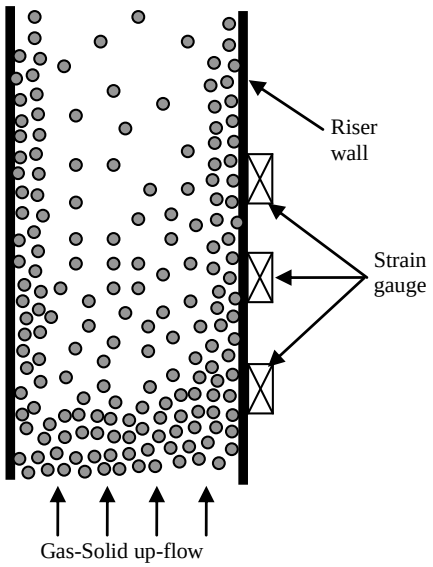

Figure 4.11 Strain gauge set up for riser wall stress measurement due to particle collision.

The strain gauges can be used for the measurement of the particle collision induced wall stress. As shown in Figure 4.11, the strain gauge can be installed along the riser height, to measure the strain in the wall which can be converted in to the wall stress. In absence of measurements for σ_{sw}, the radial wall stress due to particle collision can be expressed in terms of particle axial acceleration as;

$$\sigma_{ws} = k_1 \bar{\alpha}_s \rho_s \bar{u}_s^{\,2} \tag{4.28}$$

Here k_1 is coefficient to express radial solid wall stress in terms of axial acceleration of particles.

4.4.2.3 Axial Momentum Transfer

Gas phase: The wall friction prevents the movement of gas phase in the axial direction, which results in "no slip" condition at wall.

$$u_{gw} = 0 \tag{4.28}$$

Solid Phase: The wall friction offers resistance to the movement of the solid particle at wall. Most published literature used friction force or friction factor between the solid particles and wall to determine the solid velocity at the wall, which can be presented as;

$$\tau_{sw} = \frac{1}{2} f_s \alpha_{sw} \rho_s u_{sw}^{\ 2} \tag{4.29}$$

Where, f_s represent friction factor. The above equation is derived by balancing the pressure drop per unit length with the weight of the particles and the wall-shear friction. Here, the core-annulus inter phase friction is neglected. To determine the particle velocity in the wall regime using Equation (4.29), the correlation for axial distribution of wall shear stress or friction factor should be known for different operating conditions. It is noticed that in Equation (4.29), the solid volume fraction and solid velocity is average value in the wall regime not the solid phase property at wall. In order to determine average solid phase flow properties in the wall regime, the core and wall regime should be pre-defined i.e., the core radius along the riser height should be known in advance. There are too many unknowns, to determine particle velocity at wall using Equation

(4.29). In this study, a correlation for axial distribution of particle velocity on the riser wall with single adjustable parameter is proposed.

$$u_{sw} = \bar{u}_s \exp\left(-\beta \frac{z}{H}\right) - u_{pt} \tag{4.29}$$

Where the coefficient β is a function of the riser operation conditions, here in this study it is an adjustable parameter for the prediction of the particle velocity at the wall.

Here, the number of the unknown for the radial distribution of gas and solid phase are Solid volume fraction at center $\alpha_{s0}(z)$, Solid volume fraction at wall $\alpha_{sw}(z)$, Solid velocity fraction at center $u_{s0}(z)$, Solid velocity fraction at wall $u_{sw}(z)$, gas velocity fraction at center $u_{g0}(z)$, and gas velocity fraction at wall $u_{gw}(z)$. The above unknowns can be calculated by solving coupled Equations (4.16), (4.21), (4.25), (4.27), (4.28), and (4.29) provided the axial distribution of the wall stress exerted by the gas and solid phase.

4.4.3 Drag Force

In radial nonuniform gas-solids transport, the inter-phase drag force varies along the radial locations. The total drag force on the particle can be estimated by averaging over the cross-section of the riser. The drag force on a particle in presence of neighboring particles can be expressed by modifying the drag on a single particle in unbound stationary fluid. The effect of neighboring particles can be expressed by a correction factor to a drag force on a single particle (C_{D0}), which is a function of solid volume

fraction. Taking into account the effect of neighboring particles, the total drag force per unit volume in gas-solids riser transport can be expressed as;

$$f_d = k_1 n_s C_{D0} \frac{\pi}{8} \rho_g d_s^2 (u_g - u_s)^2 \tag{4.30}$$

Here n_s is the number density of particles; k_1 is empirical correction factor to the drag coefficient of single particle in swamp of surrounding particles.

$$k_1 = (1-\alpha_s)^{-2(n-1)} \tag{4.31}$$

The exponent 'n' is the slope of the curve of $\log(u_s)$ against α. From the experiment data, the empirical correlation for exponent 'n' had been proposed by Richardson & Zaki, 1954, in terms d_p/D and particle Reynolds number.

For $0.2 < Re_p < 1$

$$n = \left(4.35 + 17.5\frac{d_p}{D}\right) \mathrm{Re}_p^{-0.03} \tag{4.32}$$

For $1 < Re_p < 200$

$$n = \left(4.45 + 18\frac{d_p}{D}\right) \mathrm{Re}_p^{-0.1} \tag{4.33}$$

For $200 < Re_p < 500$

$$n = 4.45 \mathrm{Re}_p^{-0.1} \tag{4.34}$$

4.4.4 Collision Force

The inter-particle collision force is dues to the inelastic normal compression and rebounding, sliding, non-sliding micro-slip and rolling effects among particles during the transport. The high slip velocity or low solid velocity in the dense phase regime is mainly due to energy dissipation by inter-particle collision, which accounts for turbulence induced solids movements and solids volume fraction. The order of magnitude of collision force is in the same order of magnitude in the dense phase regime and its reaches almost zero in the dilute phase regime. The formulation of the collision force from the basic principles is very complicated due to normal, tangential and oblique collision among the particles. In this study, following the semi-empirical model for "S" shape axial distribution of solid volume concentration (Kwauk *et al*., 1986), we present the phenomenological semi-empirical correlation for collision force as a function of drag force.

$$F_c = F_D \left(1 - K_1\right) \tag{4.35}$$

Where K_1 is the coefficient represents the "S" shaped distribution along the riser height, which can be written as;

$$K_1 = A + \tan^{-1}\left(\frac{H - z_i}{B}\right) / C \tag{4.36}$$

Where A, B, and C are the coefficient which can be adjusted to fit the experiment data. The constants A, B, and C are the function of the operating conditions, physical and hydrodynamic properties of phases. The formulation of the function K_1 is similar to that proposed by Kwauk *et al*., 1986 for "S" shape distribution of the solid volume fraction.

4.5 Problem Closure

For continuous prediction of axial and radial non-uniform distribution of phases, a mechanistic model is proposed for radial non-uniform distribution of phases. By using cross-sectioned average flow properties (uniform flow) modeling approach, the axial non-uniform distribution of the gas and solid phase can be determined from Equation (4.1) to (4.4) and (4.6) by integrating the phase properties over a cross-section. The proposed model has 11 unknowns namely, average solid volume fraction $\bar{\alpha}_s$, solid volume fraction at center of riser α_{s0}, solid volume fraction at wall α_{sw}, average particle velocity $\bar{u}_s$, particle velocity at center of riser u_{s0}, particle velocity at wall u_{sw}, average gas velocity $\bar{u}_g$, gas velocity at center of riser u_{g0}, gas velocity at wall u_{gw}, average pressure P, and average gas density ρ_g, which can be determined by solving governing Equations (4.1) to (4.4), (4.6), (4.16), (4.21), (4.25), (4.27), (4.28), and (4.29).

4.6 Results and Discussion

In this section, the proposed continuous model for axial and radial nonuniform distribution of gas-solids transport properties was validated by comparing model predictions against literature experimental data for both axial and radial evolution of phase transport properties. The model was calibrated for axial predictions by comparing model predictions for cross-sectional averaged solids volume fraction and pressure gradient against experiment data. From model predictions, the core-wall boundary and particle back-mixing mass flux were calculated and analyzed. The core-regime radius was determined as a radial location where the slope of radial particle velocity distribution is zero (excluding the center of the riser) i.e., a radial location at any cross-section of riser where the radial particle velocity changes its direction. Together with the core-wall regime area determination, the solids mass flow rates in the core and wall regime are equally important for the understanding of riser transportation. The back-mixing of the particle from wall regime was determined by mass-balance of particles in core-regime. The back-mixing of the particle is presented as back-mixing ratio, which is defined as the ration of the solids mass flow rate in the wall regime to the net mass flow rate of solids.

4.6.1 Inlet Conditions

To solve the foregoing system of governing equations requires appropriately prescribed inlet (boundary) conditions. We set proper inlet condition as follow. At riser inlet, we assumed uniform flow for the particle phase, while used nonuniform conditions for gas phase. The centerline velocity for gas phase was determined from power law model for turbulent flow through pipe. At a given inlet pressure P_o, the inlet catalyst volume

fraction was estimated so that the resulting pressure at the riser exit would reasonably agree with the measurements. The detailed formulations of all radial transport coefficients for gas-solids phase are essential for radial phase transfer. The focus of this study is to lay down the modeling approach for axial and radial nonuniform distribution of gas-solid transport properties in risers. At this stage, the radial transport coefficients for gas-solids phase were presumed to predict appropriate axial and radial distribution of transport properties. The detailed formulation for radial transport coefficients can be carried out as a separate study in future.

4.6.2 Model Validation

The proposed continuous model was validated for axial distribution of solid volume fraction and pressure gradient against literature experiment data. As a demonstrative case study the operation conditions of experiment data and transport coefficients are listed in Table 4.7.

Table 4.7 Riser Operation Condition and Model Inputs

Case	Pugsley and Berruti, 1996
Particle Type	Glass beads
Particle diameter (μm)	76
Particle density (kg/m^3)	1712
Solid mass flux (kg/m^2s)	489
Superficial gas velocity (m/s)	5.2
Inlet pressure (atm)	2.5
Riser Diameter (m)	0.1
Riser Height (m)	6.4
D_{Ds} (m^2/s)	0.01
K_{sT}	0.01
D_{Dg} (m^2/s)	0.001
K_{gT}	0.001
X_{sT}	0.5
X_{sD}	0.001
X_{gT}	0.05
X_{gD}	0.001
K	0.005
B_3	1.0
K_1	0.001

Source: T. S. Pugsley and F. Berruti, "A predictive hydrodynamic model for circulating fluidized bed risers", *Powder Technology*, 89, pp.57-69, 1996.

As a part of model validation, the model predictions of axial distribution of solid volume fraction for experiment conditions of (Pugsley and Berruti, 1996) were compared against same experiment data, which is shown in Figure 4.12.

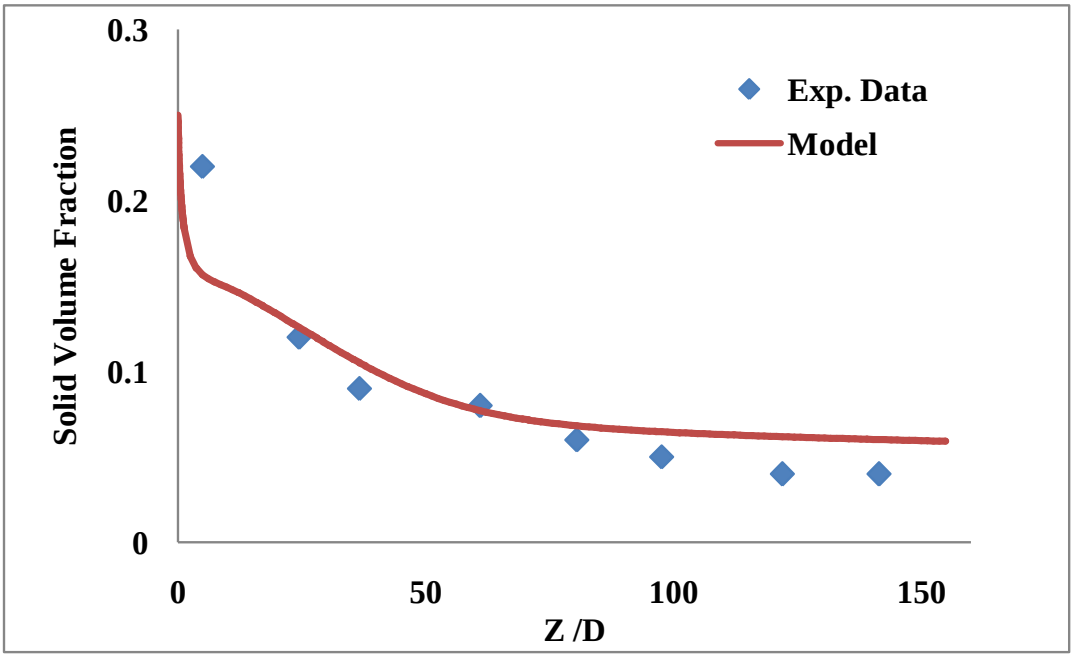

Figure 4.12 Model predictions of solid volume fraction against experiment data (Pugsley and Berruti, 1996).

The proposed model predictions of solid volume fraction reasonably agree with experiment data along the entire riser height, especially in the dense phase regime. The proposed model, which includes both radial nonuniformity and particle backflow, reasonably predicts the solid volume fraction distribution in dense, acceleration and dilute phase transport regime. The volume fraction in the bottom dense phase regime is much higher than any other part of the riser due to inter-particle collision, which restricts the particle acceleration and back-flow of the particles from the wall regime. The particles are then accelerated when solid volume fraction reduces below 0.13 (Zhu *et al.*, 2007), and reaches to steady state condition in dilute phase transport regime at the top of the reiser. The model also predicts "S" shape axial distribution of solid volume fraction for high flux riser as shown in Figure 4.12.

The model prediction of axial distribution of pressure gradient is also compared against experiment data (Knowlton, 1995), which is shown in Figure 4.13.

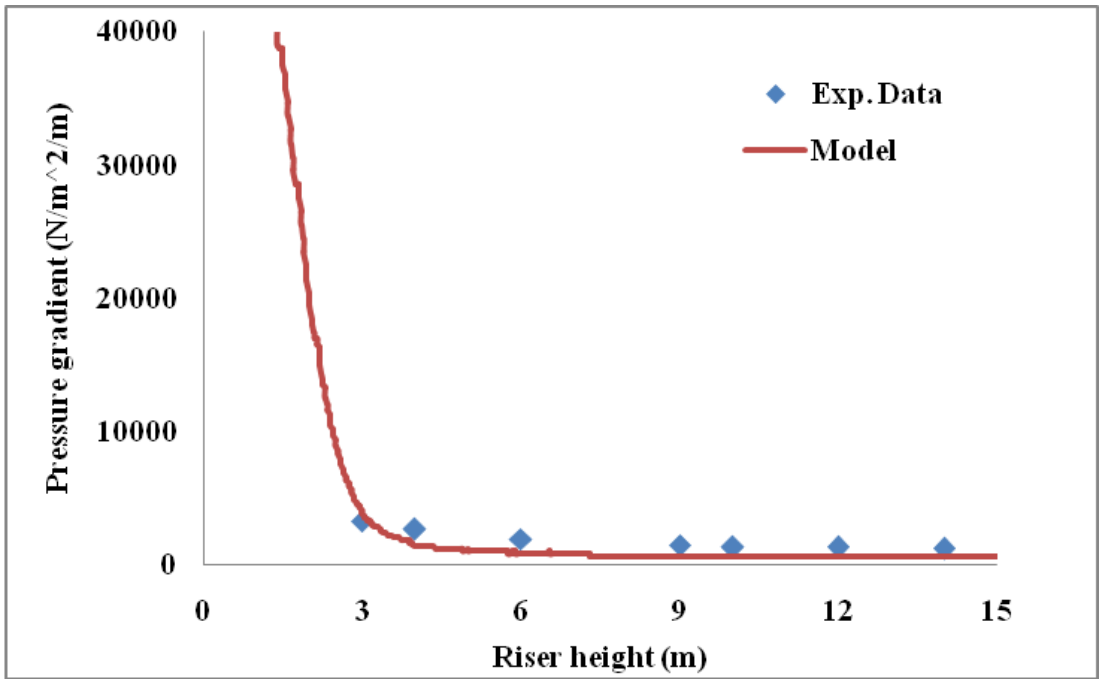

Figure 4.13 Model predictions of axial pressure gradient against experiment data (Knowlton, 1995).

The model prediction reasonably matches with the experiment data of pressure gradient along the entire riser. The pressure drop in the bottom dense phase regime is the highest, which is due to intensive energy dissipation due to strong inter-particle collision in this regime. While the pressure drop into the top dilute regime of the riser is very small, where the pressure drop is only due to the friction between the riser wall and gas/solid phase and the pressure loss due to inter-particle collision is null due to very dilute solid volume fraction in this regime.

Figure 4.14 shows the dimensionless core radius along the riser height. The dimensionless core radius is defined as the ratio of the core radius to the riser radius. The

results show that the core radius increases marginally along the riser height i.e., the wall regime area reduces along the riser height. For the case under the study, the dimensionless core radius is around 0.65. In the bottom dense phase regime of the riser, due to the up-flow of high volume fraction particles against down-flow of particles in the wall regime, the core radius reduces initially and then steadily increases along the riser height.

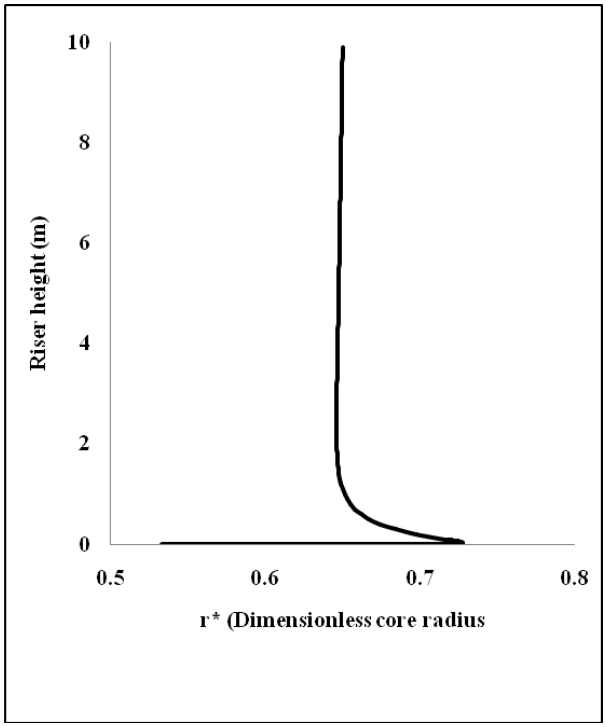

Figure 4.14 Dimensionless core radius along the riser height.

Figure 4.15 shows the results of backmixing ratio estimation along the riser height. The back-mixing ration is defined as the ration of the flow rate of particles in the wall regime to the net flow rate of particles. The results shows that, initialy for some length of the riser, there is a back-mixing of particles from the wall to core regime, which

is shown as the negative back-mixing ratio. The pisitive back-mixinf ratio alog the riser height shows the radial transfer of particles from the core to wall regime. In the top dilute regime of the riser the back-mixing ratio is almost remaining constant. The back-mixing ratio is very useful parameter to decide the radial transfer of particles from the core-to-wall regime or vice versa.

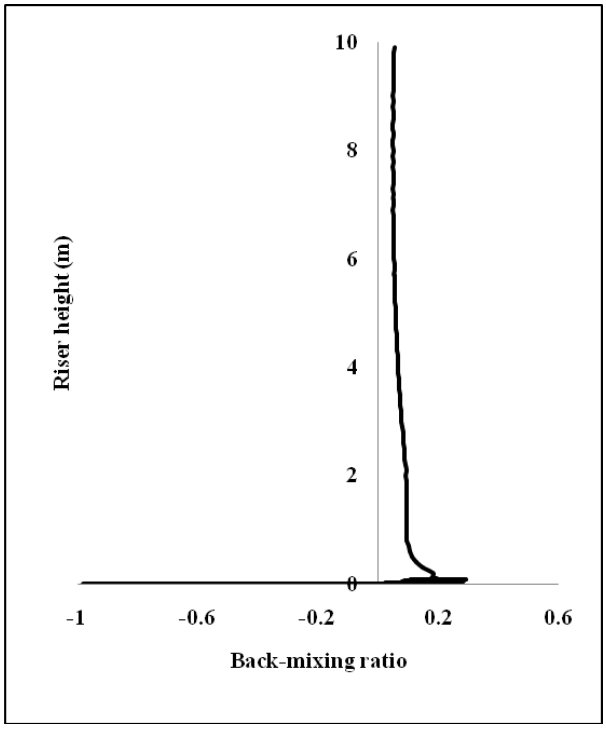

Figure 4.15 Backmixing ratio along the riser height.

4.7 Summary of Chapter

1. A contineous modeling approach has been proposed for one-dimensional axial non-uniform distribution of the gas-solds transport properties taking into the account the radial nonuniform distribution of phase transport properties.

2. The radial nonunifrom distributions of the phases were approximated by the 3rd order polynomial distribution, which is supported by the 3rd order polynial fit for experiment data of rdial phase distribution.

3. The mechanism for radial nonuniform distribution of the phases is discussed and based on which a mechanistic model for radial nonuniform phase distribution is proposed for problem closure.

4. The proposed model is validated for axial distribution of solid volume fraction and pressure gradient against the literature data.

5. A demonstrative case study is also shown to represent the model estimation of the core regime radius along the riser height and particle radiadial mass transfer in terms of the back-mixing ratio.

6. The future direction from this study should be towards the determination of transport coefficient and use of proposed model for riser reaction model to identify the core-wall boundary and to identify the motion of fresh/deactivating or deactivated catalyst.

CHAPTER 5

HYDRODYNAMICS AND REACTION CHARACTERISTICS IN SPRAY INJECTION REGIME OF RISER REACTOR

5.1 Problem Statement and Challenges

Injection of liquid spray into a hot gas-solids fluidized bed has been used widely in many industrial processes such as fluidized catalytic cracking (FCC), polyethylene synthesis, and spray-assisted coal gasification etc. In FCC process, the liquid hydrocarbon feed (VGO) is injected into the dense cross-flow of hot gas-solids flow through the multiple feed injection nozzles. The schematic representation of the feed injection regime with single ring of multiple nozzles is shown in Figure 5.1. With the injection of high-momentum spray jet into a cross flow of hot gas-solids flow, the collision of high momentum cold droplets with hot catalyst particles promote strong momentum transfer which affects the spray hydrodynamics such as penetration of spray jet and scattering. The collision of the droplets with the hot catalysts also causes a significant heat transfer resulting in a rapid vaporization of the droplets as well as significant cooling of the catalysts. The rapid vaporization of feed droplets results in three phase flow (catalyst, liquid hydrocarbons, and vapor hydrocarbons) along the spray trajectory. With the vaporization of feed oil (VGO), the cracking reaction starts in which, heavy molecules of oil vapor is cracked into the useful light molecules e.g., Gasoline and other petro-chemical feed-stocks. Part of ambient solids can penetrate through the spray regime by convection, where they collide with droplets in the spray region. Whereas some part of ambient solids either flow around the spray region or enter the spray region by entrainment.

The collision between droplets and cross-flowing solids and drag force by gas convection causes considerable bending of spry jet along spray trajectory. While bending of the gas-vapor mixture is caused by ambient gas-solids flow around the gas-vapor mixture in spray regime. The bending of spray jet and the gas jet is quite different due to difference in momentum of gas and droplet phase, which is shown in Figure 5.1. In the inertial regime, the jet momentum is significantly reduced and the hydrocarbon vapor in this regime is carried by the cross-flowing ambient solids and so the jet does not follow its characteristics in this regime.

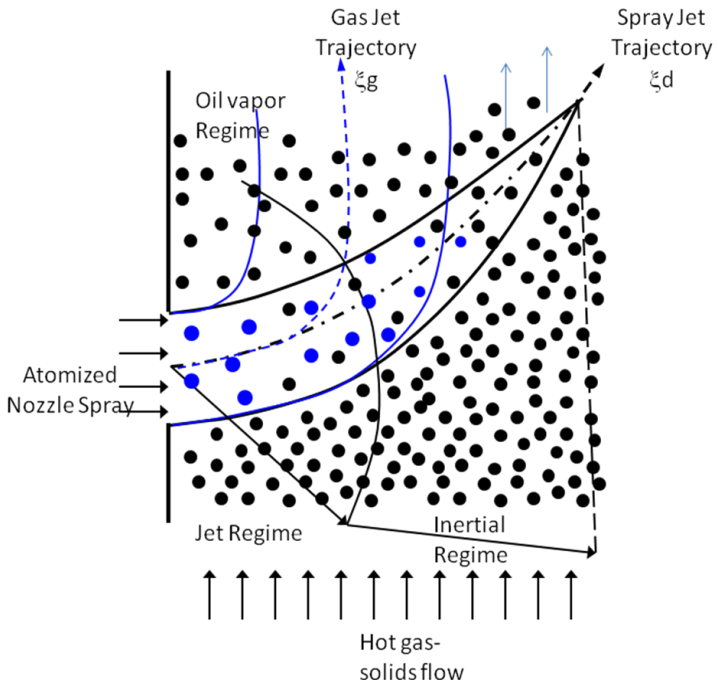

Figure 5.1 Interaction between evaporating jet and cross-flow of hot gas and solids in FCC riser reactor.

The cross-flow convection of ambient gas-solids flow also digress part of vapor-gas mixture from spray region. The cracking of digressed hydrocarbon vapor is much higher than along spray jet due to high solid volume fraction, high temperature of catalyst

and very low velocity of solids and hydrocarbon feed in ambient fluidized. The process of feed vaporization in the feed injection regime is important in determining performance of FCC unit, even dominating the product distribution and quality (e.g., Gupta and Rao, 2003; Chen, 2006). The conversion of VGO into useful product (gasoline) occurs as soon as the liquid feed spray vaporizes. A significant portion of cracking occurs in the ambient fluidized bed, above spray regime, where escaped hydrocarbon vapor from spray regime contact with hot catalyst. The cracking reaction is highest in this regime as the catalysts are fresh and its temperature is highest. In case of multiple feed injection nozzles, due to very high momentum of the spray jet, the jet profiles overlaps in the center of the riser. In this study, eight feed injection nozzles were used to study the reaction and hydrodynamics in the feed injection regime. For simplicity, the overlapping of the four spray jets is shown in Figure 5.2. In the overlapping regime, the feed droplets coming from the individual jets vaporize and intensive reaction occurs in this regime.

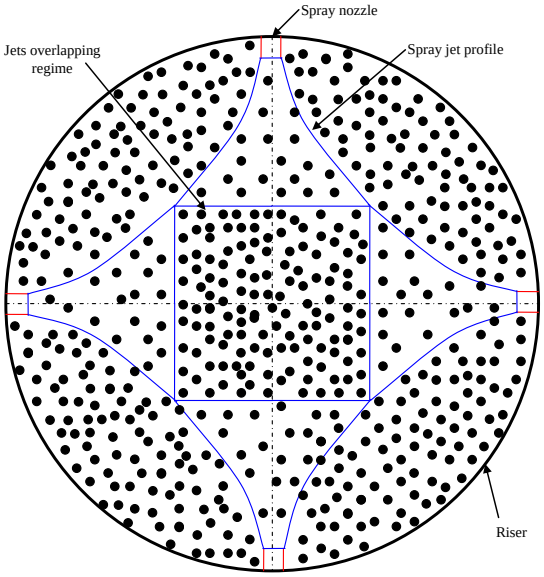

Figure 5.2 Schematic representations of multiple jets overlapping in feed injection regime of FCC reactor.

As the mixture moves along the riser after completion of the feedstock vaporization, becomes a two phase flow (catalyst and vapor hydrocarbons) in the main body of the riser reactor. With today's high-activity catalysts, the contact time in the FCC riser has been shortened significantly over the years, thus the feed injection zone plays an increasingly important role in determining the FCC riser performance. Despite this little if any work has been done on the investigation of the transition from a vapor-liquid-solid spray flow to a vapor-solid flow and reaction in this regime. Due to the lake of information on the reaction in the feed injection regime, most published literature model for FCC riser reactor are based on the assumption of instantaneous vaporization or no catalytic reaction in the feed injection regime. Hence, the understating of three phase interaction, heat transfer, vaporization and reaction in the this regime is very important to determine the actual performance of the riser reactor in terms of the input boundary conditions for existing riser reactor model.

Research endeavor has been made for better understanding of hydrodynamics of evaporating spray jet into gas-solids fluidized beds by conducting experiments, theoretical modeling, and numerical simulation of process. The literature review related to the development of single and multiphase evaporating spray jets is given in Chapter 2. It is concluded from the literature review that, the literature models may be inadequate for simulating complex three phase flows along spray jet regime in cross-flow fluidized beds at high solids flux, for handling droplet-particles collisions and other interactions in the dense phase regime of solid transport. In absence of credible hydrodynamics-coupled-reaction models, models for droplet-particle collision dominated heat transfer and droplet vaporization, and interaction between spray jet and cross-flow gas-solids flows, the

applicability of such models are in questions. Even for simple process model, due to large number of lumps for reaction kinetics and complex three phase flow, a full-scale CFD simulation require tremendous computational time and resources.

The literature review in the Chapter 2 shows that, there have been no systematic studies for the reaction-hydrodynamics coupling in a vaporizing spray jet penetrating into hot gas-solids flows. This is hardly surprising given the complexity of the problem, which involves transfers of momentum, heat and mass transfer in a three-phase interacting system that is coupled with catalyst-influenced cracking reaction. Due to the lack of information on the extent of cracking reactions in the feed injection zone, previous investigators on FCC reactor models neglect this regime and assume instantaneous vaporization of feed droplets (Zhu *et al.*, 2010). However, the validity of this assumption has not been established. The reactions in the feed injection zone are believed to be significant and should not be ignored without justification. After all, within the feed injection regime, the temperature of catalyst and feed concentration both are both highest and the catalyst has the highest activity. Cracking reactions inside this regime are expected to affect the vapor composition, volume fractions and catalyst activity, which in turn influence the spray penetration behavior.

Against above backdrop, in this study, we proposed a mechanistic model that gives a quantitative understanding of the interplay of three phase flow hydrodynamics, heat/mass transfer, vaporization and cracking reactions in the feed injection zone of a fluid catalytic cracking (FCC) riser reactor. The major objectives of the proposed study are: to predict the multiphase flow hydrodynamics coupled with reaction characteristics along the jet trajectory, the reaction in ambient gas-solids fluidized bed in presence of

hydrocarbon vapor escaped from spray regime, the cross-section averaged hydrodynamics and reaction properties of phases at the end of multiple nozzles feed injection regime. The model has three main components: (1) hydrodynamics and reaction characteristics of single evaporating nozzle spray jet in cross-flow of hot gas-solids fluidized bed with gas and solids entrainment; (2) Cracking of hydrocarbon vapor in ambient fluidized bed (3) Cross-section averaging of hydrodynamics properties of three phase flow and molar concentration of lumps of hydrocarbon vapor. The catalytic cracking reaction is represented by a simple four-lump reaction model, while the ambient gas-solids transport is represented by a dense-phase riser flow. The emphasis is on the effects of chemical reactions on the behavior of a vaporizing liquid spray penetrating into a high-temperature gas-solids flow. The proposed model takes into account gas and particles entrainment in to the jet; collision dominated heat transfer between droplets and particles and interaction between local flow hydrodynamics and reaction kinetics, bending of spray jet due to cross-convection and gas drag, and partition function for escape of gas-vapor mixture from spray jet. The cracking of hydrocarbon feed along the spray jet and into the ambient fluidized bed was reasonably modeled. The governing equations are based on the conservation of mass, momentum and energy in all three phases. The cross-section averaged hydrodynamics and reaction characteristics were calculated and analyzed at the end of feed injection regime.

5.2 Modeling Approach

The detailed modeling of multiphase flow hydrodynamics and coupled reaction characteristics of feed injection regime of FCC riser is very complicated due to

heterogeneous gas-solid-liquid flow structure, intensive momentum exchange between phases, heat and mass transfer, endothermic reactions, etc. In case of multiple spray jet injection into the hot cross-flowing gas-solids flow, there is overlapping of the jets trajectories at the center of the riser reactor, due to high initial momentum of the spray jet. A schematic diagram of overlapping of four spray jets is shown in Figure 5.2.

Conceptually, the feed injection regime can be divided into the three regimes, a spray jet regime, oil vapor regime and jet overlapping regime. The hydrodynamics and reaction characteristics in these three regimes are completely different. To find the average hydrodynamics properties of phases and reaction characteristics at the end of the feed injection regime, this study is divided into four parts: 1) modeling of hydrodynamics of three phase flow and reaction kinetics along a single spray jet 2) modeling of the reaction and hydrodynamics of two-phase flow in the vapor regime of fluidized bed 3) modeling of reaction characteristics in the overlapping regime and finally 4) cross-section averaging of hydrodynamics and reaction characteristics at the end of the feed injection regime.

5.2.1 Hydrodynamics and Reaction Kinetics of Single Spray Jet

Let's consider a single nozzle vapor-droplets jet that is injected into the dense mixing zone of an FCC riser with an injection angle of θ_j, where it interacts with hot gas-solids suspension flow, as shown in Figure 5.3.

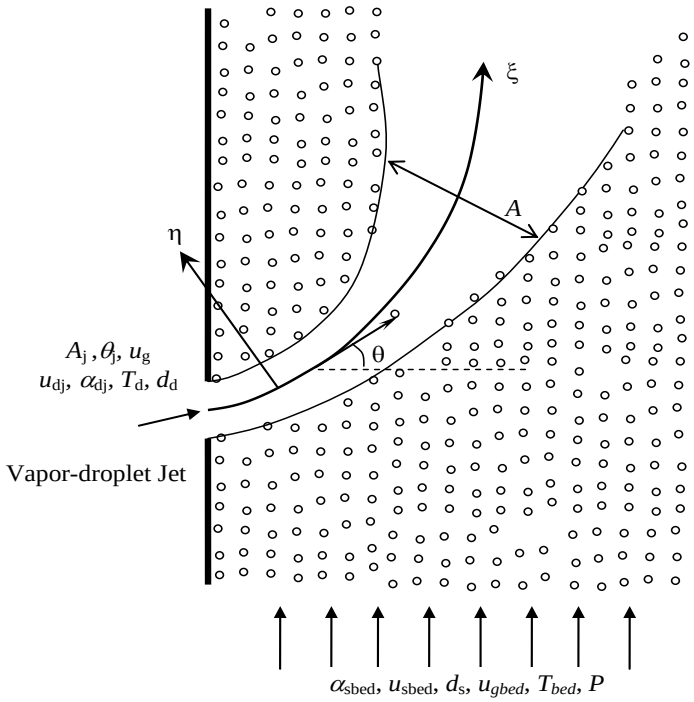

Figure 5.3 Schematic diagram of spray jet into gas-solids riser flow.

The detailed modeling of coupled characteristics of evaporating jet flow hydrodynamics and reaction kinetics in the mixing zone of the riser is very complicated due to heterogeneous gas-solid-liquid flow structure, intensive momentum exchange between phases, heat and mass transfer, endothermic reactions, etc. Some simplifying assumptions are made while capturing the salient features of the system. It is assumed that a thermal equilibrium is maintained between hot particles and carrying gas in the ambient gas-solids flow. In the jet region, the vapor phase behaves like an ideal gas. The centerline trajectory of gas-vapor mixture always coincides with the centerline of the liquid spray. In addition, the spray jet trajectory is assumed to be symmetric to the centerline spray jet. To further simplify the problem, the effects of gravity, surface wall, as well as size distributions of solids and droplets are neglected. Heat transfer between

gas and particles follows a lumped heat capacity model**,** while heat transfer between particles and droplets occurs only by solid-droplet collision**,** where particles are assumed to be attached with droplets upon collision. In case of multi-jet injection, it is assumed that, the jet profiles never overlaps. Thermo-physical properties of parameters are constants. Each-spray jet will have identical hydrodynamics and reaction characteristics along spray jet. The average hydrodynamic and reaction characteristics at the end of feed injection regime can be found by simply averaging individual properties in cross-section area of spray jet and remaining riser area over riser cross-section.

5.2.1.1 Transport Equations for Spray Jet. The governing equations for describing the hydrodynamics of the three-phase flow in feed injection zone involves dynamic interactions among phases via the strong coupling of momentum, heat and mass transfer. The phase trajectory and mixing characteristics in the jet region can be described using a deterministic Lagrangian trajectory approach represented by a (ξ,η) coordinate system along the centerline of the jet, as shown in Figure 5.3. All phases are assumed to be moving along the ξ direction inside the jet mixing region, while the ambient gas and solids are engulfed into the mixing stream by jet entrainment.

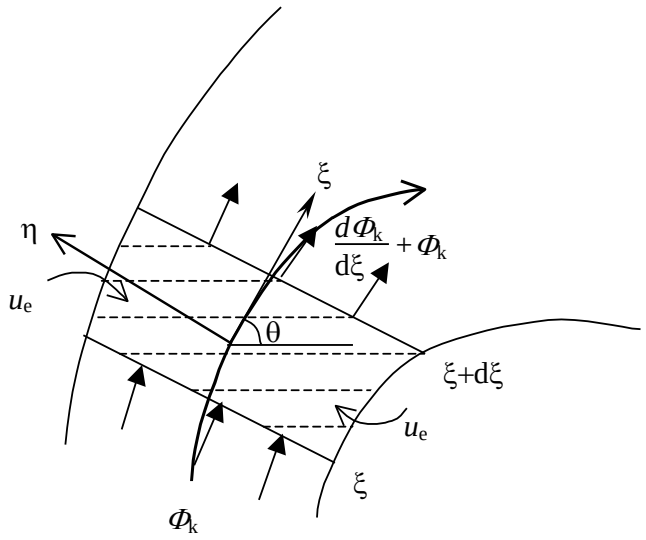

Figure 5.4 Schematic diagram of control volume of jet trajectory.

Based on the mass, momentum, and energy balance over a control volume in the (ξ, η) coordinates, as shown in Figure 5.4, the governing equations for each phase can be written in differential forms. It is noted that, due to the assumption of the identical flow centerline of each phase in the mixing region, only one momentum equation in the η direction is independent. The most representative η-momentum equation should be selected from the phase in which the inertia effect is the least among the three phases. Hence, in the following, the η-momentum equation for the gas-vapor mixture is used to define the bending of the centerline of jet trajectory.

5.2.1.1.1 Deflection angle of Spray Jet. The deflection of the spray jet is due to the increasing in its η-component momentum by the ambient gas-solids entrainment, penetration as well as drag forces from the gas-solids flow around the jet. The deflection of jet in the ξ direction can be expressed by a ratio of η-component momentum to its total momentum.

$$\frac{d\theta}{d\xi}=\frac{n_d\left(3\pi\mu d_d u_{g\infty}\sin\theta\right)A}{\left(\alpha_g\rho_g u_g^2+\alpha_d\rho_d u_d^2+\alpha_s\rho_s u_s^2\right)A}+\frac{\alpha_{s\infty}\rho_s\left(u_{s\infty}\sin\theta\right)^2 l}{\left(\alpha_g\rho_g u_g^3+\alpha_d\rho_d u_d^3+\alpha_s\rho_s u_s^3\right)A} \tag{5.1}$$

Where, the first term on the right hand side represents the increase in η-component momentum due to gas-solids entrainment and diffusive penetration; the second term represents the effect of drag force on jet trajectory due to gas-solids flow around the jet.

5.2.1.1.2 Vapor-gas Phase. The continuity equation based on mass balance of gas entrainment rate across jet boundary, gas diffusion rate from jet due to convection and vapor generation rate by droplet evaporation over a control volume along ξ-direction, which can be written as;

$$\frac{d}{d\xi}\left(\alpha_g\rho_g u_g A\right)=\dot{m}_{ge}l_e+\dot{m}_v A-\gamma\alpha_g\rho_g u_g l \tag{5.2}$$

where the terms on the right hand side represent the contribution of entrainment, the droplet evaporation rate, and the gas diffusion rate from the jet area which is expressed as a partition function γ of the total gas mass flow rate through the jet respectively.

The momentum equation for vapor phase is derived by a force balance over cross section of jet along ξ-direction as shown in Figure 5.4.

$$\frac{d}{d\xi}\left(\alpha_g\rho_g u_g^2 A\right)=\dot{m}_v u_d A+\dot{m}_{ge}u_{ge}l_e\cos\theta-\gamma\,\alpha_g\rho_g u_g^2 l-\left(F_{Dd}+F_{Ds}\right)A \tag{5.3}$$

where the four terms on the right hand side represent the momentum change due to drop vaporization, gas entrainment, gas diffusion from jet and drag forces on droplets and solids which are denoted as F_{Dd} and F_{Ds}, respectively.

The thermal energy equation is derived from the energy exchange between gas and liquid-solid phase over a control volume. The energy balance over the control volume can be written as;

$$\frac{d}{d\xi}\left(\alpha_g \rho_g u_g C_{pg} T_g A\right) = \dot{m}_{ge} l_e C_{pg} T_{bed} - \gamma \alpha_g \rho_g u_g C_{pg} T_g l + \dot{m}_v LA + \left(E_{Cs} - E_{Cd}\right) A - E_R \tag{5.4}$$

where the five terms on right hand side represent the heat transfer due to gas entrainment, gas diffusion from the jet area, droplet vaporization, convective heat transfer with solids and droplet, and heat absorption for endothermic reaction, respectively.

5.2.1.1.3 Droplet Phase. Note that the spray of fast vaporizing liquid drops vaporizes inside the jet mixing zone. The continuity equation is based on the fact that the mass flow rate of droplet decreases due to the vaporization along the ξ direction, which can be described as follows;

$$\frac{d}{d\xi}\left(\alpha_d \rho_d u_d A\right) = -\dot{m}_v A \tag{5.5}$$

The momentum equation for droplet phase is derived from the ξ-component of force balance over a control volume among the increase rate of droplet momentum flow,

interfacial forces between droplets and the gaseous mixture, solids-droplets collision, and the momentum transfer due to droplet vaporization as shown in Figure 5.4, which leads to;

$$\frac{d}{d\xi}\left(\alpha_d \rho_d u_d^2 A\right) = -\dot{m}_v u_d A + \left(F_{Dd} - F_{Cds}\right) A \tag{5.6}$$

where F_{Dd} and F_{Cds} represents respectively, the drag force between gas and droplet and solids-droplets collision force.

The thermal energy equation for droplet phase is derived from the balance of energy exchange between droplet and gas-solids phase over a control volume as shown in Figure 5.4.

$$\frac{d}{d\xi}\left(\alpha_d \rho_d u_d C_{pd} T_d A\right) = E_{Cds} + E_{Cd} - \dot{m}_v L.A + E_{Rad} \tag{5.7}$$

The terms on right-hand side represent the convective heat transfer from the gaseous mixture, the heat transfer from particles by collision, latent heat released due to droplet vaporization, and radiative heat transfer from ambient solid particles, respectively.

5.2.1.1.4 Solids Phase. It is assumed that particles enter the mixing region only by jet entrainment and diffusion-induced penetration and that all entrained particles flow along the ξ-direction. Thus the mass conservation equations can be written as;

$$\frac{d}{d\xi}\left(\alpha_s u_s \rho_s A\right) = \dot{m}_{se} l_e + \dot{m}_{sp} D_d \tag{5.8}$$

The corresponding momentum equation is derived from the force balance of the ξ-component over a control volume as shown in Figure 5.4.

$$\frac{d}{d\xi}\left(\alpha_s \rho_s u_s^2 A\right) = (\dot{m}_{se} l_e + \dot{m}_{sp} D_d) u_{se} \cos\theta + \left(F_{Ds} + F_{Cds}\right) A \tag{5.9}$$

The terms on the right-hand side represent, respectively, the momentum transfer by entrained particles, interfacial forces from the gaseous mixture, and momentum changes due to droplet-solids collision.

The energy equation for the solid phase is derived from the energy balance between solid and gas-liquid phases over a control volume as shown in Figure 5.4.

$$\frac{d}{d\xi}(\alpha_s \rho_s u_s C_{ps} T_s A) = -E_{Cds} - E_{cs} + (\dot{m}_{se} l_e + \dot{m}_{sp} D_d) C_{ps} T_{bed} \tag{5.10}$$

The terms on the right-hand side represent, respectively, heat transfer by droplet-solids collision, convection heat transfer between solid and gaseous mixture and heat transfer due to entrainment and convection of the particle into the jet regime.

5.2.1.2 Reaction Kinetics and Feed Component Mass Balance. Here we adopted a simple four-lumped reaction scheme (Lee *et al.*, 1989) to describe cracking reactions. In typical FCC riser reactors, steam is injected upstream of the feed injection zone to help

disperse the catalyst. While the impact of steam is still important for the hydrodynamics in the spray region, its impact for kinetics and component mass balance can be ignored. This is due to the extremely low molecular weight of steam with respect to that of the oil vapor. The cracking reaction network used here is simplified four hydrocarbon lumps. As shown in Figure 5.3, VGO is simultaneously cracked into gasoline, light gases, and coke as primary reactions, which are second order. Due to the high temperatures, gasoline is further cracked to coke and gases. These secondary reactions are first order.

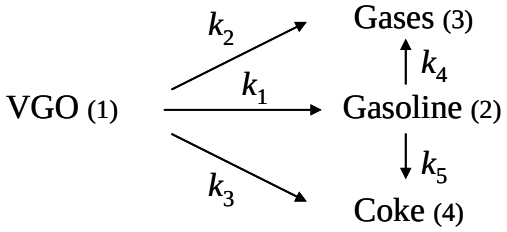

Figure 5.5 Four-Lump model for gas oil cracking.

The component mass balance equations for each chemical lump as well as steam can be written as follows;

VGO:

$$\frac{d}{d\xi}(C_1 u_g A) = -\Phi_s \left(k_1 + k_2 + k_3\right) C_1^{\,2} A + \frac{\dot{m}_v A}{M_1} - \gamma C_1 u_g l \tag{5.11}$$

Gasoline:

$$\frac{d}{d\xi}(C_2 u_g A) = \Phi_s \left(\frac{M_1}{M_2} k_1 C_1^{\,2} - (k_4 + k_5) C_2 \right) A - \gamma C_2 u_g l \tag{5.12}$$

Light Gases:

$$\frac{d}{d\xi}(C_3 u_g A) = \Phi_s \left(\frac{M_1}{M_3} k_2 C_1^{\,2} + \frac{M_2}{M_3} k_4 C_2 \right) A - \gamma C_3 u_g l \tag{5.13}$$

Coke:

$$\frac{d}{d\xi}(C_4 u_g A) = \Phi_s \left(\frac{M_1}{M_4} k_3 C_1^{\,2} + \frac{M_2}{M_4} k_5 C_2 \right) A - \gamma C_4 u_g l \tag{5.14}$$

Steam:

$$\frac{d}{d\xi}(C_5 u_g A) = \frac{\dot{m}_{ge} l_e}{M_5} - \gamma C_5 u_g l \tag{5.15}$$

The reaction rate constants (k_i's) were taken from Ref. (Zhu *et al*., 2010, Han and Chung, 2001), which rate given in Tables 5.1 & 5.2.

Table 5.1 Catalyst and Feed Oil Properties

Operation parameters and properties		Case 1	Case 2
Catalyst diameter (μm)		70	75
Inlet riser pressure (atm)		2.9	3.15
Catalyst density (kg/m^3)		1800	1800
Gas specific heat (J/kg-K)		3299	3299
Liquid specific heat (J/kg-K)		2671	2671
Catalyst specific heat (J/kg-K)		1150	
Molecular weight (kg/kmol)	VGO	400	
	Gasoline	100	
	Gas	50	
	Coke	400	

Table 5.2 Heat of Reaction, Pre-exponential Factor, and Activation Energy

Cracking Reaction	ΔH_i kJ/kg	k_{io} g oil/(s · g cat)	E kJ/kmol
VGO → Gasoline	195	1457.5	57359
VGO → Light Gases	670	127.59	52754
VGO → Coke	745	1.98	31830
Gasoline → Light Gases	530	256.81	65733
Gasoline → Coke	690	0.022	66570

The reaction rate constants (k_i's) can be written as according to (Zhu *et al.*, 2011, Han and Chung, 2001).

$$k_i = \bar{k}_{i0} CTO \exp\left(-\frac{E_i}{RT_i}\right) \tag{5.15-1}$$

Here CTO is local catalyst-to-oil ratio along the spray jet, which can be expressed as;

$$CTO = \frac{\alpha_s \rho_s u_s}{\alpha_g \rho_g u_g} \tag{5.15-2}$$

Note that the pre-exponential factor ($\bar{k}_{io}$) is molar-based, which can be expressed in terms of mass-based pre-exponential factors (k_{io}) by the following expression;

$$\bar{k}_{io} = \left(\frac{M_i}{\alpha_g \rho_g}\right) k_{io} \tag{5.15-3}$$

The parameter Φ_s represent the decay of catalyst activity due to coke deposition. Following (Pitault *et al.,* 1994), we set

$$\Phi_s = \frac{A+1}{A+\exp(BC_c)} \tag{5.15-4}$$

where A and B are deactivation constants, taken as 4.29 and 10.4, respectively and C_c is the concentration of coke (weight percent) on catalyst.

5.2.2 Hydrodynamics and Reaction Kinetics of Oil Vapor Regime

5.2.2.1 Hydrodynamics of Gas-solids Flow. The oil vapor regime is located just above the spray jet as shown in Figure 5.1, where the hydrocarbon vapor escaped from the spray jet will be cracked into the useful product. The catalytic cracking of hydrocarbon vapor in this regime will cause dilution of catalyst concentration by acceleration, catalyst cooling due to endothermic reactions and catalyst acceleration due to vapor expansion during cracking process. For modeling of hydrodynamics of gas-solids flow and reaction kinetics in oil vapor regime, the vapor regime is divided into number of small channels as shown in Figure 5.6, and each channel behaves like a small reactor. The cracking inside the channel will cause catalyst dilution and cooling.

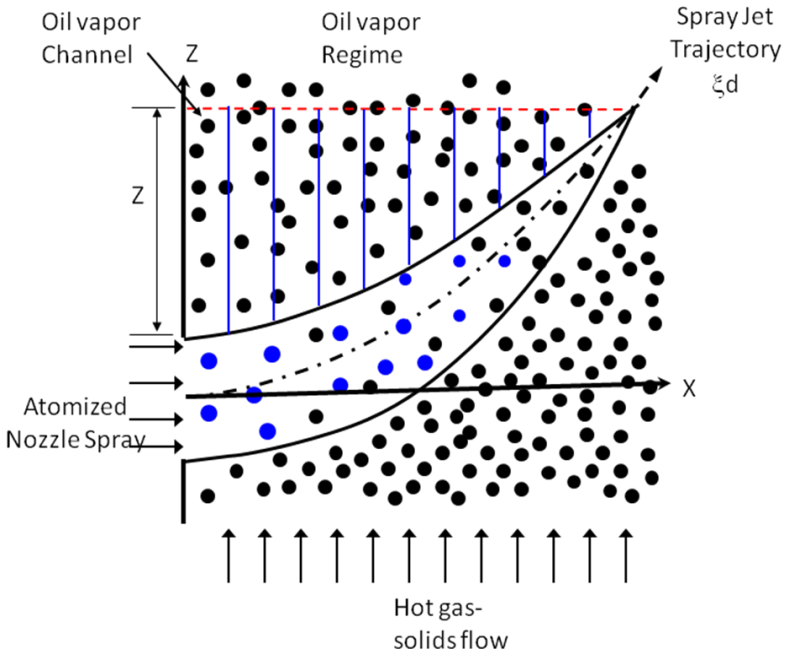

Figure 5.6 Channeling concept for modeling of hydrodynamics and reaction in oil vapor regime.

The following simplifying assumptions are made. Thermal equilibrium is maintained between catalyst and hydrocarbon vapor. The cross-section area of each channel is remaining constant. The hydrocarbon feed behaves like ideal gas. In this study, the modeling approach proposed by Zhu *et al.*, 2011 is adopted for hydrodynamics and reaction kinetics of each channel.

The overall mass balance of the gas phase is given by;

$$\frac{d\left(\alpha_g \rho_g U_g\right)}{dz} = -\left(r_3 + r_5\right) \tag{5.16}$$

The two terms on the right hand side represent the mass loss due to coke formation. The average gas density can be calculated from the ideal gas law as Equation (5.17);

$$\rho_g = \frac{P.\sum_{i=1}^{3}\left(C_i M_i\right)}{RT\sum_{i=1}^{3} C_i} \tag{5.17}$$

The solid phase mass balance is given by;

$$\frac{d(\alpha_s \rho_s U_s)}{dz} = \left(r_3 + r_5\right) \tag{5.18}$$

The gas phase momentum balance can be described as;

$$-\frac{dP}{dz} = \alpha_g \rho_g g + \frac{d\left(\alpha_g \rho_g U_g{}^2\right)}{dz} + F_D \tag{5.19}$$

The drag force per unit volume, F_D, is expressed by a modified Richard-Zaki equation as;

$$F_D = \frac{18\mu}{d_s^2} \cdot \frac{\alpha_s}{(1-\alpha_s)^4} \cdot (U_g - U_s)\xi_1 \tag{5.19-1}$$

Here ξ_1 is a correction factor that accounts for the wake effect of the neighboring particles on the particle-fluid interfacial force.

$$\xi_1 = 1-\left(1-A\right)\exp\left(B.\sqrt[3]{\frac{\pi}{6\alpha_s}} - 1\right) \tag{5.19-2}$$

where A and B are empirical coefficients related to local particle Reynolds number.

The momentum balance for the solid phase can be expressed as;

$$F_D = \alpha_s \rho_s g + \frac{d\left(\alpha_s \rho_s U_s^{\,2}\right)}{dz} + F_c \tag{5.20}$$

where F_c is a collision force that restricts the axial acceleration of solids in the dense phase and acceleration regions. A semi-empirical model for the axial collision force proposed by You *et al.*,2010 is of the form;

$$F_c = (1-\xi_2\xi_3)F_D - (1-\xi_3)\alpha_s \rho_s g \tag{5.20}$$

where ξ_2 and ξ_3 are correction factors representing an S-shaped axial profile of solids volume fraction, which may be estimated by;

$$\xi_2 = 1 - \exp\left(-\left(\frac{\alpha_s + 0.2}{\alpha_{sc}}\right)^2\right) \tag{5.20-1}$$

$$\xi_3 = \frac{0.3}{\pi}\tan^{-1}\left(26 - 100\alpha_s\right) + 0.15 \tag{5.20-2}$$

The overall energy balance equation reads;

$$\left(\alpha_s \rho_s U_s c_{ps} + \alpha_g \rho_g U_g c_{pg}\right)\frac{dT}{dz} + \left(r_3 + r_5\right)\left(c_{ps} - c_{pg}\right)T = -\sum_{i=1}^{5} r_i . \Delta H_i \tag{5.21}$$

where ΔH_i is the heat of reaction for the i^{th} endothermic cracking reaction.

5.2.2.2 Reaction Kinetics and Component Mass Balance. Since the component mass balance involves chemical reactions, we use molar concentrations to account for volume expansion. Based on the reaction scheme shown in Figure 5.1, we have

Gas-oil:

$$U_g \frac{dC_1}{dz} + C_1 \frac{dU_g}{dz} = -\Phi_s (k_1 + k_2 + k_3) C_1^{\,2} \tag{5.22}$$

Gasoline:

$$U_g \frac{dC_2}{dz} + C_2 \frac{dU_g}{dz} = \Phi_s \left(\frac{M_1}{M_2} k_1 C_1^{\,2} - (k_4 + k_5) C_2 \right) \tag{5.23}$$

Light Gases:

$$U_g \frac{dC_3}{dz} + C_3 \frac{dU_g}{dz} = \Phi_s \left(\frac{M_1}{M_3} k_2 C_1^{\,2} + \frac{M_2}{M_3} k_4 C_2 \right) \tag{5.24}$$

Coke:

$$U_g \frac{dC_4}{dz} + C_4 \frac{dU_g}{dz} = \Phi_s \left(\frac{M_1}{M_4} k_3 C_1^{\,2} + \frac{M_2}{M_4} k_5 C_2 \right) \tag{5.25}$$

The reaction rate constants, activation energy, catalyst deactivation functions and catalyst-to-oil ratio (CTO) will follow the same form as discussed in previous section.

5.2.3 Reaction in Overlapping Regime

In case of multiple spray jet injection into the hot cross-flowing gas-solids flow, there is heat and mass transfer, vaporization of feed droplet and cracking reaction along the jet and in the oil vapor regime. Due to the high momentum of the spray jet, there is

overlapping of the jets trajectories at the center of the riser reactor. A schematic diagram of overlapping of four spray jets is shown in Figure 5.7. To simplify the problem, the overlapping regime is defined as the regime at the center of the riser to the jet reference plane, where spray jets overlapping starts, which is shown in the Figure 5.7.

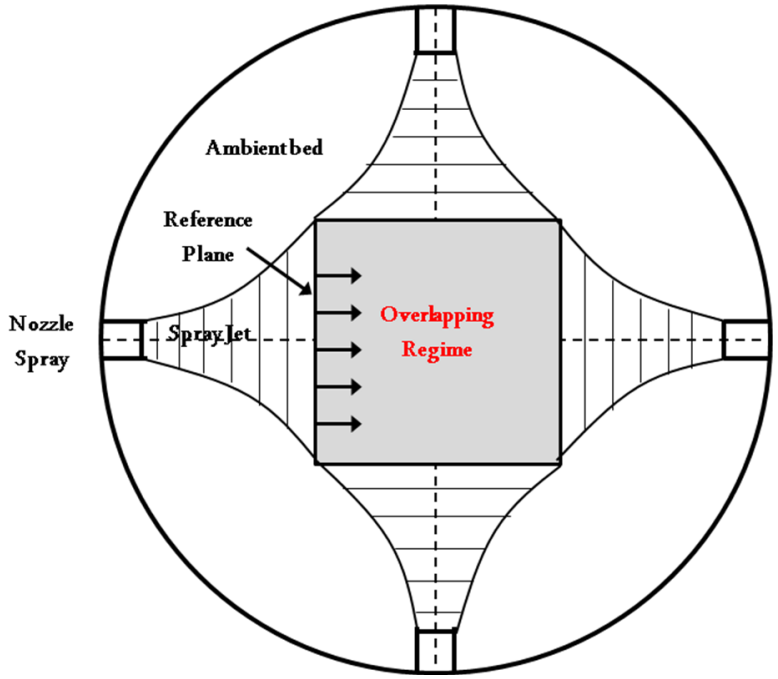

Figure 5.7 Schematic representations of four spray jet interaction with overlapping regime.

To reduce the mathematical complexity it is assumed that, the droplets entering into the overlapping regime from the spray jet (from reference plane as shown in Figure 5.7) will instantly vaporizes into this regime. It is also assume that, the height of the feed injection regime is equivalent to the single jet single jet vertical penetration. The VGO moles generated due to the droplet vaporization and the moles of four lumps entering from the spray jets are uniformly distributed over the overlapping regime. The reaction in the overlapping regime is treated as the single riser reactor of overlapping regime cross-

section area and corresponding height is shown in Figure 5.8. The energy balance is carried out over the overlapping regime to find the average catalyst and feed temperature. The hydrodynamic and reaction characteristics were calculated from riser reactor discussed in the Section 5.2.2.

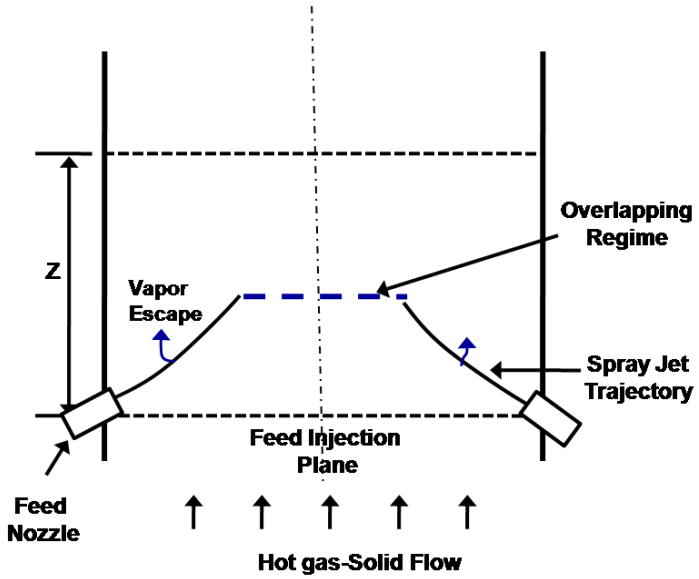

Figure 5.8 Schematic representation of jet overlapping, height of feed injection regime and reference plane for overlapping regime.

The inlet boundary conditions for the reaction in the overlapping regime were calculated from the properties of the droplet and particle phase at reference plane and overlapping regime. Consider a single spray jet with overlapping, similarly there will be other three spray jet sharing the overlapping area which shown by regime 1 in the Figure 5.9. The transport properties of the gas and droplet phase entering the overlapping regime from the spray jet are indicated at reference plane which is numbered 2 in the Figure 5.9.

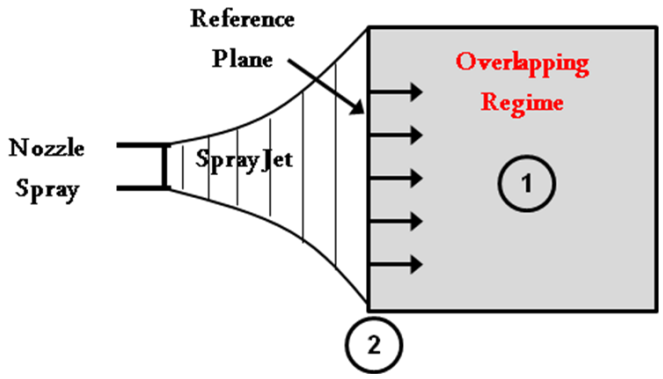

Figure 5.9 Regime defination for overlapping regime model boundary condition calculation.

The mass flow rate of the droplet entering into the overlapping regime can be written as;

$$\dot{m}_{d2} = n\alpha_{d2}\rho_d u_{d2} A_{j2} \tag{5.26}$$

Here n represents number of nozzles.

The fraction of vapor of four lumps at reference plane 2 can be written as;

$$Y_i = \frac{M_i C_i}{\sum M_i C_i} \tag{5.27}$$

Here i represent lump of hydrocarbon vapor, according to four lump scheme i=1 to 4. Here 1, 2, 3, 4 corresponds to VGO, gasoline, light gases and coke respectively.

The VGO mole generation due to the droplet vaporization into the overlapping regime can be written as;

$$C_1 = \frac{\dot{m}_{d2}}{MW1} \tag{5.28}$$

Here C_1 and MW_1 represent molar fraction and molecular weight of the VGO respectively.

The average gas velocity on the overlapping regime due to the droplet vaporization can be written as Equation (5.29);

$$\bar{u}_{g1} = \frac{\dot{m}_{d2}}{\alpha_{g1}\rho_{g2}A_1} \tag{5.29}$$

Here we assumed that the droplets entering from the jets instantly vaporize into the overlapping regime. Let's assume that, $\bar{T}$ represent the average thermal equilibrium temperature of the gas-solids phase in the overlapping regime after the droplet vaporization. T∞ represents temperature of the overlapping regime before vaporization. Assuming the instant vaporization of droplets into the overlapping regime, the energy balance for the droplet, solid and gas phase can be written as;

$$\bar{T} = \frac{\alpha_{s\infty}\rho_s u_{s\infty} c_{ps} T_{s\infty} A_1 + \dot{m}_d c_{pd} T_d - \dot{m}_d L}{\alpha_{s\infty}\rho_s u_{s\infty} c_{ps} A_1 + \dot{m}_d c_{pd}} \tag{5.30}$$

It is assumed that the solid volume fraction of the particles in the overlapping regime will not be diluted due to droplet vaporization, and will be same as the ambient fluidized bed particle concentration.

5.2.4 Cross-section Averaging of Transport and Reaction Characteristics

Once the transport and reaction characteristics in the overlapping regime, oil vapor regime are calculated from models discussed in Sections 5.2.1 and 5.2.3 and assuming no reaction in ambient bed (shown in Figure 5.9 without hatching lines) the cross-section average transport and reaction properties of the phases at the end of the feed injection regime were determined by averaging over the riser cross-section area as;

$$\bar{\phi} = \frac{\phi_0 A_0 + \phi_\infty A_\infty + n\sum_{i=1}^{n} \phi_{ci} A_{ci}}{A} \tag{5.31}$$

Were, ϕ represent either transport or reaction property, while 'A' represents area, 'k' represent number of channels and 'n' represent number of nozzles. Subscripts ∞, 0 and c represent ambient, overlapping and channel regime respectively.

5.3 Modeling of Constitutive Relations

In order to solve above governing equations for single spray jet hydrodynamics and reaction kinetics, additional constitutive correlations for the flow entrainment velocity, particle collision frequency, and collision efficiency and heat transfer models are needed. Here is the description and formulation of constitutive models required for this study

5.3.1 Gas and Solid Entrainment

Although the presence of the particles and droplets in jet regime does affects the gas solid entrainment characteristics, but there is no simple correlation to quantify this effect. In this study, as a first order approximation, we used correlation of gas entrainment velocity of single-phase gas jet flow correlation proposed by Platten and Keffer, 1968 to determine the mass flux of entrained gas into the jet regime.

$$\dot{m}_{ge} = \alpha_{ge}\rho_{ge}\left[0.06(u_g - u_{ge}\cos\theta) + 0.3u_{ge}(\cos\theta - \cos\theta_0)\right] \tag{5.32}$$

Using the similarity concept, a single-phase gas jet entrainment velocity is extended to write the solid phase entrainment into the jet regime;

$$\dot{m}_{se} = \alpha_{se}\rho_s\left[0.06(u_s - u_{se}\cos\theta) + 0.3u_{se}(\cos\theta - \cos\theta_0)\right] \tag{5.33}$$

Although the above equation for gas entrainment velocity was originally obtained from the study of oblique jets, the extension of this equation to co-current jet resembles the equations directly derived from co-current jet studies, for example, $u_e = 0.026(u - u_\infty)$ from Rajaratnam (1976). For simplicity and generality of the mechanistic modeling, the above equations for entrainment velocity may be adopted as a general equation to cover all injection angles.

The mass flux of particles penetrated into the spray jet region is dependent on the ratio of momentum of ambient particles into the fluidized bed perpendicular to the jet and the momentum of jet flow, which can be written as;

$$\dot{m}_{sp} = \alpha_{se}\rho_s u_{se} \exp\left(-\frac{\alpha_{se}\rho_{se}u_{se}^2 \sin\theta}{\alpha_s\rho_s u_s^2 + \alpha_g\rho_g u_g^2 + a_d\rho_d u_d^2}\right) \tag{5.34}$$

5.3.2 Vaporization Model

In FCC unit, the cracking reaction starts as soon as the feed vaporizes; hence, the modeling of the droplet vaporization is very important for FCC unit.

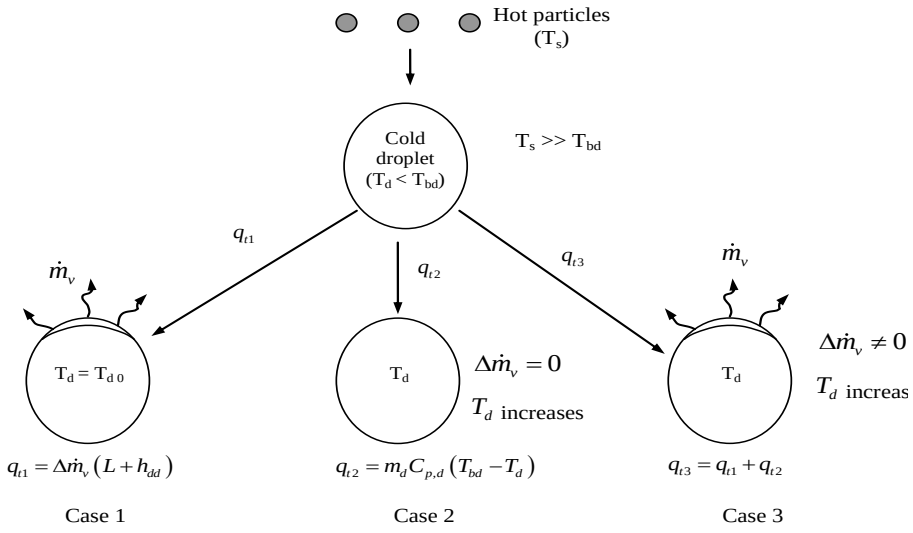

Figure 5.10 Droplet vaporization modeling: case-1: Droplet vaporization without sensible heating case-2: Sensible heating of droplet without vaporization and case-3: simultaneous droplet heating and vaporization.

For the droplet vaporization modeling, there are two limiting cases; in first case as show in Figure 5.10 (case-1), all the heat transfer to the droplet is first utilized for the sensible heating of droplet up to boiling point and any additional heat transfer to the droplet will be utilized for vaporization. In second case as show in Figure 5.10 (case-2), the heat transfer to the droplet will cause vaporization at its surface without altering its core temperature. Either of the case is not appropriate for droplet vaporization because the sensible heating of droplet and vaporization are simultaneous process. Hence, in this study the total heat transfer to the droplet phase is partitioned into the sensible heating and vaporization of the droplet which is shown in Figure 5.10 (case-3). The partition function for heat transfer for sensible heating and droplet vaporization is proposed as in terms of the latent heat and sensible heat as;

$$\chi_v = \frac{L}{L + C_{pd}\left(T_{bd} - T_b\right)} \tag{5.35}$$

The droplet vaporization rate can be determined from;

$$\dot{m}_v = \chi_v \frac{E_{Cds} + E_{cs} + E_{rad}}{L} \tag{5.36}$$

5.3.3 Spray Jet Coverage

The expansion of the jet into the fluidized beds can be expressed as a function of momentum ratio between ambient gas-solids fluidized bed and gas-droplet spray at inlet to nozzle, which can be expressed by Equation (5.37);

$$R = R_j + 0.11\left(1 + \frac{\alpha_{g\infty}\rho_g + \alpha_{s\infty}\rho_s}{\alpha_{gj0}\rho_{g0} + \alpha_{dj0}\rho_d}\right)\xi \tag{5.37}$$

5.3.4 Drag Force

The drag force on the single particle is extended for the drag force for particle and droplet. The extension of the single particle drag is reasonable because the concentration of droplet and particle is low in the jet regime.

$$F_{Di} = n_i c_{di} \frac{\pi}{8} d_i^2 \rho_g \left|u_g - u_i\right|(u_g - u_i) \qquad i = d, s \tag{5.38}$$

Where the drag coefficient for single particle can be written as;

$$C_d = \begin{cases} \dfrac{24}{\mathrm{Re}} & \mathrm{Re} < 2 \\ \dfrac{18.5}{\mathrm{Re}^{0.6}} & 2 < \mathrm{Re} < 500 \\ 0.44 & 500 < \mathrm{Re} < 2\times10^5 \end{cases} \tag{5.39}$$

The *Re* represent Reynolds number base on the relative velocity between gas and solids or droplet phase, respectively.

5.3.5 Collision Frequency

In this study we used the collision frequency model proposed by Fan and Zhu (1998) to determine collision frequency among droplets and solid particles can be calculated by;

$$f_{ds} = \eta_{co} n_d n_s \frac{\pi \left(d_s + d_d \right)^2}{4} \left| u_s - u_d \right| \tag{5.40}$$

where the collision efficiency, η_{co}, is given from an analytical approximation, which is derived based on the rigid sphere collisions in Stokesian flows (Zhu, 2000)

$$\eta_{co} = \left(1 + 34 \frac{d_d}{d_s} \frac{\rho}{\rho_s} \frac{1}{\mathrm{Re}_{sd}} \right)^{-2} \tag{5.41}$$

where Re_{sd} is the particle Reynolds number based on the relative velocity between particle and droplet.

5.3.6 Collision Heat Transfer Model

When droplet collides with the hot particle, heat transfer from the particle causes the vaporization of the droplet. It is assumed that when adequate amount of vapor is generated, the particle is pushed back and the heat transfer due to droplet-particle collision is terminated. It is also assumed that with the collision of the droplet with particle, the heat transfer from the particle is equivalent to its thermal capacity which can be written as;

$$E_{Cds} = f_{ds}\frac{\pi}{6}d_s^3\rho_s C_{p,s}(T_s - T_d) \tag{5.42}$$

5.3.7 Momentum Exchange due to Collision

The total momentum exchange to particles due to droplet-particle collision can be expressed in terms of collision frequency, physical properties of droplet and particles, and slip velocity as;

$$F_{Cds} = f_{ds}\frac{m_s m_d}{(m_s + m_d)}(u_d - u_s) \tag{5.43}$$

5.3.8 Reaction Heat

The endothermic reaction heat in equation E_R in Equation (5.4) can be written as;

$$E_R = -\sum_{i=1}^{5} r_i.\Delta H_i A \tag{5.44}$$

where r_i and ΔH_i represents the mass transfer rates due to the cracking and heat of reaction for the i^{th} endothermic cracking reaction respectively. The details of reaction rate constants k_i and local catalyst-to-oil ratio (CTO) is given elsewhere (Zhu *et al*., 2010).

5.3.9 Heat Transfer Model

5.3.9.1 Convection Heat Transfer Model. The total convective heat transfer to the droplets from the gas E_{cd} in Equation (5.7) can be written as;

$$E_{cd} = n_d \pi d_d^2 h_d (T_g - T_d) \tag{5.45}$$

where h_d is the convective heat transfer coefficient, which can be presented as;

$$h_d = \frac{Nu_d K}{d_d} \tag{5.46}$$

Where Nu_d, Nusselt number for evaporating droplet suggested by Buchanan, 1994 is adopted in this study, which can be written as;

$$Nu_d = \frac{2 + 0.6\,\mathrm{Re}_d^{*\,0.5}\,\mathrm{Pr}^{0.333}}{\left[1 + \dfrac{C_p (T_g - T_d)}{L}\right]^{0.7}} \tag{5.47}$$

where Re_d represent the relative Reynolds number of droplets in a gas-solids mixture, which is defined as;

$$\mathrm{Re}_d^* = \frac{(\rho_d \alpha_d + \rho_m)(u_d - u_g) d_d}{\mu} \tag{5.48}$$

The convective heat transfer between gas and solids E_{cs} in Equation (5.10) can be presented as;

$$E_{cs} = n_s \pi d_s^2 h_s (T_s - T_g) \tag{5.49}$$

Where h_s, the convection heat transfer coefficient can be presented as;

$$h_s = \frac{Nu_s K}{d_s} \tag{5.50}$$

Nusselt number Nu_s in above equation can be presented by heat transfer coefficient of a single particle can be calculated from the Ranz-Marshall correlation;

$$Nu_s = 2 + 0.6 \mathrm{Re}_s^{0.5} \mathrm{Pr}^{0.333} \tag{5.51}$$

Where, $\mathrm{Re_s}$ and $\mathrm{P_r}$ represents relative Reynolds number for particle and Prandtl number respectively.

5.3.9.2 Radiation Heat Transfer Model. The radiation heat transfer from ambient particles to the droplets in the jet regime per unit volume can be present in terms of the droplet number density as Equation (5.52);

$$E_{rad} = n_d \pi d_d^2 \varepsilon_s F \sigma (T_{s\infty}{}^4 - T_d{}^4) \tag{5.52}$$

5.3.10 Partition Function for Vapor Flux Convection (γ). Portion of gas-vapor mixture is convicted from the spray regime by the cross-flow convection of ambient gas-solids flow. The convection of hydrocarbon vapor depends on the momentum ratio of the cross-flow to the jet flow in a power low from; which can be expressed as;

$$\gamma = \left(\frac{\alpha_{s\infty} \rho_s u_{s\infty}{}^2 + \alpha_{g\infty} \rho_g u_{g\infty}{}^2}{\alpha_s \rho_s u_s{}^2 + \alpha_g \rho_g u_g{}^2 + \alpha_d \rho_d u_d{}^2} \right)^n \tag{5.53}$$

The value of "n" varies from 0 to 1. In this study "n" is selected as 0.75.

5.4 Problem Closure

The relation between the molar concentrations of chemical lumps in the gas phase and the gas density can be obtained from the ideal gas law, which gives;

$$\rho_g = \frac{P}{RT_g} \frac{\sum_{i=1}^{5} (C_i . M_i)}{\sum_{i=1}^{5} C_i} \tag{5.54}$$

A constraint on the volume fractions of the three phases is given as;

$$\alpha_s + \alpha_g + \alpha_d = 1 \tag{5.55}$$

There are 17 coupled Equations (5.1) to (5.15), (5.54) and (5.55) for hydrodynamics and reaction characteristics along the single spray jet, which can be solved using the Runge-Kutta method for 17 independent variables (θ, u_g, α_g, T_g, u_d, α_d, T_d, u_s, α_s, T_s, C_1, C_2, C_3, C_4, C_5, ρ_g, A_j). The boundary conditions for droplet size and droplet velocity were determined from typical commercial nozzles used for FCC riser reactors. The feed contains only VGO so C_2, C_3 and C_4 were set to be zero.

For the reactions into the oil vapor regime and over lapping regime we have nine governing Equations (5.16), (5.18-5.25) and nine unknowns (u_g,, T, u_s, α_s,C_1, C_2, C_3, C_4, ρ_g,), which were solved coupled by Runge-Kutta method.

5.5 Results and Discussion

The proposed model can predict the hydrodynamic and reaction characteristics of vaporizing gas-droplet into the entrance regime of FCC riser reactor. In this section we discuss some of the important hydrodynamic features of the spray jet and reaction rates in the feed injection zone. This section is basically split into three sections, namely, the model predictions hydrodynamics and reaction characteristics along the spray jet, overlapping regime and in the oil vapor regime.

First, the hydrodynamic model for single spray jet was validated by comparing the results of model predictions with measured jet penetration length (Ariyapadi *et al.*, 2004) and liquid-induced solid entrainment (Felli, 2002) without reactions. The operating conditions for experiment in Ref. (Ariyapadi *et al.*, 2004) are shown in Table 5.3.

Table 5.3 Experimental Cases for Model Validation (Ariyapadi *et al*., 2004)

Case	Nozzle Type	Liquid flow rate (Kg/s)	Gas flow rate (Kg/s)	ALR	UMF	U0
C1	I A	0.057	0.001	1.75	0.012	0.1
C2	I A	0.065	0.001	1.54	0.012	0.1
C3	I A	0.071	0.001	1.41	0.012	0.1
C1-C3 Model	-	0.065	0.001	1.54	0.012	0.1
C4	I B	0.026	0.00045	1.73	0.012	0.1
C5	I B	0.028	0.00045	1.61	0.012	0.1
C6	I B	0.032	0.00045	1.40	0.012	0.1
C4-C6 Model	-	0.028	0.00045	1.61	0.012	0.1
D1	II C	0.03	0.001	3.33	0.012	0.1
D2	II C	0.04	0.001	2.5	0.012	0.1
D3	II C	0.054	0.001	1.85	0.012	0.1
D1-D3 Model	-	0.04	0.001	2.5	0.012	0.1
D4	II D	0.014	0.00045	3.21	0.012	0.1
D5	II D	0.018	0.00045	2.5	0.012	0.1
D6	II D	0.023	0.00045	1.96	0.012	0.1
D4-D6 Model	-	0.018	0.00045	2.5	0.012	0.1

Source: Ariyapadi, S., Berruti, F., Briens, C., McMillan, J., Zhou, D. (2004). Horizontal Penetration of Gas-Liquid Spray jets in Gas-solids Fluidized Beds. *International Journal of Chemical Reactor Engineering*, 2 (A22).

Here, UMF, U0, and ALR are the minimum fluidization velocity, gas velocity, and the air-to-liquid ratio, respectively.

The experiment data presented in Tables 5.3 and 5.4 are for the spray jet into the fluidized bed under the isothermal conditions i.e., there is no evaporation of droplets, no cracking reaction and there is no convection of ambient gas-solids fluidized bed into the spray jet. To make the comparison of model predictions with the experiment data, the evaporation of the droplets, reaction kinetics and convection of cross-flowing gas-solids

fluidized bed was set to be zero for the proposed model. There is no literature experiment data for evaporating spray jet into the circulating fluidized bed; so the best way to validate the proposed hydrodynamic model for the evaporating and reacting spray jet is to convert the governing equations into the form of the experiment conditions. There are published experiment data for evaporating spray jet into the cross-flow of gas and solids (Qureshi and Zhu, 2006), but the experiment doesn't provide the important information about the droplet size and droplet velocity at the inlet of the nozzle, which are the input boundary conditions for the proposed model.

Figure 5.11 shows the comparison of model predictions with experimental data on jet penetration length in the absence of chemical reactions and evaporation. The simulation conditions used in our hydrodynamics model are chosen to match those shown in Table 5.3. The results show that the penetration length varies with nozzle type. The model prediction on spray penetration matches well with experiment for all nozzle types and ALRs.

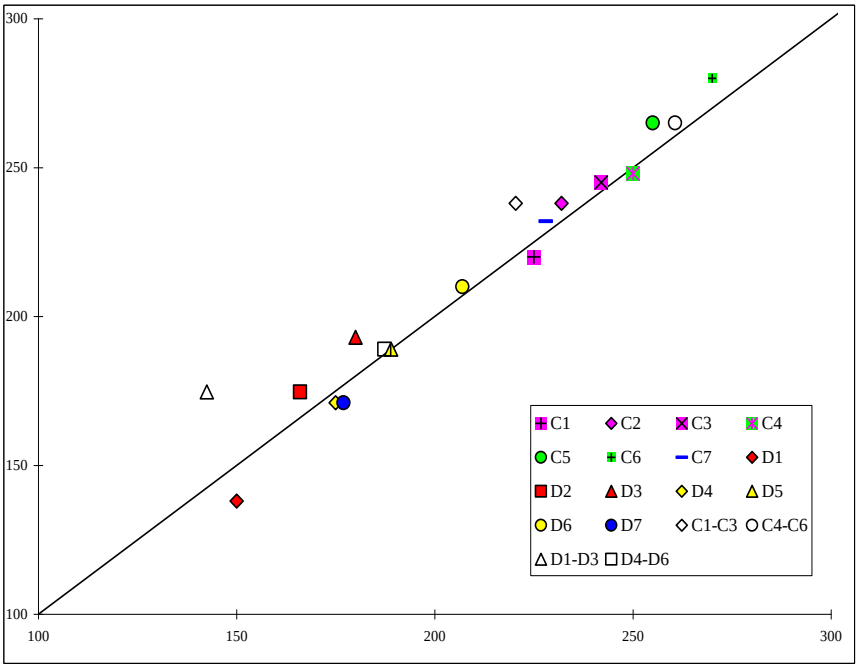

Figure 5.11 Model prediction of jet penetration length against measured penetration length (Ariyapadi *et al.*, 2004).

Figure 5.12 compares the predicted and measured (Ariyapadi *et al.*, 2004) solid entrainment flow rates. The model predicts that the entrained solids mass flow rate increases along the jet penetration direction in the near-nozzle field, as expected on physical grounds.

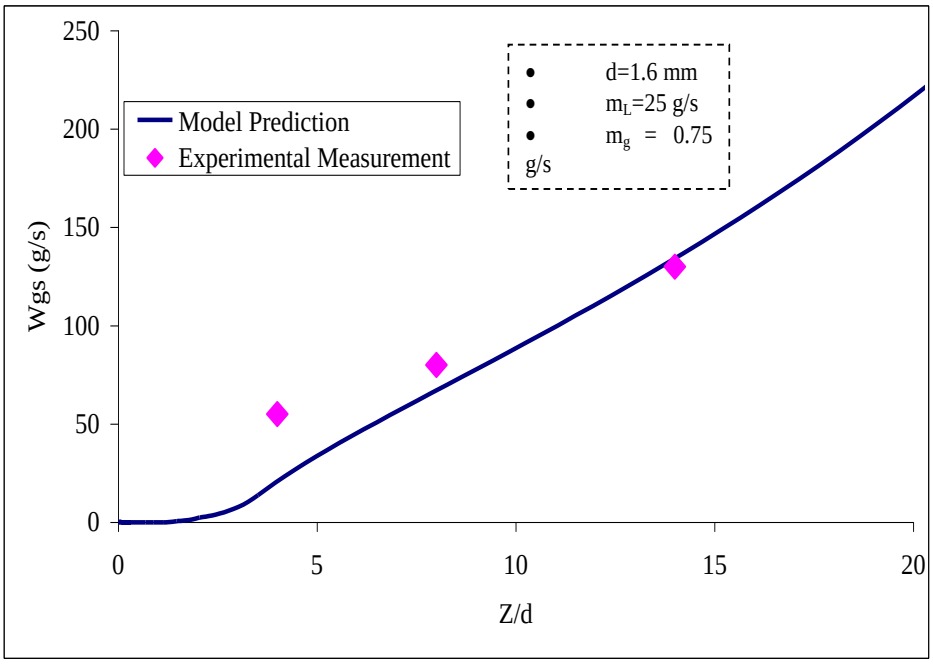

Figure 5.12 Model prediction of solid entrainment mass flow rate along jet trajectory against experiment data (Ariyapadi *et al*., 2004).

There have been no published data on spray jet penetrating into a gas-solids fluidized bed in the presence of chemical reactions. In what follows we present the results of model predictions on the behavior of a reacting single spray jet in terms of penetration length and jet expansion/trajectory, phase temperature and concentration distribution and reaction characteristics. The input conditions for single spray jet model predictions are listed in Table 5.4.

Table 5.4 Model Input Parameter for Injection of Single Spray Jet in Hot Gas-solids Cross-Flow Convection

Parameter	Value
Gas velocity (m/s)	53
Droplet volume fraction	0.0764
Droplet velocity (m/s)	35
Droplet size (μm)	100
Droplet density (kg/m^3)	900
Nozzle radius (Inch)	0.6
Droplet temperature (K)	350
Jet penetration angle (degree)	30
Bed steam velocity (m/s)	1.7
Fluidized bed solids volume fraction	0.35
Bed solids velocity (m/s)	0.5
Solids density (kg/m^3)	1400
Solids size (μm)	75
Bed temperature (K)	925
Droplet saturated temperature (K)	425
Droplet latent heat (J/kg)	220160
Gas thermal conductivity (w/m·K)	0.0415
Gas viscosity (Pa.s)	5e-5
Gas thermal capacity (J/kg·K)	2250
Droplet thermal capacity (J/kg·K)	2093
Solids thermal capacity (J/kg·K)	1214
Droplet surface tension (N/m)	0.7
Solids emissivity	1.0
Crude oil molecular weight (kg/kmol)	400
Gasoline molecular weight (kg/kmol)	108
Light gases molecular weight (kg/kmol)	28
Coke molecular weight (kg/kmol)	32
Steam molecular weight (kg/kmol)	18

Figures 5.13 to 5.15 demonstrates typical hydrodynamic characteristics of a spray jet into the gas-solids riser flow in the presence of cracking reactions, which include the temperatures, volume fractions and velocities of gas, solids and droplet phases. The abscissa is the penetration length along the ξ-coordinate.

Figure 5.13 shows the temperature profiles of gas, solids and droplet phases along the spray trajectory. The droplet temperature steadily reaches to the saturation

temperature due to the partition of heat supplied to the droplet into the sensible heating and vaporization. The intense heat transfer the droplet is from hot particles by collision and convective heat transfer from hot gases. On the other hand, the surrounding gas temperature initially increases and then steadily approaching to thermal equilibrium temperature between gas and solid phase. Along the way, the solid temperature decreases due to the intensive heat transfer to the gas phase resulting from endothermic cracking and vaporization.

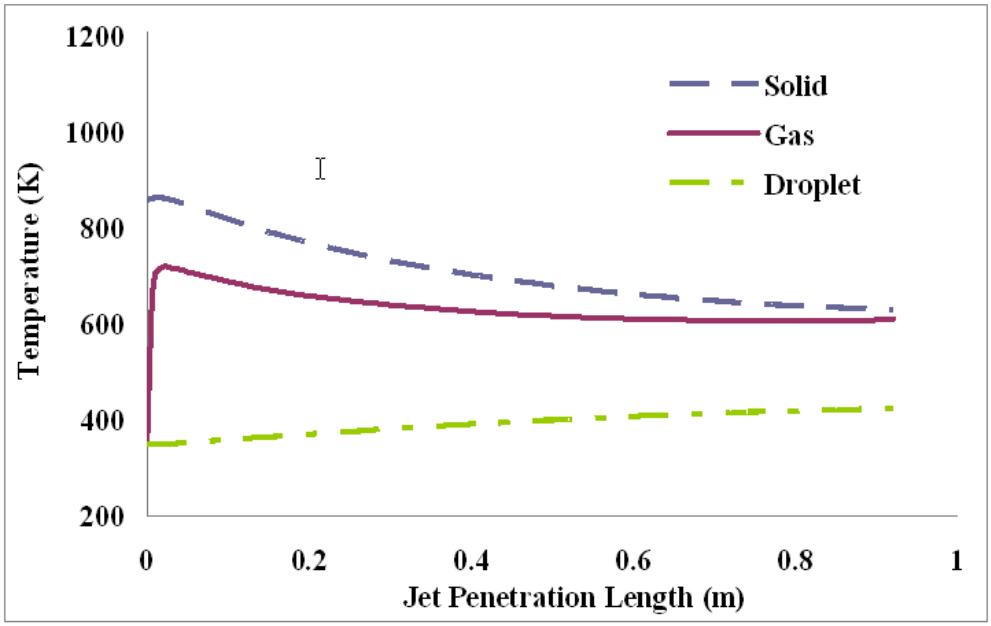

Figure 5.13 Model predictions of phase temperatures along spray jet.

The velocity profiles for the gas, liquid and solid phases are shown in Figure 5.14. Due to the entrainment of surrounding gas and solid at the riser base, the velocity of gas and droplet phase each phase decreases along the trajectory, which is attributed to the momentum transferred to the entrained solids by drag force and droplet-particle collision. Hence, the velocity of the gas decreases much faster than that of droplets, but it is always

larger than the solids phase velocity. The droplet velocity also decreases due to the gas-droplet inter-phase frictional loss and collisional momentum transfer with the solids phase. The particle velocity increases initially due to the momentum transfer by gas and droplet by slip velocity between gas-solids and collision respectively. At the end of the jet three phases attain steady state equilibrium velocity.

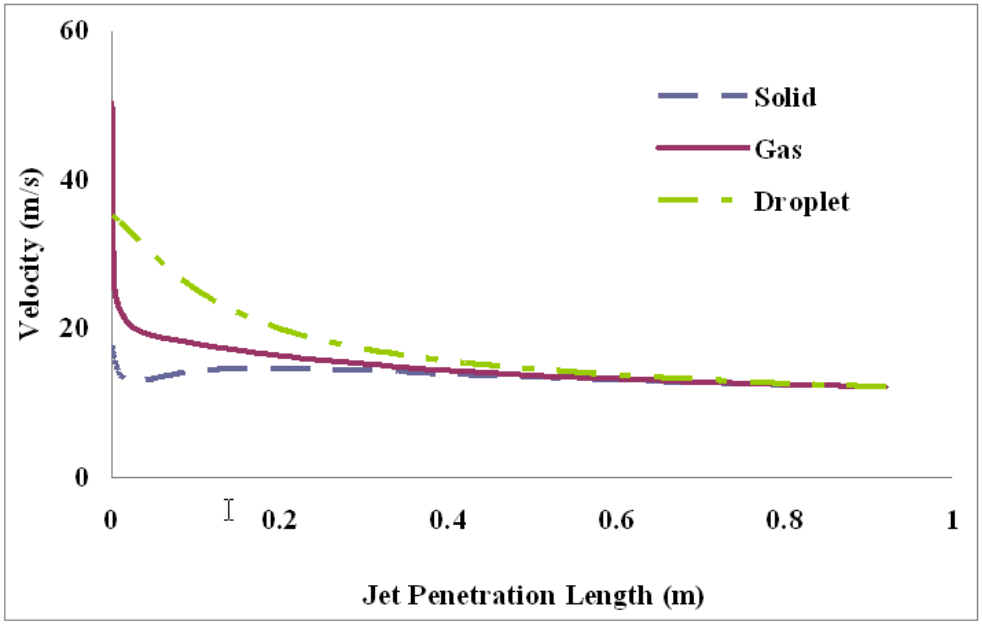

Figure 5.14 Model predictions of phase velocities along spray jet.

Figure 5.15 shows the result of the volume fraction of phases along the spray trajectory. With the intense vaporization and jet expansion, the volume fraction of the droplet phase decreases dramatically along the spray trajectory. The corresponding solids volume fraction increases with the continuous entrainment and diffusive penetration across the jet boundary. The solid volume fraction at the end of the jet reaches to ambient fluidized bed solid volume fraction. The gas volume also changes due to the gas entrainment and cracking of the reactant along the jet trajectory.

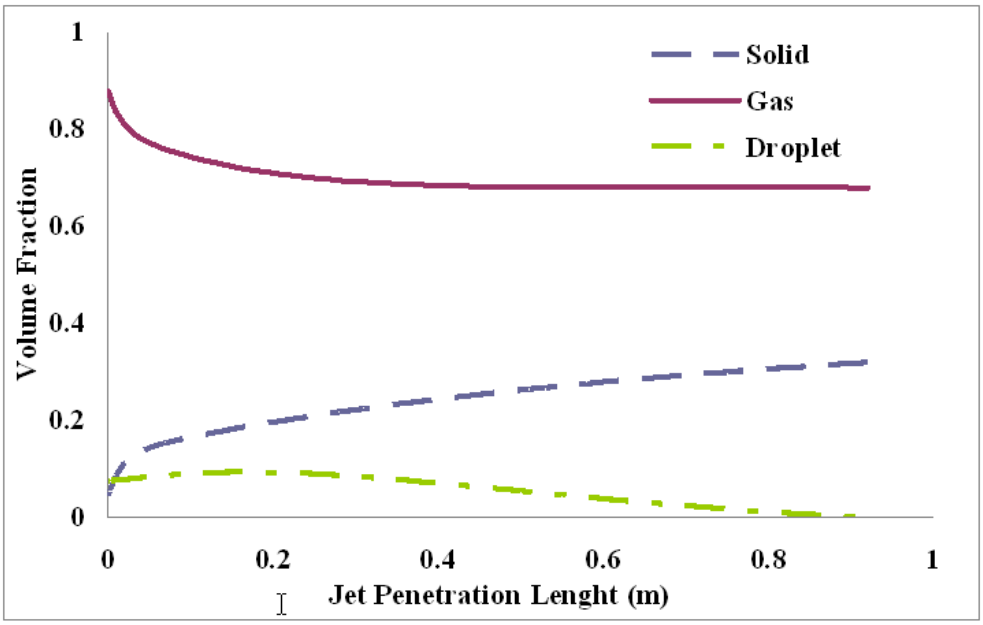

Figure 5.15 Model predictions of phase volume fractions along spray jet.

At the beginning of the spray jet, the temperature of the hydrocarbon of vapor is not high so, there is no reaction and vapor that serves as carried gas of the spray jet. But due to liquid vaporization, the concentration of gas phase increases significantly. As the liquid feed vaporizes and cracking reactions take place, and feed VGO is cracked into gasoline, light gases and coke as shown in Figure 5.16.

As show in Figure 5.16, along the spray jet, the molar concentration of VGO increases which is due to the vaporization of droplet, while the gasoline and light gases molar concentration increases due to conversion of VGO into the gasoline and light gases. Due to very high temperature of catalyst in this regime, there must be secondary reactions, this is the reason for high molar concentration of light gases at the end of spry jet. At the end of the jet the droplets are almost vaporized hence the molar concentration of VGO vapor decreases slightly, while the gasoline and light gases molar concentration increases due to the conversion of VGO into the gasoline and light gases.

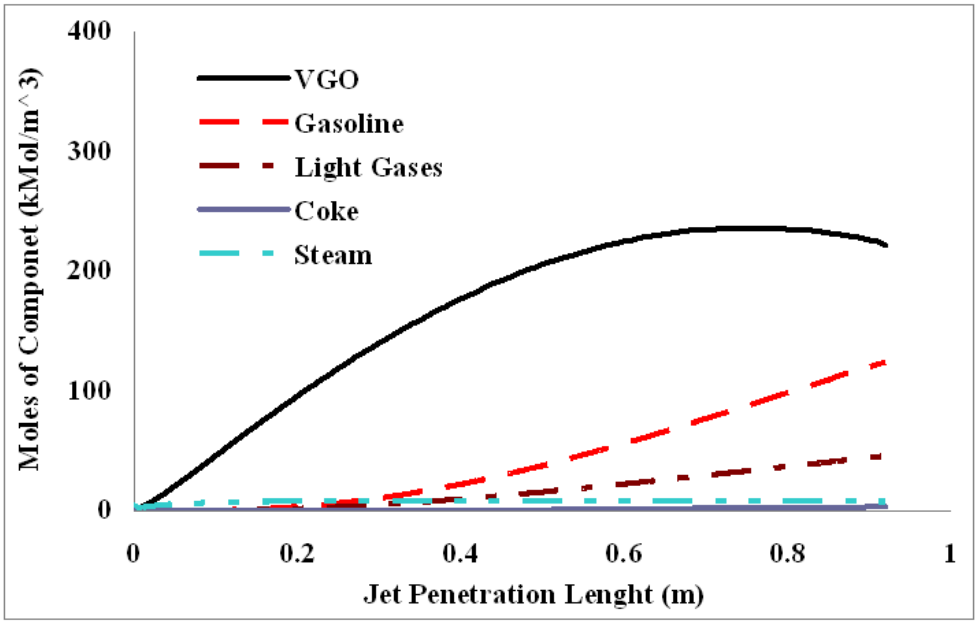

Figure 5.16 Model predictions of mole concentrations of hydrocarbon feed lumps along spray jet.

Figure 5.17 shows the jet penetration profile into the fluidized bed. The axial and radial penetration of jet is plotted by projection the centerline of jet trajectory (ξ) on the horizontal and vertical plane respectively. The result shows that the jet penetrates around 0.41 m in vertical direction from the point of injection, while the jet penetrates around 0.6m in radial direction.

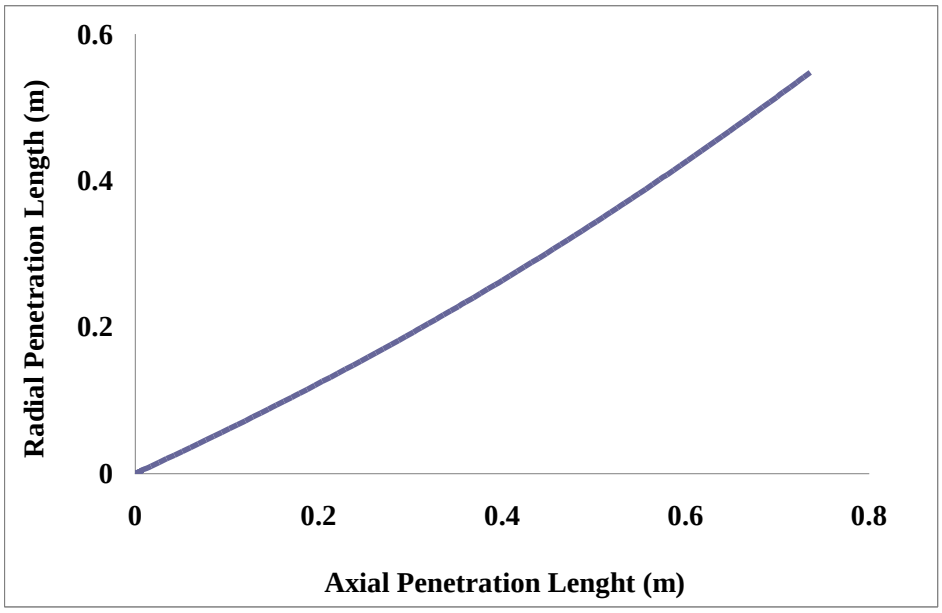

Figure 5.17 Model predictions of jet penetration into the fluidized bed.

Figure 5.18 shows the model prediction of jet bending along its trajectory. The jet is injected into the gas-solids fluidized bed at 30° with horizontal plane. As spray jet penetrates into the cross-flowing gas-solids flow, the momentum transfer by cross-flowing solids to droplets by collision and drag force of gas will cause bending of spray jet. As shown in Figure 5.18, before the end of spray jet, the spray jet bending is around 12° (i.e., the spray jet bending is from 30° to 42° with horizontal plane).

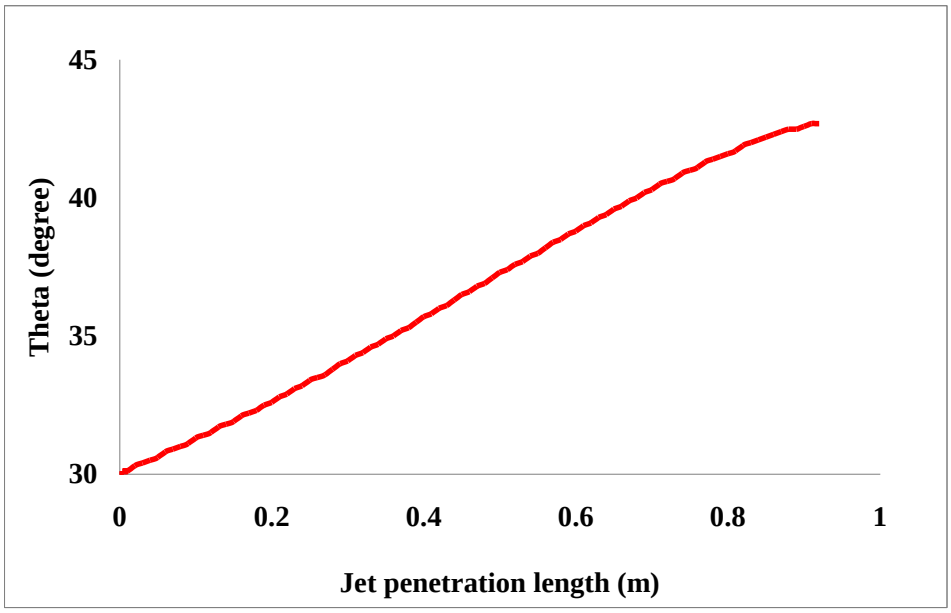

Figure 5.18 Model predictions of jet bending along jet trajectory.

5.5.1 Impact of Feed Injection Regime on Riser Reactor Performance

As the spray penetrates toward the riser center, the concentrations of chemical components keep changing, and finally entering into the overlapping regime of multiple jets spray. At the end of the feed injection regime, the gasoline component becomes an important constituent of the vapor phase. The concentrations of these reactants at the end of the feed injection regime will directly influence the "boundary" (or "initial") conditions for feed components in its immediate downstream gas-solids reaction region of riser. In this study, eight spray nozzle injections into the confined riser are used to determine the hydrodynamic and chemical reaction characteristics at the end of the feed injection regime. In order to study the influence of vaporization and reactions into the feed injection regime on the performance of the FCC reactors, the results of reaction characteristics of hydrodynamics coupled reaction model (Zhu *et al*., 2011) predictions were presented and compared for two different inlet boundary conditions. In the first

case, instant vaporization of feed at riser inlet without reactions was assumed while in the second case, we used inlet boundary conditions calculated from model presented in this study. The input boundary conditions for riser reactor are presented in the Table 5.5.

Table 5.5 Catalyst Properties at Regenerator Exit

Model inputs and and properties	With Reaction in feed injection regime	Without Reaction in feed injection Regime
Catalyst feed rate (kg/s)	192	192
Catalyst volume fraction	0.5	0.5
A_2/A_1 (Ratio of area)	3	3
Area of regenerator pipeline, A_2 (m^2)	0.262	0.262
Lubrication steam velocity (m/s)	5.7	5.7
Catalyst temperature (K)	925	925

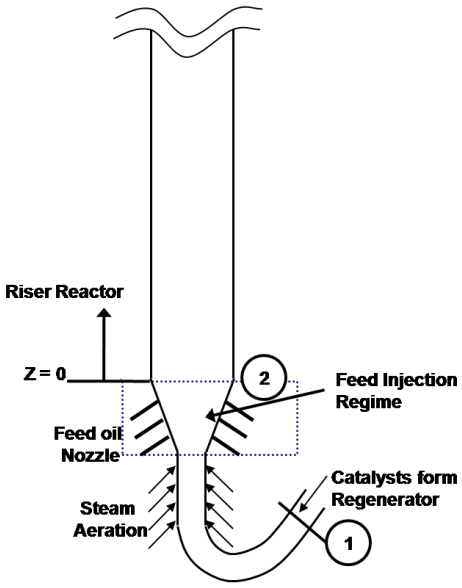

Figure 5.19 Schematic representation of feed injection regime with J-bend connection with regenerator.

Table 5.6 Reaction Model Input Conditions and Properties

Model inputs and and properties		With Reaction in feed injection regime	Without Reaction in feed injection Regime
Catalyst feed rate (kg/s)		192	192
VGO feed rate (kg/s)/CTO ratio		25.2/7.6	25.2/7.6
Number of nozzles		8	8
Inlet temperature of VGO feed (K)		350	350
Inlet temperature of catalyst (K)		809	826.7
Fraction of VGO (%)		73.3	100
Fraction of Gasoline (%)		22.9	0
Fraction of Light Gases (%)		2.4	0
Fraction of Coke (%)		1.4	0
Inlet pressure (atm)		3.0	3.0
Inlet solid volume fraction		0.245	0.32
Riser diameter (m)		1.0	
Riser height (m)		35	
Catalyst diameter (μm)		75	
Inlet riser pressure (atm)		3.15	
Catalyst density (kg/m^3)		1400	
Gas specific heat (J/kg-K)		3299	
Liquid specific heat (J/kg-K)		2671	
Catalyst specific heat (J/kg-K)		1150	
Droplet latent heat (J/kg)		220160	
Molecular weight (kg/kmol)	VGO	280	
	Gasoline	108	
	L-Gas	28	
	Coke	32	

To make the model predictions more realistic, we consider the effect of the shape of the feed injection regime and lubrication steam which is supplied for the catalyst transport from the feed regenerator to the feed injection regime on the catalyst concentration dilution (as shown in Figure 5.19). For the most FCC units, the ratio of the area of stand pipe to the riser reactor is usually 1:3. We take into the account the effect of the catalyst concentration dilution effect due to expansion of the area of the feed injection regime.

With above inlet boundary conditions, the reaction characteristics along the main body of riser reactor was estimated from the flow hydrodynamics coupled reaction model, recently proposed by Zhu *et al.,* 2011. The distribution of product yield and VGO conversion were estimated and compared.

Figure 5.20 shows the comparison of model predictions of VGO yield with and without the reaction in the feed injection regime. The results show that, the VGO conversion in presence of reaction in the feed injection regime is almost similar. With considering the reaction in the feed injection regime, the conversion of the VGO is 5% less than, without reaction. Due to the reaction in the feed injection regime, the initial yield of the VGO is 72%.

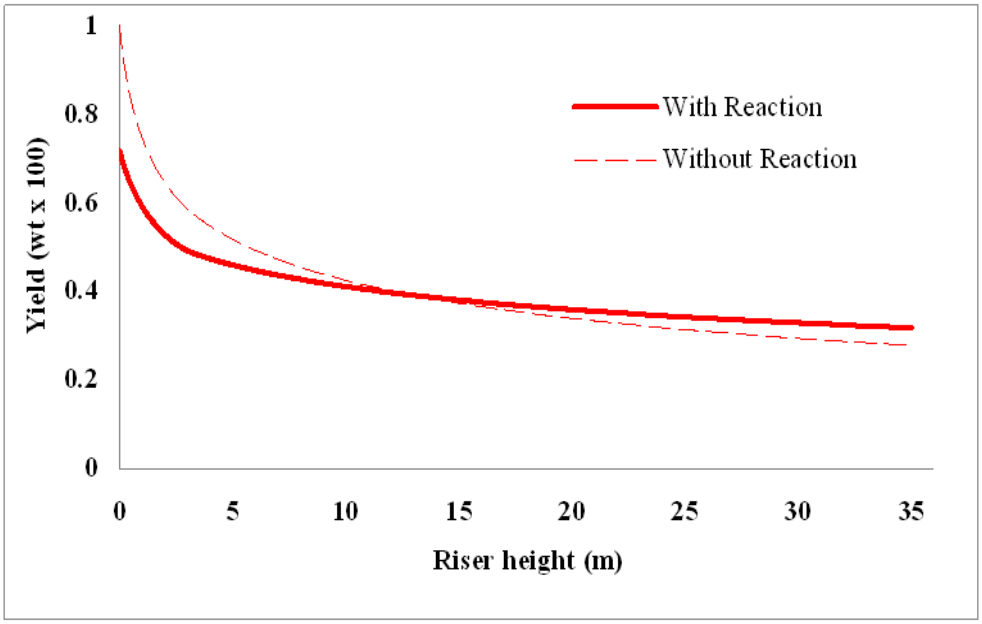

Figure 5.20 Comparison of riser reactor model prediction of VGO Yield: with and without reaction in feed injection regime.

Figure 5.21 shows the effect of reaction in feed injection regime on the gasoline yield distribution along the main body of reactor. In presence of reaction in feed injection

regime, the yield of gasolie is high in the dense phase reigne of the riser reactor, which is due to very high solid concentration and temperature of the catalyst. The gasoline yield distribution shows assymptotic trend in dilute phas transport regime of the riser reactor. With pre-reaction in the feed injection regime, the gasoline yield in the dense phase regime is much higher than without pre-reaction, while at the exit of the riser there is no appreciable diffrence in the gasoline yield prediction. At riser height of 5m, the gasoline yied is with pre-reaction in the feed injection regime is around 16% higher (gasoline yield with and without pre-reaction in feed injection regine are 42% and 35% respectively) than without pre-reaction.

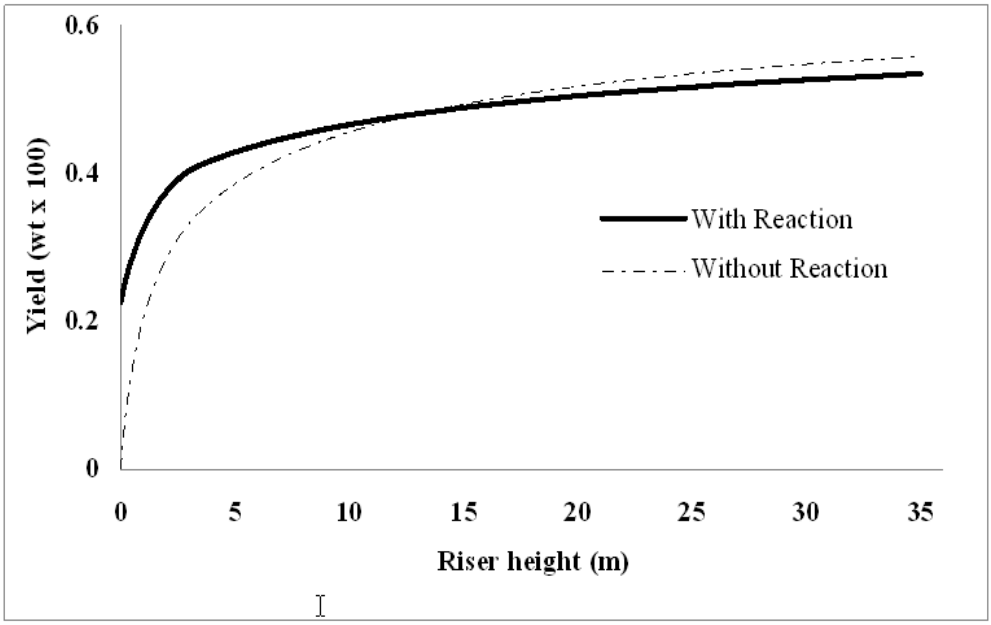

Figure 5.21 Comparision of gasoline yield prediction of riser reaction model: with and without reaction in feed injection regime.

Figure 5.22 shows the comparision of riser reaction model preidctions of light gases and coke yield with and without reaction in the feed injection regime. In presence

of reaction in feed injection regime, the yield of non-product, light gases and coke is much higher than without reaction in the feed injection regime.

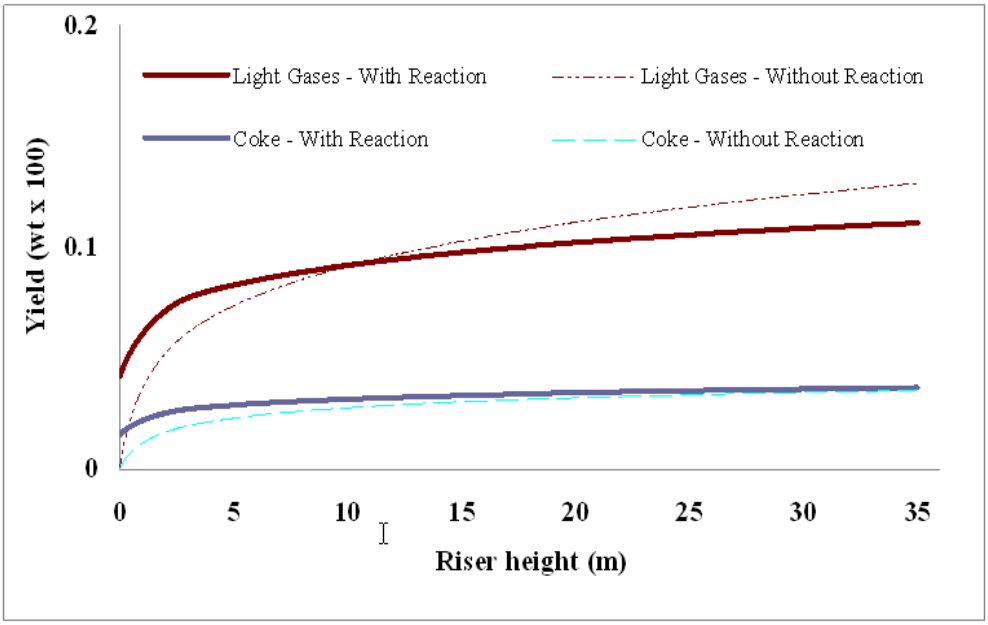

Figure 5.22 Comparison of reaction model prediction of light gases and coke: with and without reaction in the feed injection regime.

5.6 Summary of Chapter

1. This study is focused on the development of a mechanistic model aimed at gaining a quantitative understanding of the coupled characteristics of hydrodynamics, heat-mass transfer by vaporization, and catalytic reaction in the feed injection zone of a high-temperature gas-solids reactor.
2. Proposed mechanistic model for hydrodynamics and reaction characteristics along the single spray jet, in the oil vapor regime and in the overlapping regime. From the results of hydrodynamics and reaction characteristics in these three regime, cross-section average properties of hydrodynamics and reaction characteristics

were estimated at the end of the feed injection regime by cross-section averaging concept.

3. The inlet boundary conditions for riser reaction model can be estimated from the proposed model for feed injection regime.

4. It is also shown that in presence of reaction in the feed injection regime, the conversion and yield distribution along the main body of the reactor was considerably different.
5. The length of the feed injection regime can be identified using the proposed model.

CHAPTER 6

COUPLING OF NON-UNIFORM FLOW HYDRODYNAMICS AND REACTION KINETICS IN RISER REACTOR

6.1 Problem Statement and Challenges

The Fluid catalytic cracking (FCC) process has been the most widely used technology for the conversion of various refinery hydrocarbon streams into high-octane gasoline and high-value petrochemical feed-stocks (King, 1992; Ali & Rohani, 1997; Arandes *el al.*, 2000). Higher selectivity to these intermediate products is more desirable for FCC reactor performance. For a typical refinery, FCC offers the greatest potential for increasing its profit margin; even a small improvement in FCC process can make a big difference because of the sheer volume of oil converted. Thus, the incentives for a better predicative understanding of the FCC process are immense (Krishna and Parkin, 1985). Over the years, the residence (or contact) time in the FCC riser reactor has been shortened significantly, thanks to the development of high-activity catalysts. As a result, the transport and hydrodynamic effects on cracking reactions have played an increasingly important role in determining conversion and product quality (Chang and Zhou 2003).

Riser reactor is the most important part of this unit as the cracking reactions take place in the riser. Modern FCC units have short diameter risers (0.8-1.2 m) with lengths varying from (30-40 m). In typical FCC unit as shown in Figure 6.1, Hydrocarbon feed (gas oil) is atomized and fed to a riser reactor along with hot catalyst at the bottom of the reactor. Feed droplets entering the riser get vaporized by contacting with hot catalyst in the feed injection zone of riser and the reaction starts as soon as the hydrocarbon feed is vaporized.

The hydrocarbon vapors cracks down to lighter molecules as it travels upwards with hot catalyst. Hot regenerated catalyst act as heat source for vaporization of feed and for endothermic cracking reactions. As a result of cracking reactions the density of the oil decreases causing an increase in the velocity of the vapor/gas phase, which accelerates the catalyst. During cracking, the by-product of the process, coke gets deposited on catalyst and thus catalyst loses its activity. Cracked hydrocarbon vapors are separated from deactivated catalyst in a separator at the top of the riser reactor. Deactivated catalyst flows into a regenerator (after passing through stripper) where coke deposited on catalyst is burnt off that makes catalyst sufficiently hot. This hot-regenerated catalyst is recycled back to the riser reactor.

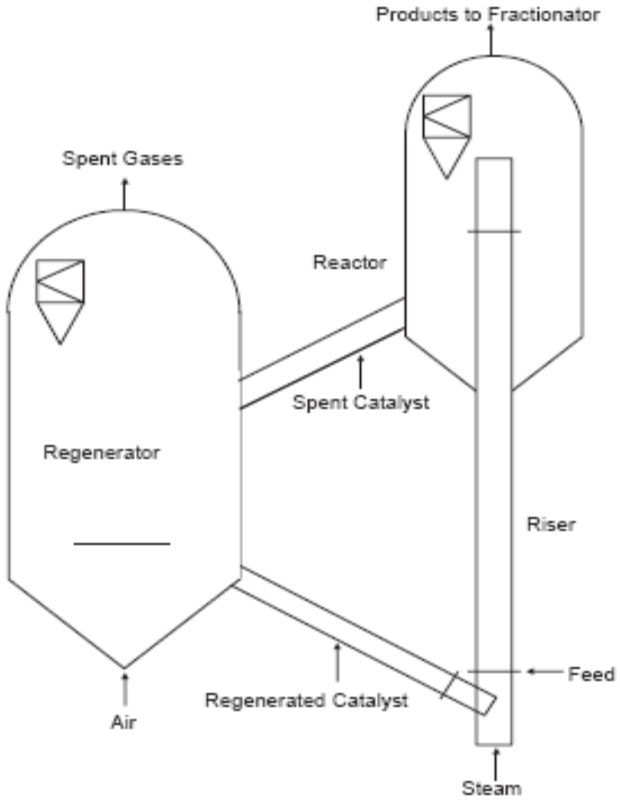

Figure 6.1 Industrial Fluid Catalytic Cracking (FCC) Unit (Nayak *et al.*, 2005).

The hydrodynamic characteristics of catalyst and hydrocarbon flows in riser reactors are highly heterogeneous both in the axial and radial direction with severe catalyst back-mixing (Herb *et al.*, 1992; You *et al.*, 2008; Wang *et al.*, 2010). Riser reactor exhibit an "S" shaped axial holdup distribution of catalyst with dense catalyst holdup at bottom and dilute catalyst holdup at top of riser. The holdup decreases along the riser height as the catalyst are accelerated by the gas (acceleration zone) and eventually the fully developed flow condition is reached where the catalyst holdup is invariant with the riser height (fully developed flow region).

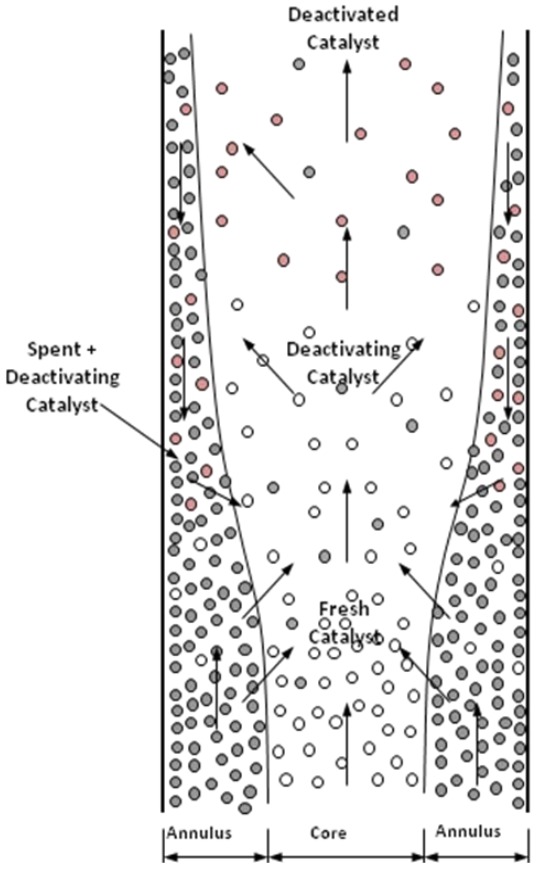

Figure 6.2 Motion of fresh and deactivating catalyst in two-zone (core-annulus) regime of riser reactor.

The radial non-uniform flow structure in the riser reactor is presented as core-annulus gas-solids flow structure with severe back-mixing of deactivated catalyst. Such heterogeneity has a significant impact on reaction rates. The reaction characteristics in core and wall regions are very different. The majority of the cracking reactions occur in the core region in which gaseous hydrocarbons and fresh catalysts move upward concurrently, whereas the cracking contribution of the descending catalysts against up-flowing hydrocarbons in the wall region is less significant, where deactivated catalyst moves downward. The extents of catalyst deactivation in the two regions are also very different: as most of the descending catalysts are more severely deactivated than the rising catalysts. Internal circulation of deactivating catalyst significantly affects the reactor performance. The up-moving fresh catalyst in core regime, downward motion of deactivated in wall regime and back-mixing of deactivating catalyst is shown in Figure 6.2

A low-cost approach to improve FCC performance is the development of a robust process model that can be used for predicting product quality and real-time optimization. This is why tremendous efforts have been expended on the development of FCC process models. The related literatures are summarized in the Chapter 2 in details. Most modeling efforts discussed above assumes thermal equilibrium between the hydrocarbon feed and the catalyst, which is not the case for real FCC process. In FCC process, most reaction occurs inside the pores of the catalyst, which results in significant cooling of the catalyst compare to gas feed. Hence, the temperature of the gas phase and solid phase (catalyst) is different along the riser height. With the rapid advancement of CFD techniques and computing capacity, a full-scale numerical simulation of gas–solids riser flows becomes a

useful approach for simulation of FCC process. Most literature CFD models kinetic theory of granular flows has been introduced to account for inter-particle collisions for hydrodynamic modeling. The restitution coefficient represents the elasticity of particle collisions and ranges from fully inelastic (e = 0) to fully elastic (e =1). The proper selection of restitution coefficient is important for correct prediction of hydrodynamic characteristics. However, these models may be inadequate for simulating complex gas–solid flows at high solids flux (Ranade, 2002) and for handling inter-particle collisions and other interactions in the dense-phase and transition/acceleration regimes of solids transport (You *et al.*, 2008; You *et al.*, 2010; Wang *et al.*, 2010). In addition it requires significantly increased requirement on computational resources. Even with today's prodigious computing power, full-scale CFD simulations are not ideally suited for routine applications such as real-time optimization, on-line control, feedstock selection, and plant monitoring.

The efficiency of the FCC process is strongly influenced by the effective contact of catalyst with feed oil. Vacuum gas oils (VGO, 340-560^{o}C boiling range) are typical FCC feed-stocks whose conversion depends on temperature, pressure, oil residence time, and the local catalyst-to-oil ratio (CTO). The conversion or product yield structure is governed by the vapor transport and local reaction rate r_i (various reactions from j species):

$$U\frac{d}{dz}(\rho Y_i) = -\sum_j r_{ij} \tag{6.1}$$

The local reaction rate of i^{th} species is generally linked to vapor mass concentration (Y_i), reaction temperature (T_i), catalyst deactivation factor (Φ_c), overall catalyst-to-oil ratio (C/O), and reaction parameters (e.g., order of reaction n_i, activation energy E_{ai} and pre-exponential factor k_{i0}) by the following expression:

$$r_i = k_{io} Y_i^{n_i} \overline{\left(\frac{C}{O}\right)} \Phi_c \exp\left(-\frac{E_{ai}}{RT_i}\right) \tag{6.2}$$

The vapor transport velocity U is typically treated as constant and the role of catalyst is only reflected by a constant overall catalyst-to-oil ratio (C/O) - with the untenable assumption of a uniform vapor-catalyst flow throughout the entire riser. From a mechanistic point of view, the hydrodynamics of catalyst particles should play a nontrivial role in determining FCC conversion and yield structure. To make the case, let us consider the following factors that have been overlooked in prior studies.

(1) Local Catalyst-to-Oil Ratio (rather than overall C/O). The rate of cracking reactions depends strongly on the C/O. The C/O in core and wall regime is completely different due to radial non-uniform flow structure of catalyst and hydrocarbon gas feed. Due to vaporization and cracking, the hydrocarbon vapor expands, thus drastically increasing the velocities of vapor and catalysts and the consequent decrease in the catalyst concentration. Hence, the C/O decreases significantly from the bottom (dense phase) to the top (dilute phase) of the riser in core regime.

(2) Coupling of Hydrodynamics and Reaction. The catalysts in a riser undergo an accelerating process or a continuously diluting process, which is significantly influenced by the non-uniform cracking along the riser. On the other hand, the reaction rates are a

strong function interaction between catalyst and hydrocarbon feed i.e., catalyst temperature and catalyst concentration. The hydrodynamics of both phases are completely different in core and wall regime and hence reaction rates. The upshot is that the interacting gas/solids flows and reaction kinetics are strongly coupled.

(3) Reaction Temperature. Due to the endothermic reaction and different thermal capacities of vapor and catalysts, the temperature of reacting vapors can be significantly lower than that of catalysts. Since catalytic reactions predominantly occur on the catalyst surface inside the pores and heat of reaction is supplied by regenerated catalyst, the temperature that drives the reaction should lie intermediate between the catalyst and vapor temperature.

(4) Backmixing of Deactived Catalysts. The heterogeneous structure (core-annulus, as well as axial non-uniformity) of solids flow in the riser has been well recognized (Brereton *et al.*, 1988; Werther *et al.*, 1992). In most of the annulus (wall) region, deactivated catalysts move downwards, causing the so-called back flow or back-mixing. These deactivated catalysts not only affect the hydrodynamics of fresh/deactivating catalysts and energy balance but also contribute to the cracking with a lower activity.

In summary, the traditional reaction models neglect the effects of heterogeneous gas-solids flows on reaction characteristics in FCC risers, whereas the plant data for FCC unit clearly point to the strong influence of gas-solids flow hydrodynamics on cracking kinetics and selectivity. The recent study (Zhu *et al.*, 2010) proposed formulation for two-way coupling mechanisms of local gas-solids hydrodynamics and chemical reactions in FCC reactors. In fact, the impacts of radial flow heterogeneity in gas-solids systems under non-thermal equilibrium conditions have not been investigated. Given the above, in

this study we proposes a mechanistic modeling approach that systematically incorporates two-zone (core-wall) hydrodynamics of gas-solids flow and the local hydrodynamics-reaction interactions along the riser reactor. The proposed model will take into account the effects of gas-solids concurrent/countercurrent flow on FCC reactions, which are subjected to varying degrees of catalyst deactivation. The four lumps reaction kinetic model is still popular because of its simplicity, and ease of formulation and solution of kinetic, material and energy equations. Hence, in this study we adopted four lumps reaction kinetic model for an example. The extension of simple four lumps to more complicated ten lump reaction kinetic is simple.

6.2 Modeling Approach

Consider a two-phase, two-zone gas-solids flow with the back mixing of the solid as shown in Figure 6.2. The fresh catalyst are moving upward while the deactivated catalyst are moving downward in the wall regime with the mixing of fresh/deactivating catalysts in the core region and deactivated catalyst from the wall region. The cross-section area of each zone and inter-zone mass transfer of solids (also known as back mixing) can be estimated from our recent continuous model which is discussed in the previous chapter. The adoption of core-annulus two-zone approximation instead of a direct radial-continuous-distribution approach is important at the current stage to ensure the mathematical simplicity without the loss of generality of riser transport and reaction characteristics. To further simplify the problem, following more simplifying assumptions are made. The non-thermal equilibrium condition doesn’t change the core boundary, which is estimated from the cold flow riser model. The modeling domain excludes the

quick vaporization region where feed oil vaporizes upon the contact with hot catalysts from the regenerator. It is assumed that the extent of conversion in this region is insignificant. All the variables are locally averaged over the cross-section area of core and wall regime for both hydrodynamic and reaction model. The riser wall is assumed to be adiabatic and the axial wall temperature function is assumed to be known. The heat transfer from catalyst to gas phase is by convection only and the catalyst receive radiation heat transfer from hot riser wall. Steam and by-product H_2 are neglected in hydrodynamic and reaction mode, this assumption is justified as % of mass of steam in H_2 is very small in the gas mixture. Coke formed is assumed to attach on catalyst surface, which will change the catalyst activity on cracking, and the change in catalyst size is neglected. The activity decay function for catalyst is different for catalyst in core and wall regime. Here it is noticed that all equations for the core and wall regime are for cross-section average properties of respective regimes.

6.2.1 Core-Regime

6.2.1.1 Hydrodynamic Model. Consider a small cross-section of the two-zone, two phase riser reactor, based on the balance of the mass, momentum and energy in the core regime as shown in Figure 6.3, the conservation equation for the mass, momentum and energy in the core regime can be written as Equations (6.3) to (6.6).

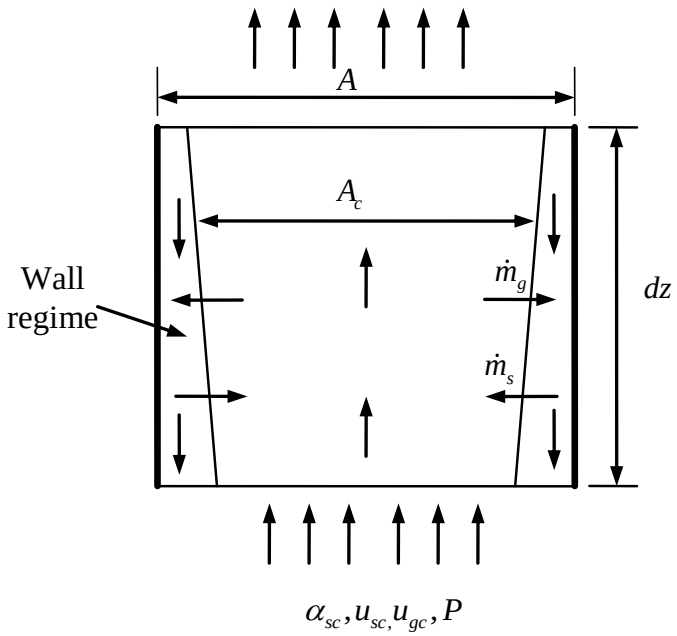

Figure 6.3 Schematic representation of control volume for two-zone riser reactor.

The overall mass balance of gas phase:

$$\frac{d\left(\alpha_{gc}\rho_g u_{gc} A_c\right)}{dz} = -\left(\gamma_3 + \gamma_5\right)_c . A_c - \dot{m}_{gr} l_c \tag{6.3}$$

Where l_c represent the periphery of the core regime. The term on right hand side of the above equation represents the reduction in gas phase due to conversion into the coke and radial transport of the hydrocarbon from core to wall regime.

The mass balance of solid phase:

$$\frac{d(\alpha_{sc}\rho_s U_{sc} A_c)}{dz} = \left(r_3 + r_5\right)_c . A_c + \dot{m}_s \tag{6.4}$$

Where $\dot{m}_s$ is catalyst mass transfer across the core-wall boundary. The mass transfer of catalyst transfer from wall-to-core is positive, while from core-to-wall is negative.

The momentum balance for gas phase can be written as;

$$-\alpha_{gc}\frac{d\left(PA_c\right)}{dz}=\tau_{gc}l_c+\alpha_{gc}\rho_g g.A_c+\frac{d\left(\alpha_{gc}\rho_g {U_{gc}}^2.A_c\right)}{dz}+F_{Dc}.A_c-\dot{m}_{gr}v_g l_c \qquad (6.5)$$

Where v_g represent the radial transport velocity of the hydrocarbon gases. The terms on the right hand side of the equation represents frictional force between the gas and core boundary, weight of the gas, acceleration of gas drag force and momentum loss due to the as transport from core to wall regime respectively.

The momentum balance for the catalyst phase can be written as;

$$\frac{d\left(\alpha_{sc}\rho_s {U_{sc}}^2.A_c\right)}{dz}=F_{Dc}.A_c-\alpha_{sc}\frac{d\left(PA_c\right)}{dz}-F_c.A_c-\alpha_{sc}\rho_s g.A_c-\tau_{sc}l_c-\dot{m}_{sr}v_s l_c \quad (6.6)$$

The terms on the right hand side of the equation represents the drag force, force on catalyst due to pressure gradient in riser reactor, inter-particle collision force, weight of the catalyst, friction between catalyst and wall and momentum transfer due to radial catalyst transfer respectively.

The average gas density can be calculated from the ideal gas law as Equation (6.7):

$$\rho_{gc} = \frac{P.\sum_{i=1}^{3} C_{ci} M_i}{RT_g \sum_{i=1}^{3} C_{ci}} \tag{6.7}$$

A constraint on the volume fractions of the two phases in the core regime is that

$$\alpha_{sc} + \alpha_{gc} = 1 \tag{6.8}$$

6.2.1.2 Reaction Model for Core regime. In this study, a simple four lump reaction scheme proposed by (Lee *et al*., 1989) is used for cracking reaction both in core and wall regime which is show in Figure 6.3.

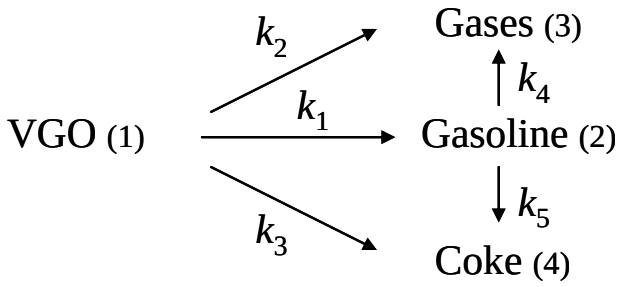

Figure 6.4 Four-lump kinetic model for gas oil cracking in FCC riser reactor (Lee *et. al*., 1989).

Since the component mass balance involves chemical reactions, we use molar concentrations to account for volume expansion. Based on the reaction scheme shown in Figure 6.4, we have

Gas-oil:

$$\frac{d\left(C_{1c}U_{gc}A_c\right)}{dz} = -\Phi_{sc}\left(k_{1c}+k_{2c}+k_{3c}\right)C_{1c}{}^{2}.A_c - \gamma C_{1c}v_g l_c \tag{6.9}$$

Gasoline:

$$\frac{d\left(C_{2c}U_{gc}A_c\right)}{dz} = \Phi_{sc}\left(\frac{M_1}{M_2}k_{1c}C_{1c}{}^{2} - (k_{4c}+k_{5c})C_{2c}\right)A_c - \gamma C_{2c}v_g l_c \tag{6.10}$$

Light Gases:

$$\frac{d\left(C_{3c}U_{gc}A_c\right)}{dz} = \Phi_{sc}\left(\frac{M_1}{M_3}k_{2c}C_{1c}{}^{2} + \frac{M_2}{M_3}k_{4c}C_{2c}\right)A_c - \gamma C_{3c}v_g l_c \tag{6.11}$$

Coke:

$$\frac{d\left(C_{4c}U_{gc}A_c\right)}{dz} = \Phi_{sc}\left(\frac{M_1}{M_4}k_{3c}C_{1c}{}^{2} + \frac{M_2}{M_4}k_{5c}C_{2c}\right)A_c - \gamma C_{4c}v_g l_c \tag{6.12}$$

Where γ represents the fraction of hydrocarbon transport from the core to wall regime. The reaction rate constant for the i^{th} reaction in the riser reactor can be written as (Zhu *et al*., 2010);

$$k_{ic} = k_{ci0}\lambda_c\left(z\right)\exp\left(-\frac{E_{ai}}{RT_s}\right) \tag{6.13}$$

where λ_c is defined as a local catalyst-to-oil ration (CTO) in the core regime . The catalyst concentration distribution along the riser in the core regime of the reactor is highly nonlinear, which has a significant effect on the reaction rates. The local CTO can be presented in terms of local hydrodynamics properties of catalyst and feed as Equation (6.14);

$$\lambda_c(z) = \left(\frac{C}{O}\right)_c = \frac{\alpha_{sc}\rho_s}{\alpha_{gc}\rho_{gc}} \tag{6.14}$$

Note that the pre-exponential factor k_{cio} in Equation (6.13) is molar-based, whereas k_{io}, the pre-exponential factor in the pseudo-homogeneous model, is mass-based. They are related by the following expression;

$$k_{cio} = \left(\frac{M_i}{\alpha_{gc}\rho_{gc}}\right) k_{io} \tag{6.15}$$

The parameter Φ_s represent the catalyst decay of activity due to coke deposition.

$$\Phi_{sc} = \frac{X+1}{X+\exp(Y.C_{cc})} \tag{6.16}$$

where X and Y are deactivation constants, taken as 4.29 and 10.4, respectively and C_{cc} is the weight percent of coke on catalyst in core regime.

6.2.2 Wall Regime

6.2.2.1 Hydrodynamic Model. Consider a small cross-section of the two-zone, two phase riser reactor, based on the balance of the mass, momentum and energy in the wall regime of the riser reactor can be written by balancing the mass, forces and energy over a small cross-section area as shown in Figure 6.3.

The mass conservation equation for the gas phase can be written as;

$$\frac{d\left(\alpha_{gw}\rho_g u_{gw}A_w\right)}{dz} = -\left(\gamma_3+\gamma_5\right)_w .A_w + \dot{m}_{gr}l_c \tag{6.17}$$

The term on the right hand side of the equation represents the reduction in mass of gas phase due to conversion into coke in wall regime.

The mass conservation equation for the deactivated catalyst in the wall regime can be written as;

$$\frac{d(\alpha_{sw}\rho_s u_{sw}A_w)}{dz} = \left(\gamma_3+\gamma_5\right)_w .A_w - \dot{m}_s\, l_c \tag{6.18}$$

Where, the terms on the right hand side of the equation represents the increase in the mass of solid phase due to formation of coke and mass transfer of catalyst to and from the core regime respectively. The mass transfer of catalyst from the core to wall regime is taken as positive in this study.

The momentum equation for the gas phase can be written as;

$$-\alpha_{gw}\frac{d\left(PA_w\right)}{dz}=F_{Dw}.A_w+\alpha_{gw}\rho_g g.A_w+\tau_{gw}.l_w+\tau_{gc}.l_c+\dot{m}_{gr}v_g l_c \tag{6.19}$$

Where the terms on the right hand side of the above equation represents, the drag force in wall regime, weight of the gas, friction force between the gas and wall of the reactor, friction force between the gas and core-annuls inter phase and momentum transfer due to the radial transport of the hydrocarbon gases respectively.

The momentum equation for the solid phase can be written as;

$$-\alpha_{sw}\frac{d\left(PA_w\right)}{dz}+F_{Dw}.A_w=\alpha_{sw}\rho_s g.A_w+\tau_{sw}l_w+\tau_{sc}l_c-\dot{m}_{sr}v_s l_c \tag{6.20}$$

Where the terms on the right hand side of the equation represents, weight of the catalyst in the wall regime, friction force between the catalyst and wall regime, friction force between the catalyst and the core-annulus inter phase and momentum transfer due to radial transport of catalyst respectively.

The energy conservation for the gas phase across entire cross-section of the riser reactor can be written as;

$$\frac{d\left(\alpha_{gc}\rho_g u_{gc}c_{pg}A_c T_{gc}\right)}{dz}+\frac{d\left(\alpha_{gw}\rho_g u_{gw}A_w T_g\right)}{dz}=-\chi.\sum_{i=1}^{5}\left(r_i\Delta H_i\right)_w A-\left[\left(\gamma_3+\gamma_5\right)_c+\left(\gamma_3+\gamma_5\right)_w\right]c_{pg}T_g A+\left(n_{sc}+n_{sw}\right)A_s h_c\left(T_s-T_g\right)A \tag{6.21}$$

Where the terms on the right hand side of the equation represents, the heat of reaction supplied by the gas phase, heat lost due to conversion of hydrocarbon feed into the coke, and the convection heat transfer from catalyst to gas.

Similarly the energy conservation for the catalyst across the entire cross-section of the riser reactor can be written as;

$$\frac{d\left(\alpha_{sc}\rho_s u_{sc} c_{ps} A_c T_s\right)}{dz} + \frac{d\left(\alpha_{sw}\rho_s u_{sw} A_w T_s\right)}{dz} = -(1-\chi)\sum_{i=1}^{5} r_i \Delta H_i A + (\gamma_3 + \gamma_5) c_{pg} T_g A - \left(n_{sc} + n_{sw}\right) A_s h_c \left(T_s - T_g\right) A + \left(n_{sc} + n_{sw}\right) A_s F \varepsilon_s \sigma \left(T_w^{\,4} - T_s^{\,4}\right) A \tag{6.22}$$

The terms on the right hand side of the equation represents the reaction heat supplied to the hydrocarbon gas feed, Convection heat transfer to the hydrocarbon feed and the radiation heat transfer from the riser wall.

The average gas density can be calculated from the ideal gas law as:

$$\rho_{gw} = \frac{P.\sum_{i=1}^{3} C_{wi} M_i}{RT_g \sum_{i=1}^{3} C_{wi}} \tag{6.23}$$

A constraint on the volume fractions of the two phases in the core regime can be written as;

$$\alpha_{sw} + \alpha_{gw} = 1 \tag{6.24}$$

6.2.2.2 Reaction Model for Wall regime. Following the four lumps reaction kinetic scheme, the molar concentration of the each phase due to the cracking reaction can be written as

Gas-oil:

$$\frac{d\left(C_{1w}U_{gw}A_w\right)}{dz} = -\Phi_{sw}\left(k_{1w}+k_{2w}+k_{3w}\right)C_{1w}{}^{2}.A_w + \gamma C_{1c}v_g l_c \tag{6.25}$$

Gasoline:

$$\frac{d\left(C_{2w}U_{gw}A_w\right)}{dz} = \Phi_{sw}\left(\frac{M_1}{M_2}k_{1w}C_{1w}{}^{2} - (k_{4w}+k_{5w})C_{2w}\right)A_w + \gamma C_{2c}v_g l_c \tag{6.26}$$

Light Gases:

$$\frac{d\left(C_{3w}U_{gw}A_w\right)}{dz} = \Phi_{sw}\left(\frac{M_1}{M_3}k_{2w}C_{1w}{}^{2} + \frac{M_2}{M_3}k_{4w}C_{2w}\right)A_w + \gamma C_{3c}v_g l_c \tag{6.27}$$

Coke:

$$\frac{d\left(C_{4w}U_{gw}A_w\right)}{dz} = \Phi_{sw}\left(\frac{M_1}{M_4}k_{3w}C_{1w}{}^{2} + \frac{M_2}{M_4}k_{5w}C_{2w}\right)A_w + \gamma C_{4c}v_g l_c \tag{6.28}$$

The reaction rate constant for the riser flow is give by;

$$k_{wi} = k_{wi0}\lambda_w\left(z\right)\exp\left(-\frac{E_{ai}}{RT_s}\right) \tag{6.29}$$

λ_w represents the local catalyst to oil ratio, which is given as;

$$\lambda_w = \left(\frac{C}{O}\right)_w = \frac{\alpha_{sw}\rho_s |u_{sw}|}{\alpha_{gw}\rho_g u_{gw}} \tag{6.30}$$

The parameter Φ_{sw} represents the catalyst decay of activity due to coke deposition in wall regime. The proposed function for catalyst deactivation takes into account the coke deposition on the catalyst in wall regime and catalyst deactivation in the core regime.

$$\Phi_{sw} = f\left(C_{cw}, \Phi_{sc}\right) \tag{6.31}$$

6.2.3 Problem Closure

The numbers of unknowns for the proposed models are solid concentration in core α_{sc}, solid velocity in core u_{sc}, gas velocity in core u_{gc}, VGO concentration in core, C_{1c}, gasoline concentration in core C_{2c}, light-gases concentration in core C_{3c}, coke concentration in core $C_{4c,}$ gas density in core ρ_{gc}, solid concentration in wall α_{sw}, solid velocity in wall u_{sw}, gas velocity in u_{gw}, VGO concentration in wall C_{1w}, gasoline concentration in wall C_{2w}, light-gases concentration in wall C_{3w}, coke concentration in wall C_{4w}, gas density in wall ρ_{gw}, solid phase temperature T_s, hydrocarbon feed temperature T_g, and pressure P, which can be solved by coupled governing Equations (6.1) to (6.5), (6.7) to (6.10), (6.15) to (6.20), and (6. 22) to (6.25).

6.2.4 Modeling of Constitutive Relations

In order to solve above governing equations for heterogeneous reaction model, we need to provide constitute equations for drag force, collision force, convective heat transfer coefficient between hydrocarbon feed and catalyst and friction force between phase and reactor wall.

6.2.4.1 Drag Force. Here the drag coefficient for particle settling in swamp of neighboring particle from the experiment of Khan & Zaki, 1990, to predict the drag force in the core regime of the riser reactor.

The total drag force on the particles in the core regime of gas-solids riser flow can be written as;

$$F_{Dc} = \frac{3}{4} C_{D0} \rho_f \left(u_{gc} - u_{sc}\right).\left|u_{gc} - u_{sc}\right|.\frac{\alpha_{sc}}{\left(1-\alpha_{sc}\right)^{-2(n-1)}}.\frac{1}{d_s} \tag{6.32}$$

Where the exponent 'n' is the slope of the curve of log u_s against α. The results of experiment, the empirical correlation for exponent 'n' had been proposed by Richardson & Zaki, 1954, in terms d_p/D and particle Reynolds number.

$$n = \left(4.35 + 17.5\frac{d_p}{D}\right)\mathrm{Re}_p^{-0.03} \qquad \text{For } 0.2 < \mathrm{Re_p} < 1 \tag{6.33}$$

$$n = \left(4.45 + 18\frac{d_p}{D}\right)\mathrm{Re}_p^{-0.1} \qquad \text{For } 0.2 < \mathrm{Re_p} < 200 \tag{6.34}$$

$$n = 4.45\,\mathrm{Re}_p^{-0.1} \qquad \text{For } 0.2 < \mathrm{Re_p} < 500 \qquad (6.35)$$

Where Re_p represents the particle Reynolds number for core flow.

6.2.4.2 Collision Force. The phenomenological semi-empirical correlation for inter-particle collision force is used for this study, which is presented as function of drag force.

$$F_c = F_{Dc}\left(1 - K_1\right) \qquad (6.36)$$

Where K_1 is the coefficient represents the "S" shaped distribution along the riser height, which can be written as;

$$K_1 = A + \tan^{-1}\left(\frac{H - z_i}{B}\right) / C \qquad (6.37)$$

Where A, B, and C are the coefficient which can be adjusted to fit the experiment data. The formulation of the function K_1 is similar to that proposed by Kwauk *et al*., 1986 for "S" shape distribution of the solid volume fraction. The value of B is unity for high solid flux risers.

6.2.4.3 Interfacial Frictional Shear Forces. The correlations for frictional shear force between each phase and wall/core-wall inter phase was adopted from the study of (Bai *et al*., 1995). Here the direction of the flow is taken into the account.

The frictional shear force of the gas and catalyst against the wall in the annulus regime can be written as;

$$\xi_{gw} = \frac{1}{2} f_{gw} \rho_g \alpha_{gw} u_{gw} |u_{gw}| \tag{6.38}$$

$$\xi_{sw} = \frac{1}{2} f_{sw} \rho_s \alpha_{sw} u_{sw} |u_{sw}| \tag{6.39}$$

Where the gas phase friction factor f_{gw} can be estimated based on the Reynolds number in the annulus regime.

$$f_{gw} = \frac{16}{\mathrm{Re}_w} \qquad \text{For } \mathrm{Re}_w \le 2000 \tag{6.40}$$

$$f_{gw} = \frac{0.079}{\mathrm{Re}_w^{0.313}} \qquad \text{For } \mathrm{Re}_w > 2000 \tag{6.41}$$

Similarly solid phase friction factor f_{sw}, following the correlation proposed by the Reddy and Pi, 1966, can be written as;

$$f_{sw} = 0.046 |u_{sw}| \tag{6.42}$$

For prediction of shear force of gas and particles at the interface between the core and annulus regime, an approximation of suspension flow within the core regime in equivalent to pipe flow having the equivalent diameter of core regime is made here. With

the above approximation, he shear force of gas and particles at the interface between the core and annulus regime can be written as Equations (6.43) and (6.44);

$$\xi_{gi} = \frac{1}{2} f_{gi} \rho_g \alpha_{gc} \left(u_{gc} - u_{gw}\right) \left|u_{gc} - u_{gw}\right| \tag{6.43}$$

$$\xi_{si} = \frac{1}{2} f_{si} \rho_s \alpha_{sc} \left(u_{sc} - u_{sw}\right) \left|u_{sc} - u_{sw}\right| \tag{6.44}$$

The friction factors for the gas and the solid phase can be written as

$$f_{gi} = \frac{16}{\mathrm{Re}_c} \qquad \text{For } \mathrm{Re}_c \le 2000 \tag{6.45}$$

$$f_{gw} = \frac{0.079}{\mathrm{Re}_c^{\,0.313}} \qquad \text{For } \mathrm{Re}_c > 2000 \tag{6.46}$$

$$f_{sw} = 0.046 \left|u_{sc} - u_{sw}\right| \tag{6.47}$$

6.2.4.4 Inter-phase Heat Transfer. The (Ranz and Marshall, 1952) correlation for heat transfer from single particle to gas may be used to predict the solid to gas heat transfer coefficient for both core and wall regime of the FCC riser reactor.

$$Nu_c = \frac{h_c d_s}{K_g} = 2.0 + 0.6\,\mathrm{Re}_p^{\,0.5}\,\mathrm{Pr}^{1/3} \tag{6.48}$$

Where K_g represents the thermal conductivity of the gas, 'Pr' Prandtl number and Re_p represents particle Reynolds number for core flow regime.

Similarly, solid to gas heat transfer coefficient for wall regime can be written as;

$$Nu_c = \frac{h_{cw} d_s}{K_g} = 2.0 + 0.6\,\mathrm{Re}_p^{\,0.5}\,\mathrm{Pr}^{1/3} \tag{6.49}$$

Here Re_p represents particle Reynolds number for annulus flow regime.

6.2.4.5 Core-Wall boundary. The core-wall boundary for this model is determined from the hydrodynamic model for axial and radial non-uniform distribution of the phases in cold riser flow. The key assumption in implementation of this correlation is that, the axial non-isothermal condition in the riser reactor doesn't affect the core-wall boundary conditions.

$$A_c = f\left(G_s, G_g, \alpha_s, z\right) = f\left(z\right) \tag{6.50}$$

The constrain for the wall regime area can be written as;

$$A_c + A_w = A \tag{6.51}$$

6.2.4.6 Radial Mass Transfer of Catalyst. The radial mass transfer of the catalyst across the core-wall boundary can be presented in terms of the back-mixing ratio, which is defined as the ration of the solid flow rate in the wall regime to the total flow rate of solids in the riser. The back-mixing ratio is determined from the hydrodynamic model for

axial and radial non-uniform distribution of the phases in cold riser flow. Again the similar assumption is made here, that is the axial non-isothermal condition in the riser reactor doesn't affect the radial transport of the solids.

$$\dot{m}_{sr} = f\left(G_{sw}, G_s\right) \tag{6.52}$$

6.3 Summary of Chapter

1. In this chapter, the concept of two-zone reaction modeling for FCC riser reactor is introduced.
2. The modeling concept is established by including major governing physics such as, catalyst back-mixing, reaction in core-wall regime, non-thermal equilibrium between the catalyst and hydrocarbon feed.
3. Fresh and deactivated catalyst motions are identified by defining core-wall boundary and back-mixing of catalyst

CHAPTER 7

SUMMARY OF DISSERTATION AND PROPOSED FUTURE STUDY

7.1 Summary

This dissertation is aimed to develop the mechanistic model for nonuniform hydrodynamics and catalytic reactions in a FCC riser reactor. The performance of the riser reactors is strongly dependent on the hydrodynamics of multiple jet interactions, vaporization rates of droplets and reactions in the feed injection regime of the FCC riser reactor. The dissertation is divided into the three major parts: 1) development of governing mechanisms and modeling of the axial and radial nonuniform distribution of the gas-solids transport properties 2) development of mechanistic model that gives a quantitative understanding of the interplay of three phase flow hydrodynamics, heat/mass transfer, and cracking reactions in the feed injection regime of a riser 3) modeling of nonuniform hydrodynamics coupled reaction kinetics in the core and wall regime of the riser reactors.

For the modeling of the axial nonuniform distribution of gas-solids transport properties, a new controlling mechanism in terms of impact of pressure gradient along the riser on the particles transport is introduced by partition of pressure gradient for gas and solid phase in their momentum equations. A new correlation for inter-particle collision force is proposed which can be used for any operation conditions of riser, riser geometry and particle types. The one-dimensional model for axial nonuniform phase distribution successfully predicted the axial profiles of transport properties along the riser height, including dense phase, acceleration, and dilute phase regimes.

To take into account the radial nonuniform distribution of phase transport properties, a continuous modeling approach, proposed by Wang 2010, is adopted for simultaneous prediction of axial and radial nonuniform phase distribution. In this dissertation, a mechanistic model for radial nonuniform distribution of the gas and solid phase transport properties is proposed. With the proposed model for radial nonuniform phase distribution, the continuous model can successfully predicts both axial and radial nonuniform distribution of phase transport properties. The proposed model results can be used to estimate much-needed information such as the wall boundary layer thickness and back-mixing of the particles, which establishes the base for the modeling of the reaction in the core and wall regime with the back-mixing of the deactivated catalyst.

As the performance of the riser reactor is strongly influence by the reaction in the feed injection regime, in this dissertation, a detailed mechanistic model for the hydrodynamics and reaction characteristics in feed injection regime is established. To simulate the real industrial riser reactor, the four nozzle spray jets were used in this study and overlapping of the spray jets is also studied. The proposed model is very useful tool for identifying the real input conditions for the present riser reaction models.

Finally, in this dissertation, the modeling concept for the reactions in the core and wall regime of the riser reactor is explored. The basis for the model is the success of the proposed continuous model. The proposed modeling concept takes into the account very important missed out physics such as, non-thermal equilibrium between the hydrocarbon vapor and the feed, back mixing and recirculation of the deactivated catalyst, and coupling between the flow hydrodynamics and reaction kinetics.

The major contributions and findings on the hydrodynamic modeling of gas-solids riser flow are from this study:

1. Introduced a new physics for solid phase transport by introduction of impact of pressure gradient along the riser on the particle transport.
2. Proposed new correlation for the inter-particle collision force in presence of pressure gradient force.
3. Formulated correlation for the drag force in presence of surrounding particles from the experiment of sedimentation and fluidization.
4. Proposed mechanistic model for the radial nonuniform distribution of the gas-solids phase transport properties.
5. The one-dimensional uniform flow model with proposed physics and inter-particle collision successfully predicts the axial nonuniform distribution of phase transport properties.
6. The proposed model for radial nonuniform phase distribution with continuous modeling approach can yield generic information on the core-wall boundary and backflow mixing of particles instead of empirical correlations.

The major contributions and findings from the modeling of hydrodynamics and reactions in the feed injection regime:

1. Proposed modeling approach for hydrodynamics of three phase flows and reaction into the feed injection regime by considering multiple jet injection and jets overlapping.

2. The proposed model can reasonably estimate the average hydrodynamics characteristics of the three phase flow and reaction characteristics at the end of the feed injection regime, which provides very important inlet boundary conditions for present riser reaction models.
3. The proposed model can estimate the length of the feed injection regime.

The major contributions from the modeling of non-uniform hydrodynamics and reactions in core and wall regime:

1. Explore modeling approach for the nonuniform hydrodynamics and reaction characteristics into the core and wall regime of the riser reactor.
2. Important governing physics such as non-thermal equilibrium between the hydrocarbon vapor and catalyst, back mixing and recirculation of deactivated catalyst and coupling between the flow hydrodynamics and reaction kinetics were taken into the account.

7.2 Suggested Future Study

The detailed modeling of the reactions into the FCC riser reactors is vast area of the research. Here, some important research topics are suggested to further explore the modeling for FCC the riser reactor.

7.2.1 Modeling of Reaction into the Core and Wall Regime of the FCC Riser Reactor

The radial non-uniform flow structure in the riser reactor is presented as core-annulus gas-solids flow structure with severe back-mixing of deactivated catalyst. Such heterogeneity has a significant impact on reaction rates. The reaction characteristics in core and wall regions are very different. The majority of the cracking reactions occur in the core region in which gaseous hydrocarbons and fresh catalysts move upward concurrently, whereas the cracking contribution of the descending catalysts against up-flowing hydrocarbons in the wall region is less significant, where deactivated catalyst moves downward. The extents of catalyst deactivation in the two regions are also very different: as most of the descending catalysts are more severely deactivated than the rising catalysts. Internal circulation of deactivating catalyst significantly affects the reactor performance. A detailed investigation on the reaction characteristics in the core and wall region shall be built up on the coupling of chemical reaction and hydrodynamics in this region. The modeling concept for reaction in the core and wall regimes is explored in the Chapter 6 of this dissertation. The quantification of reaction characteristics with detailed modeling of the key physics should be carried out to realize the actual reaction in FCC reactor.

7.2.2 Multiple Droplet Size and Velocity Distribution from Nozzle

Another challenge in investigating the spray characteristics is that the gas-droplet flow from complex industrial nozzles is always not uniform. There is always a wide range of droplet size distribution and velocity distribution across the cross-section of the jet from nozzle. A further investigation on this topic may be based on the grouping methodology which divides the nozzle cross-section into multiply sub-regions in each of which the droplet size and velocity are treated as uniform.

REFERENCES

Abramovich, G.N. (1963). The theory of turbulent jets. Cambridge, MA: *MIT Press*.

Abul-Hamayel, M.A., Siddiqui, M.A.B., Ino, T., Aitani, A.M. (2002). *Applied Catalysis A: General*, 237, 71-80.

Ali, H., Rohani, S., and Corriou, J. P. (1997). Modeling and control of a riser type Fluid Catalytic Cracking(FCC) unit. *Transactions of the Institution of Chemical Engineers*, 75(Part A), 401-412.

Arandes, J.M., Azkoiti, M.J., Bilbao, J., and de Lasa, H. I. (2000). Modeling FCC units under steady and unsteady state conditions. *The Canadian Journal of Chemical Engineering*, 78, 111-123.

Arandes, J.M., and Lasa, H.I. (1992). Simulation and multiplicity of steady states in fluidized FCCUS. *Chemical Engineering Science*, 47, 2535-2540.

Arbel, A., Huang, Z., Rinard, I.H., Shinnar, R., and Sapre, A.V. (1995). Dynamic and control of fluidized catalytic crackers; modeling of current generation of FCC's. *Industrial and Engineering Chemistry Research*, 34, 1228-1243.

Arbel, A., Huang, Z., Rinard, I.H., Shinnar R., and Sapre, A.V. (1995). Dynamic and control of fluidized catalytic crackers. *India Eng. Chem. Res.*, 34, 3014-3026.

Arena, U., Cammarota, A., Pistone, L. (1985). High velocity fluidization behavior of solids in a laboratory scale circulating fluidized bed. *Circulating Fluidized Bed Technology*, Halifax, Nova Scotia, Canada.

Ariyapadi, S., Berruti, F., Briens, C., McMillan, J., Zhou, D. (2004). Horizontal penetration of gas-Liquid spray jets in gas-solid fluidized beds. *International Journal of Chemical Reactor Engineering*, 2, (A 22).

Bader, R., Findlay I., and Knowlton, T.M. (1988). Gas-solid flow patterns in a 30.5-cm-diameter circulating fluidized bed. In "*Circulating Fluidized Bed Technology II, P. Basu and J.F. Large, Eds., Pergamon Press, Oxford*, UK, 123-137.

Bai, D.R, Jin, Y., Yu, Z.Q., and Zhu J.X. (1992). The axial distribution of the cross-sectionally averaged voidage in fast fluidized beds. *Powder Technology*, 71(1), 51-58.

Benyahia S., Ortiz A.G., and Paredes J.I.P. (2003). Numerical analysis of a reacting gas/solid flow in the riser section of an industrial fluid catalytic cracking unit. *International Journal of Chemical Reactor Engineering*, Volume 1, Article A41.

Blasetti, A., and de Lasa, H. (1997). FCC riser unit operated in the heat-transfer mode: Kinetic modeling. *Industrial and Engineering Chemical Research*, 36, 3223-3229.

Bollas, G. (2007). Five-lump kinetic model with selective catalyst deactivation for the prediction of the product selectivity in the fluid catalytic cracking process. *Catalyst Today*, 127, 31-43.

Bolton, L.W., Davidson, J.F. (1988). Proceedings of the second International Conference on CFB's. *P. Basu, J.F. Large*, Pergamon Press, Oxford, 139.

Brereton, C.M.H., and Grace, J.R. (1993). Microstructural aspects of the behavior of Circulating Fluidized Beds. *Chemical Engineering Science*, 48, 2565-2572.

Bussing, W., Reh, L. (2001). On viscous momentum transfer by solids in gas-solids flow through risers. *Chemical Engineering Science*, 56, 3803-3813.

Campbell, J. F., & Schetz, J.A. (1973). Flow properties of submerged heated effluents in a waterway. *AIAA Journal*, 15, 223.

Campbell, J. F., Schetz, J. A. (1973). Flow Properties of Submerged Heated Effluents in a Waterway. *AIAA Journal*, 11 (2), 8.

Chang, S.L., Lottes, S.A., Zhou, C.Q., Bowman, B.J., Petrick, M. (2001). Numerical study of spray injection effects on the heat transfer and product yields of FCC riser reactors. *Journal of Heat Transfer-Transactions of the ASME*, 123 (3), 544-555.

Chang, S.L., and Zhou, C.Q. (2003). Simulation of FCC riser flow with multiphase heat transfer and cracking reactions. *Computational Mechanics*, 31(6), 519-532.

Chen, T.H., Roe, L.A., Nejad, A.S. (1994). Multifunction droplet imaging and velocimetry system for spray jets. *Journal of Propulsion and Power*, 10 (6), 6.

Corella, J.; Frances, E. (1991). Analysis of the riser reactor of a fluid cracking unit: Model based on kinetics of cracking and deactivation from laboratory tests. In M. L. Occelli (Ed.), Fluid Catalytic Cracking II: *Concepts in catalyst design, ACS Symposium Series*, 452, 165-182.

Derouin, C., Nevicato, D., Forissier, M., Wild, G., Bernard, J.R. (1997). Hydrodynamics of riser units and their impact on fcc operation. *Ind. Eng. Chem. Res.*, 36, 4504-4515.

Edelman, R.B., Economos, C., and Boccio, J. (1971). Mixing and combustion in two-phase flows with application to the boron-oxygen-hydrogen-nitrogen system. *AIAA Journal*, 9, 1935.

Fan, L.S., Lau, R., Zhu, C., Vuong, K., Warsito, W., Wang, X., Liu, G. (2001). Evaporative liquid jets in gas–liquid–solid flow system. *Chemical Engineering Science*, 56, 5871-5891.

Farag, H., Ng, S., and de Lasa, H. (1993). Kinetic modeling of catalytic cracking of gas oils using in situ traps (FCCT) to prevent metal contamination. *Industrial and Engineering Chemistry Research*, 32, 1071-1080.

Field, M. A. (1963). Entrainment into an Air Jet Laden with Particles . BCURA Inf.

Forney, L.J., & Kwon, T.C. (1979). Efficient single-jet mixing in turbulent tube flow. *AIChE Journal*, 25, 623.

Gates B.C., Katzer J.R., and Schuit G.C.A. (1979). Chemistry of catalytic processes. *McGraw-Hill*, New York.

Gianetto, A., Faraq, H., Blasetti, A., and de Lasa, H. (1994). FCC catalyst for reformulated gasoline Kinetic modeling. *Industrial and Engineering Chemistry Research*, 33, 3053-3062.

Gidaspow, D. (1994). Multiphase flow and fluidization: Continuum and kinetic theory descriptions. *Academic Press* (Boston).

Grace, J.R., Issangya, A.S., Bai, D., Bi, H.T., and Zhu, J.X. (1999). Situating the high density circulating fluidized bed. *AIChE Journal*, 45, 2108-2116.

Gupta, A., and Subba Rao D. (2003). Effect of feed atomization on FCC performance: simulation of entire unit. *Chemical Engineering Science*, 58, 4567-4579.

Han I.S., and Chung C.B. (2001). Dynamic modeling and simulation of a fluidized catalytic cracking process. Part I: process modeling. *Chemical Engineering Science*, 56, 1951-1971.

Han, I.S., & Chung, C.B. (2001b). Dynamic modeling and simulation of a fluidized catalytic cracking process, Part II: Property estimation and simulation. *Chemical Engineering Science*, 56, 1973-1990.

Han, K.S., Chung, M.K. (1992). Numerical simulation of a two-phase gas-particle jet in a crossflow. *Aerosol Science and Technology*, 16 (3), 13.

Harris B.J., and Davidson, J.F. (1994). Modeling options for fluidized beds: a core/annulus deposition model, in: A.A. Avidan (Ed.), Circulating Fluidized Bed Technology, Volume IV, *AIChE Publications*, New York.

Hartge, E.U., Rensner D., and Werther, J. (1988). Solids concentration and velocity patterns in circulating fluidized beds. In "*Circulating Fluidized Bed Technology II*, P. Basu and J.F. Large, Eds., Pergamon Press, Oxford, UK, 165-1 80.

He, Y., Rudolph, V. (1996). The volume-average voidage in the riser of a circulating fluidized bed. *Powder Technology*, 89, 79-82.

Herb, B., Dou, S., Tuzla, K., Chen, J.C. (1992). Solid mass fluxes in circulating fluidized beds. *Powder Technology*, 70, 197-205.

Hernandez-Barajas, J.R., Vazquez-Roman, R., and Felix-Flores, Ma.G. (2009). A comprehensive estimation of kinetic parameters in lumped catalytic cracking reaction models. *Fuel*, 88, 169-178.

Horio, M., and Kuroki, H. (1994). Three-dimensional flow visualization of dilutely dispersed solids in bubbling and circulating fluidized beds. *Chemical Engineering Science*, 49, 2413-2421.

Issangya, A.S., Grace, J.R., Bai, D., and Zhu, J. (2000). Further measurements of flow dynamics in a high-density circulating fluidized bed riser. *Powder Technology*, 111, 104-113.

Jacob, S.H., Gross, B., Voltz, S.E., and Weekman Jr., V.M. (1976). A lumping and reaction scheme for catalytic cracking. *AIChE Journal*, 22, 701-713.

Jia, C., Rohani, S., Jutan, A. (2003). FCC unit modeling, identification and model predictive control, a simulation study. *Chemical Engineering and Processing*, 42, 311-325.

Kumar, S., Chadha, A., Gupta, R., & Sharma, R. (1995). CATCRAK: A process simulator for an integrated FCC-regenerator system. *Industrial and Engineering Chemistry Research*, 34, 3737-3748.

Knowlton, M. (1995). Modeling benchmark exercise, Workshop at the eighth engineering foundation. *Conference on fluidization*, Tours, France, 1995.

Lan X., Xu C., Wang G., Wu L., and Gao J. (2009). CFD modeling of gas-solid flow and cracking reaction in two-stage riser FCC reactors. Chemical *Engineering Science*, 64, 3847-3858.

Larocca, M., Ng, S., De Lasa, H. (1990). Fast catalytic cracking of heavy gas oils: modeling coke deactivation. *Industrial & Engineering Chemistry Research*, 29(2), 71-180.

Lee, L., Chen, Y., Huang, T., Pan, W. (1989). Four lump kinetic model for fluid catalytic cracking process. *The Canadian Journal of Chemical Engineering*, 67, 615-619.

Li, H. S., Karagozian, A. R. (1992). Breakup of a Liquid Jet in Supersonic Cross-flow. *AIAA Journal*, 30 (7), 3.

Li, Y., Kwauk, M. (1980). In Fluidization (Eds: J. R. Grace, J. M. Matsen), Plenum Press, New York.

Louge, M. Y., Mastorakos, E., Jenkins, J.T. (1991). The role of particle collisions in pneumatic transport. *Journal of Fluid Mechanics*, 231, 345-359.

Malay, P., Milne, B.J., and Rohani, S. (1999). The modified model of a riser type fluid catalytic cracking unit. *The Canadian Journal of Chemical Engineering*, 77, 169-179.

Mathesian V., Solberg T., and Hjertager B.H. (2000). Prediction of gas/particle flow with an Eulerian model including a realistic particle size distribution. *Powder Technology*, 112, 34-35.

Nayak S.V., Joshi S.L., and Ranade V.V. (2005). Modeling of vaporization and cracking of liquid oil injected in a gas–solid riser. *Chemical Engineering Science*, 60, 6049-6066.

Neri A., Gidaspow D. (2000). Riser hydrodynamics: Simulation using kinetic theory. *AIChE Journal,* 46, 52-67.

Nieuwland, J.I., Meijer, R., Kuipers, I.A.M., and van Swaaij, W.P.M. (1996). Measurements of solids concentration and axial solids velocity in gas-solid two-phase flows. *Powder Technology*, 87, 127-139.

Parssinen, J.H., Zhu, J.X. (2001). Particle velocity and flow development in a long and high-flux circulating fluidized bed riser. *Chemical Engineering Science,* 56, 5295-5303.

Platten, J.L., Keffer, J.F. (1968). Entrainment in deflected axisymmetric jets at various angles to the stream. Department of Mechanical Engineering, University of Toronto: Tech. Rep. 6808.

Pugsley, T.S., and Berruti, F. (1995). A core-annulus solids interchange model for circulating fluidized bed and FCC risers. In "*Fluidization VIII*" preprints, p. 449-455, Tours.

Qureshi, M.M.R., and Zhu, C., (2006). Cross-flow evaporating sprays in gas-solid flows: Effect of aspect ratio of rectangular nozzles. *Powder Technology*, 166(2), 60-71.

Ranade, V.V. (2002). Computational flow modeling for chemical reactor engineering. Academic Press, London.

Rautiainen, A., Stewart, G., Poikolainen, V., Sarkomaa, P. (1999). An experimental study of vertical pneumatic conveying. *Powder Technology*, 104, 139-150.

Rhodes, M.J., Sollaart, M., Wang, X.S. (1998). Flow structure in a fast fluid bed. *Powder Technology*, 99, 194-200.

Ricou, F.P., Spalding, D.B. (1961). Measurements of entrainment by axisymmetrical turbulent jets. *Journal of Fluid Mechanics,* 11 (1), 12.

Senior, R.C., and Brereton, C. (1992). Modeling of circulating fluidized-bed solids flow and distribution. *Chemical Engineering Science*, 47, 281-296.

Skouby, D.C. (1998). Hydrodynamics studies in a 0.45-m riser with liquid feed injection. *Proceddings of the AIChE Annual Meeting*.

Subramanian, V., and Venktram, S. (1985). Particle entrainment by axisymmetric jets. *The Canadian Journal of Chemical Engineering*, 63, 853.

Subramanian, V., Ganesh, R. (1882). Entrainment by a concentric jet with particles in the secondary stream. *The Canadian Journal of Chemical Engineering*, 60 (5), 4.

Subramanian, V., Ganesh, R. (1984). Influence of free stream velocity on the entrainment by single- and two-phase axisymmetric jet. *AIChE Journal*, 30, 4.

Theologos, K.N., and Markatos, N.C. (1993). Advanced modeling of fluid catalytic cracking riser-type reactors. *AIChE Journal*, 39, 1007-1017.

Theologos, K.N., Lygeros, A.I., and Markatos, N.C. (1999). Feedstock atomization effects on FCC riser reactors selectivity. *Chemical Engineering Science,* 54, (22) 5617-5625.

Van Wachem B.G.M., Schowten J.C., Van Den Bleck C.M., Krishna R., and Sinclair, J.L. (2001). A CFD modeling of gas fluidized beds with a bimodal particle mixture, *AIChE Journal*, 1292-1301.

Wang D., (2010). Transport mechanisms and modeling of riser reactor. Ph.D. Thesis, Department of Mechanical & Industrial Engineering New Jersey Institute of Technology, Newark, New Jersey, USA

Wang, X.H., Zhu, C., and Ahluwalia, R. (2004). Numerical simulation of evaporating spray jets in concurrent gas-solids pipe flows. *Powder Technology*, 140, (1-2) 56-67.

Weekman, V.W. (1968). A model of catalytic cracking conversion in fixed, moving, and fluid bed reactors. *Industrial and Engineering Chemistry Process Design and Development*, 7, 90-95.

Wei, F., Lin, H., Cheng, Y., Wang, Z., and Jin, Y. (1998). Profile of particle velocity and solid volume fraction in a high-density riser. *Powder Technology*, 100, 183-189.

Weinstein, H., Shao, M., and Wasserzug, L. (1984). Radial solid density variations in a fast fluidized bed. *AlChE Symp. Ser.* 80, 117-121.

Wirth, K. E. (1991). Fluid mechanics of circulating fluidized beds. *Chemical Engineering and Technology*, 14, 29-38.

Wu C., Cheng Y., Ding Y., and Jin Y. (2010). CFD–DEM simulation of gas–solid reacting flows in fluid catalytic cracking (FCC) process. *Chemical Engineering Science*, 65, 542-549.

Wu, P.K., Kirkendall, K.A., and Fuller, R.P. (1998). Particle effects on free jet entrainment. *Journal of Propulsion and Power*, 14, 173.

Wu, P.K., Kirkendall, K.A., Fuller, R.P. (1998). Spray Structures of Liquid Jets Atomized in Subsonic Cross-flows. *Journal of Propulsion and Power*, 14 (2), 10.

Xiao-Bo Qi, Wei-Xing Huang and Jesse Zhu (2008). Comparison of flow structure in circulating fluidized bed risers with FCC and sand particles. *Chem. Eng. Technol*., 31(4), 542-553.

Yan, A.J., Zhu, J.X. (2004). Scale-up effect of riser reactors (1): axial and radial solids concentration distribution and flow development. *Ind. Eng. Chem. Res.*, 43, 5810-5819.

Yen, L., Wrench, R., and Ong, A. (1987). Reaction kinetic correlation for predicting coke yield in fluid catalytic cracking. *Presented at the Katalistisks' 8th Annual Fluid Catalytic Cracking Symposium*, Budapest, Hungary.

You, J., Patel, R., Wang, D., Zhu, C. (2010). Role of inter-particle collision on solids acceleration in riser. *Particuology*, 8(1), 13-18.

You, J., Wang, D., Zhu, C. (2010). Modeling of core flow in a gas–solids riser. *Powder Technology*, 199, 113-22.

You, J., Zhu, C., Du, B., Fan, L.S. (2008). Heterogeneous structure in gas-solid riser flows. *AIChE Journal*, 54(6), 1459-1469.

Zhang, W., Tung Y., and Johnsson, F. (1991). Radial voidage profiles in fast fluidized beds of different diameters. *Chemical Engineering Science*, 46, 3045-3052.

Zheng, Y.Y. (1994). Dynamic modeling and simulation of a catalytic cracking unit. *Computers and Chemical Engineering*, 18, 39-44.

Zhu C., Jun Y., Patel R.., Wang D. (2011). Interactions of flow and reaction in fluid catalytic cracking risers, *AIChE Journal*, In print.

Zhu, C., Liu, G., Wang, X., Fan, L.S. (2002). A parametric model for evaporating liquid jets in dilute gas-solid flows. *International Journal of Multiphase Flow*, 28, 1479-1495.

Zhu, C., Wang, X., Fan, L.S. (2000). Effect of solids concentration on evaporative liquid jets in gas-solid flows. *Powder Technology,* 111(1-2), 79-82.

Zhu, C., Wang, X., Liu, G., Fan, L.S. (2001). A similarity model of evaporating liquid spray jets in concurrent gas-solid flows. *Powder Technology*, 119(2-3), 292-297.

Zhu, C., You, J. (2007). An energy-based model of gas–solid transport in a riser. *Powder Technology*, 33, 33-42.

Zimmermann, S., and Taghipour F. (2005). CFD modeling of the hydrodynamics and reaction kinetics of FCC fluidized-bed reactors. *Industrial and Engineering Chemistry Research*, 44, 9818-9827.